



**HAL**  
open science

## **Emerald Deposits: A Review and Enhanced Classification**

Gaston Giuliani, Lee Groat, Dan Marshall, Anthony E. Fallick, Yannick Branquet

► **To cite this version:**

Gaston Giuliani, Lee Groat, Dan Marshall, Anthony E. Fallick, Yannick Branquet. Emerald Deposits: A Review and Enhanced Classification. Minerals, 2019, 9 (2), pp.105. 10.3390/min9020105. insu-02860887

**HAL Id: insu-02860887**

**<https://insu.hal.science/insu-02860887v1>**



Submitted on 8 Jun 2020

**HAL** is a multi-disciplinary open access archive for the deposit and dissemination of scientific research documents, whether they are published or not. The documents may come from teaching and research institutions in France or abroad, or from public or private research centers.

L'archive ouverte pluridisciplinaire **HAL**, est destinée au dépôt et à la diffusion de documents scientifiques de niveau recherche, publiés ou non, émanant des établissements d'enseignement et de recherche français ou étrangers, des laboratoires publics ou privés.

Review

# Emerald Deposits: A Review and Enhanced Classification

Gaston Giuliani <sup>1,\*</sup>, Lee A. Groat <sup>2</sup>, Dan Marshall <sup>3</sup>, Anthony E. Fallick <sup>4</sup>   
and Yannick Branquet <sup>5</sup> 

<sup>1</sup> Université Paul Sabatier, GET/IRD et Université de Lorraine, CRPG/CNRS, 15 rue Notre-Dame des Pauvres, BP 20, 54501 Vandœuvre cedex, France

<sup>2</sup> Department of Earth, Ocean and Atmospheric Sciences, University of British Columbia, Vancouver, BC V6T 1Z4, Canada; groat@mail.ubc.ca

<sup>3</sup> Department of Earth Sciences, Simon Fraser University, Burnaby, BC V5A 1S6, Canada; marshall@sfu.ca

<sup>4</sup> Isotope Geosciences Unit, S.U.E.R.C., Rankine Avenue, East Kilbride, Glasgow G75 0QF, Scotland, UK; fallickt@gmail.com

<sup>5</sup> Institut des Sciences de la Terre d'Orléans (ISTO), UMR 7327-CNRS/Université d'Orléans/BRGM, 45071 Orléans, France; yannick.branquet@univ-orleans.fr

\* Correspondence: giuliani@crpg.cnrs-nancy.fr; Tel.: +33-3-83594238

Received: 12 January 2019; Accepted: 9 February 2019; Published: 13 February 2019



**Abstract:** Although emerald deposits are relatively rare, they can be formed in several different, but specific geologic settings and the classification systems and models currently used to describe emerald precipitation and predict its occurrence are too restrictive, leading to confusion as to the exact mode of formation for some emerald deposits. Generally speaking, emerald is beryl with sufficient concentrations of the chromophores, chromium and vanadium, to result in green and sometimes bluish green or yellowish green crystals. The limiting factor in the formation of emerald is geological conditions resulting in an environment rich in both beryllium and chromium or vanadium. Historically, emerald deposits have been classified into three broad types. The first and most abundant deposit type, in terms of production, is the desilicated pegmatite related type that formed via the interaction of metasomatic fluids with beryllium-rich pegmatites, or similar granitic bodies, that intruded into chromium- or vanadium-rich rocks, such as ultramafic and volcanic rocks, or shales derived from those rocks. A second deposit type, accounting for most of the emerald of gem quality, is the sedimentary type, which generally involves the interaction, along faults and fractures, of upper level crustal brines rich in Be from evaporite interaction with shales and other Cr- and/or V-bearing sedimentary rocks. The third, and comparatively most rare, deposit type is the metamorphic-metasomatic deposit. In this deposit model, deeper crustal fluids circulate along faults or shear zones and interact with metamorphosed shales, carbonates, and ultramafic rocks, and Be and Cr ( $\pm$ V) may either be transported to the deposition site via the fluids or already be present in the host metamorphic rocks intersected by the faults or shear zones. All three emerald deposit models require some level of tectonic activity and often continued tectonic activity can result in the metamorphism of an existing sedimentary or magmatic type deposit. In the extreme, at deeper crustal levels, high-grade metamorphism can result in the partial melting of metamorphic rocks, blurring the distinction between metamorphic and magmatic deposit types. In the present paper, we propose an enhanced classification for emerald deposits based on the geological environment, i.e., magmatic or metamorphic; host-rocks type, i.e., mafic-ultramafic rocks, sedimentary rocks, and granitoids; degree of metamorphism; styles of mineralization, i.e., veins, pods, metasomatites, shear zone; type of fluids and their temperature, pressure, composition. The new classification accounts for multi-stage formation of the deposits and ages of formation, as well as probable remobilization of previous beryllium mineralization, such as pegmatite intrusions in mafic-ultramafic rocks. Such new considerations use the concept of genetic models based on studies employing chemical, geochemical, radiogenic, and stable isotope, and fluid and solid inclusion

fingerprints. The emerald occurrences and deposits are classified into two main types: (Type I) Tectonic magmatic-related with sub-types hosted in: (IA) Mafic-ultramafic rocks (Brazil, Zambia, Russia, and others); (IB) Sedimentary rocks (China, Canada, Norway, Kazakhstan, Australia); (IC) Granitic rocks (Nigeria). (Type II) Tectonic metamorphic-related with sub-types hosted in: (IIA) Mafic-ultramafic rocks (Brazil, Austria); (IIB) Sedimentary rocks-black shale (Colombia, Canada, USA); (IIC) Metamorphic rocks (China, Afghanistan, USA); (IID) Metamorphosed and remobilized either type I deposits or hidden granitic intrusion-related (Austria, Egypt, Australia, Pakistan), and some unclassified deposits.

**Keywords:** emerald deposits; classification; typology; metamorphism; magmatism; sedimentary; alkaline metasomatism; fluids; stable and radiogenic isotopes; genetic models; exploration

---

## 1. Introduction

Emerald is the green gem variety of the mineral beryl, which has the ideal formula of  $\text{Be}_3\text{Al}_2\text{SiO}_{18}$ . It is considered one of the so-called precious gems and in general the most valuable after diamond and ruby. The color of emerald is of greater importance than its clarity and brilliance for its valuation on the colored gem market. In the Munsell color chart, emerald exhibits a green color palette that is the consequence of peculiarities of its formation in contrasting environments (Figure 1). The pricing of emerald is unique in terms of the color and weight in carats. In 2000, an exceptional 10.11 ct Colombian cut gem was sold for US\$1,149,850 [1]. In October 2017, Gemfield's auction of Zambian emeralds generated revenues of US\$21.5 million and companies placed bids with an average value of \$66.21 per carat [2]. This auction included the 6100 ct. *Insufu* rough emerald extracted from the Kagem mine in 2015. Lastly, on the 2th of October, the remarkable emerald called *Inkalamu* ("the lion elephant") was extracted from the same mine [3]. Other giant crystals have been discovered in Colombia, such as *el Monstro* (16,020 ct) and *Emilia* (7025 ct), both from the Gachalá mines. In 2017, a large piece of biotite schist with several emerald crystals was discovered in the Carnaíba mine, Brazil; the specimen weighed 341 kg with 1.7 million ct of emerald, of which 180,000 ct were of gem quality. The specimen has been valued at approximately US\$309 million [4].

The present article assesses the state of our knowledge of emerald then and now, through several questions regarding their locations on the planet; their crystal chemistry; pressure-temperature conditions of crystallization; the source of the constituent elements, i.e., beryllium (Be), chromium (Cr) and vanadium (V); and their age of formation; and also proposes a new classification scheme.

Exploration beyond the 21st century may require a comprehensive data base of the typology of emerald deposits to understand why some emerald occurrences are economic in terms of quantity and quality and most are not. These future efforts will improve exploration guidelines in the field, including plate tectonics and its consequences in terms of modeling our landscape through time and within the Wilson cycle of continents.



**Figure 1.** Emeralds' worldwide photographs: (a) Emerald crystals on quartz and adularia, Panjshir Valley, Afghanistan,  $6.6 \times 4.4$  cm. Specimen: Fine Art Mineral. Photograph: Louis-Dominique Bayle, *le Règne Minéral*; (b) emerald on pyrite, Chivor, Colombia,  $3.9 \times 2.6$  cm. Collection MulitAxes. Photograph: Louis-Dominique Bayle, *le Règne Minéral*; (c) Emerald in quartz, Kagem mine, Zambia, longest crystal:  $7.9 \times 1.2 \times 1.2$  cm. The Collector's Edge. Photograph: Louis-Dominique Bayle, *le Règne Minéral*; (d) emerald in quartz vein and minor potassic feldspar, Dyakou, China, longest crystal: 1.5 cm. Specimen DYKO6-zh. Photograph: Dan Marshall; (e) emerald in plagioclase, Carnaíba, Brazil, longest crystal: 6 cm. Photograph: Gaston Giuliani.

## 2. Worldwide Emerald Deposits

Emerald is rare, but it is found on all five continents (Figure 2). Colombia, Brazil, Zambia, Russia, Zimbabwe, Madagascar, Pakistan, and Afghanistan (Figure 3) are the largest producers of emerald [5]. Emerald deposits occur mainly in the Precambrian series in Eastern Brazil, Eastern Africa, South Africa, Madagascar, India, and Australia, and younger volcano-sedimentary series or ophiolites in Bulgaria, Canada, China, India, Pakistan, Russia, and Spain. Colombian emerald deposits, which produce most of the world's high-quality emeralds, are unique in that they are located in sedimentary rocks, i.e., the Lower Cretaceous black shales (BS) of the Eastern Cordillera basin. Other deposits are hosted in Alpine-type veins, also called Alpine-type clefts. Emerald is found in veins and cavities in the European Alps (Binnental) as well as in the United States (Hiddenite). Nigerian emeralds are unique and are located in pegmatitic pods.

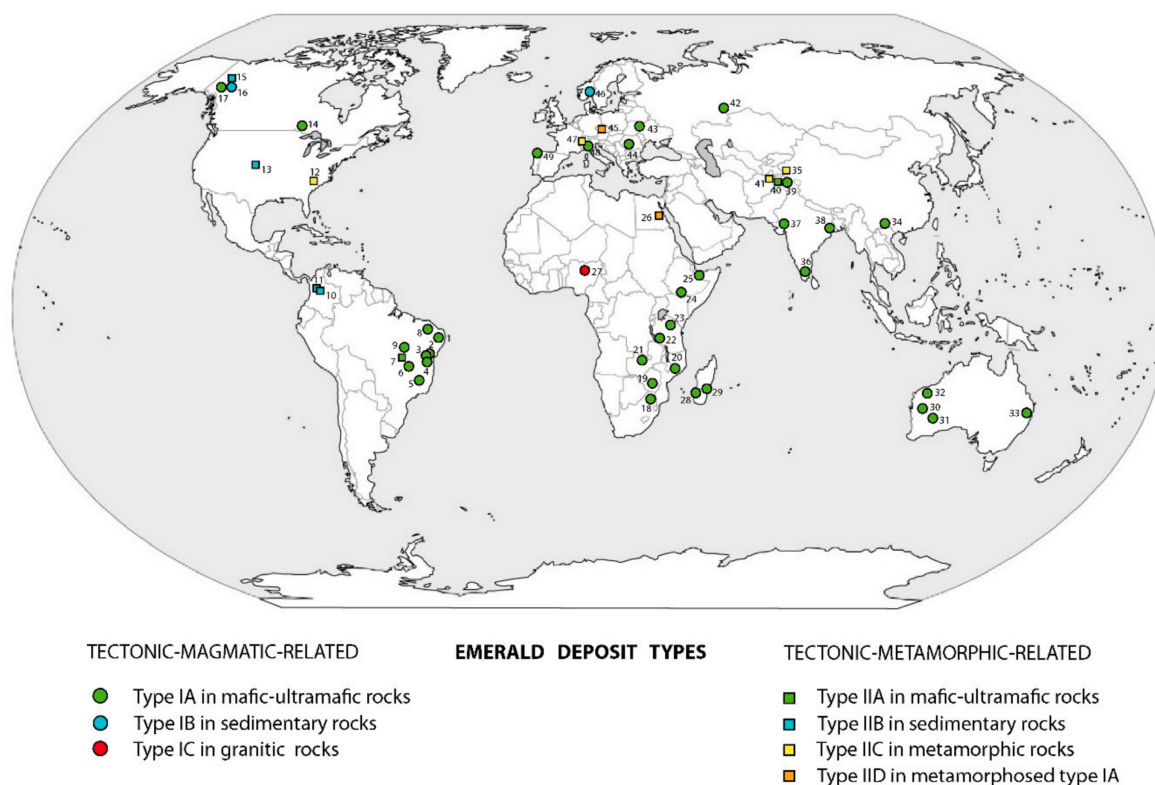


**Figure 2.** The location of emerald deposits and occurrences worldwide reported following their geological types, i.e., tectonic magmatic-related (type I) and tectonic metamorphic-related (type II): *Brazil*: 1. Fazenda Bonfim; 2. Socotó; 3. Carnaíba; 4. Anagé, Brumado; 5. Piteiras, Belmont mine, Capoierana, Santana dos Ferros; 6. Pirenópolis, Itaberai; 7. Santa Terezinha de Goiás; 8. Tauá, Coqui; 9. Monte Santo. *Colombia*: 10. Eastern emerald zone (Gachalá, Chivor, Macanal); 11. Western emerald zone (Yacopí, Muzo, Coscuez, Maripi, Cunas, La Pita, La Marina, Peñas Blancas). *United States*: 12. Hiddenite; 13. Uinta. *Canada*: 14. Dryden; 15. Mountain River; 16. Lened; 17. Tsa da Gliza. *South Africa*: 18. Gravelotte. *Zimbabwe*: 19. Sandawana, Masvingo, Filibusi. *Mozambique*: 20. Morrua. *Zambia*: 21. Kafubu, Musakashi. *Tanzania*: 22. Sumbawanga; 23. Manyara. *Ethiopia*: 24. Kenticha (Halo-Shakiso). *Somalia*: 25. Boorama. *Egypt*: 26. Gebels Sikaït, Zabara, Wadi Umm Kabu. *Nigeria*: 27. Kaduna. *Madagascar*: 28. Ianapera; 29. Mananjary. *Australia*: 30. Poona; 31. Menzies; 32. Wodgina; 33. Emmaville, Torrington. *China*: 34. Dyaku; 35. Davdar. *India*: 36. Sankari Taluka; 37. Rajasthan (Bubani, Rajgarh, Kaliguman); 38. Gubaranda (Orissa state). *Pakistan*: 39. Khaltaro; 40. Swat valley. *Afghanistan*: 41. Panjshir valley. *Russia*: 42. Urals (Malyshevo). *Ukraine*: 43. Wolodarsk. *Bulgaria*: 44. Rila. *Austria*: 45. Habachtal. *Norway*: 46. Eidswoll. *Switzerland*: 47. Binntal. *Italia*: 48. Val Vigezzo. *Spain*: 49. Franqueira.

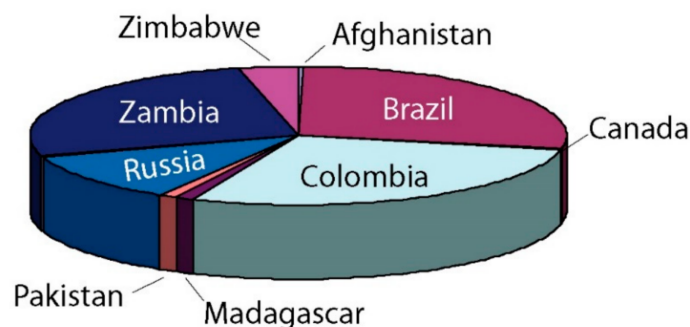


**Figure 3.** Emerald production worldwide in 2005.

### 3. Crystal Chemistry of Emerald

Beryl is hexagonal and crystallizes in point group  $6/m\ 2/m\ 2/m$  and space group  $P6/m2/c2/c$ . It is a cyclosilicate mineral. The crystal structure, as shown in Figure 4, is characterized by six-membered rings of silica tetrahedra lying in planes parallel to (0001). The Al or Y site is surrounded by six O atoms in octahedral coordination, and both the Be and silica (Si) sites are surrounded by four O atoms in tetrahedral coordination. The  $\text{SiO}_4$  tetrahedra polymerize to form six-membered rings parallel to (001); stacking of the rings results in large channels parallel to  $c$ . The channels are not uniform in diameter; in fact, they consist of cavities with a diameter of approximately 5.1 Å separated by bottlenecks with a diameter of approximately 2.8 Å. The channels can be occupied by alkali ions (such as  $\text{Na}^+$ ,  $\text{Li}^+$ ,  $\text{K}^+$ ,  $\text{Rb}^+$ ,  $\text{Cs}^+$ , etc.) whose presence is required to balance reductions in positive charges when cation substitutions occur in the structure. Neutral  $\text{H}_2\text{O}$  and  $\text{CO}_2$  molecules [6] and noble gases, such as argon, helium [7], xenon, and neon [8], are generally also present in variable amounts in the channels.

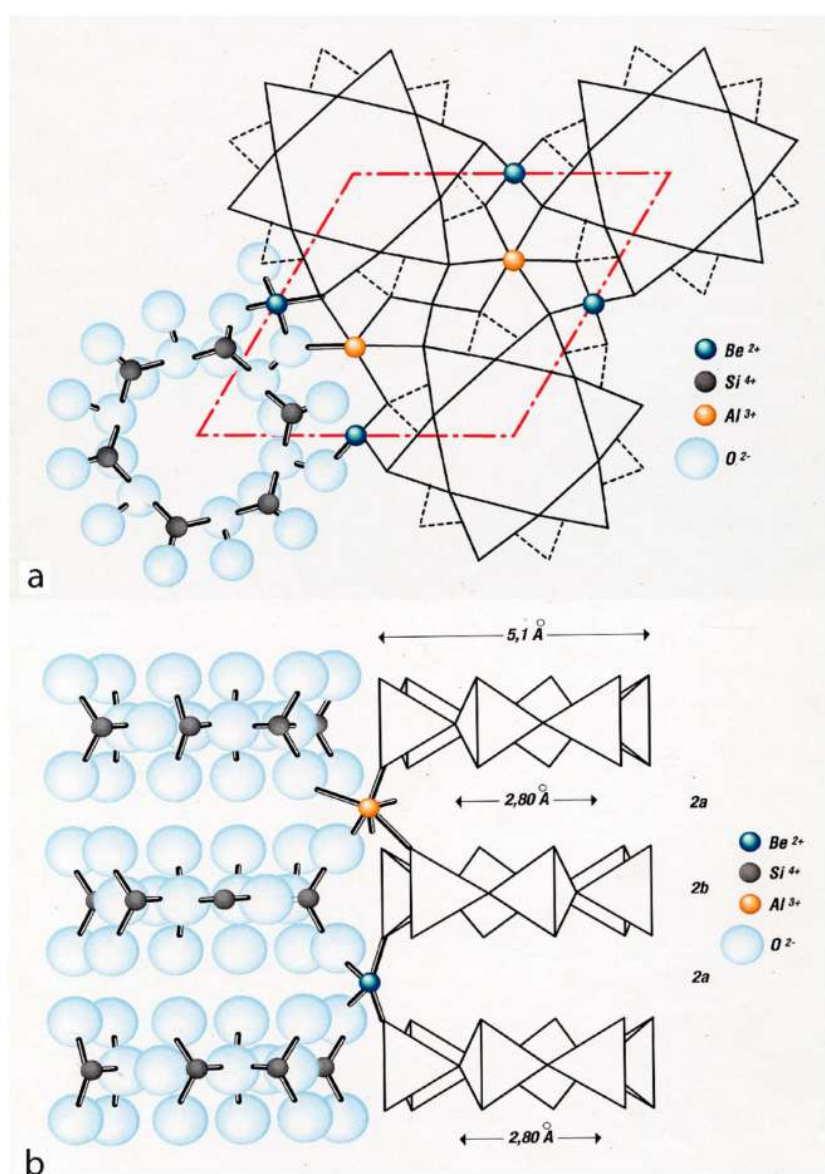


**Figure 4.** Structure of beryl [9] in: (a) Apical view: Hexagonal silicate rings stacked parallel to the  $c$  axis (normal to the drawing) are held together by  $\text{Al}^{3+}$  (octahedral site) and  $\text{Be}^{2+}$  (tetrahedral site). The radii of the ions are respected in the drawing; (b) lateral view perpendicular to the  $c$  axis showing the hexagonal silicate rings and the bottleneck ( $2b$  site) and the open cage ( $2a$  site) structure.

Emerald was defined by [10] as “the yellowish green, green or bluish green beryl which reveals distinct Cr and/or V absorption bands in the red and blue violet ranges of their absorption spectra”. Quantitatively, Cr and V substitutions range between 25 [6] and 34,000 ppm [11] for Cr and from 34 ppm [12] to 10,000 ppm [13] for V. Emerald crystals typically exhibit a prismatic habit (Figure 5) characterized by eight faces and their corresponding growth sectors: Six  $\{10\bar{1}0\}$  first order prismatic faces and two pinacoidal  $\{0001\}$  faces. Small additional  $\{10\bar{1}2\}$  and  $\{11\bar{2}2\}$  faces can also be present.

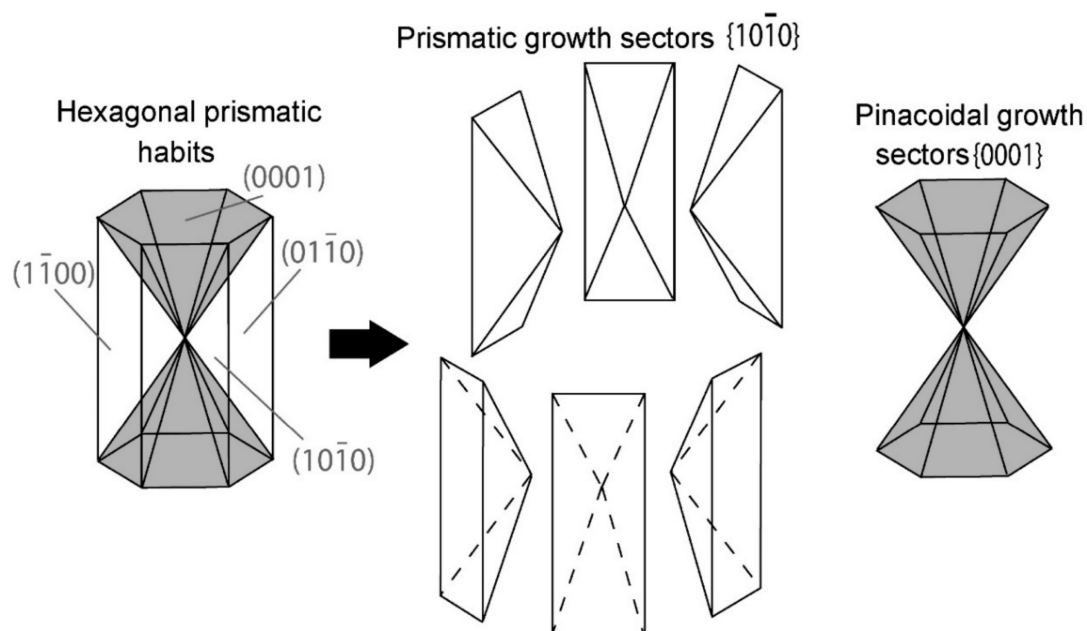


**Figure 5.** Habits of emerald crystals, characterized by eight main faces and their corresponding growth sectors: Six  $\{10\bar{1}0\}$  first order prismatic faces and two pinacoidal  $\{0001\}$  faces.

Representative emerald compositions from the literature are listed in Table 1. Most substitutions occur at the Y site. Figure 6 shows Al versus the sum of other Y-site cations for 499 emerald compositions from the literature; as expected, they show an inverse relationship. Figure 7 shows a slight deviation from a 1:1 correlation between  $Mg + Mn + Fe$  and the sum of monovalent cations. This graph suggests that, to achieve charge balance, the substitution of divalent cations for Al at the Y site is coupled with the substitution of a monovalent cation for a vacancy at a channel site. There are two sites in the channels; these are referred to as the  $2a$  (at 0,0,0.25) and  $2b$  (at 0,0,0) positions. Artioli et al. [14] suggested that in alkali- and water-rich beryls,  $H_2O$  molecules and the larger alkali atoms (Cs, Rb, K) occupy the  $2a$  sites and Na atoms occupy the smaller  $2b$  positions, but in alkali- and water-poor beryl, both Na atoms and  $H_2O$  molecules occur at the  $2a$  site and the  $2b$  site is empty. The amount of water in beryl can be difficult to determine, but Giuliani et al. [15] derived the following equation from existing experimental data for emerald:

$$H_2O \text{ (in wt.\%)} = [0.84958 \times Na_2O \text{ (in wt.\%)}] + 0.8373. \quad (1)$$

This equation has been improved [16] and is best defined by the relationship:

$$H_2O = 0.5401 \ln Na_2O + 2.1867a. \quad (2)$$

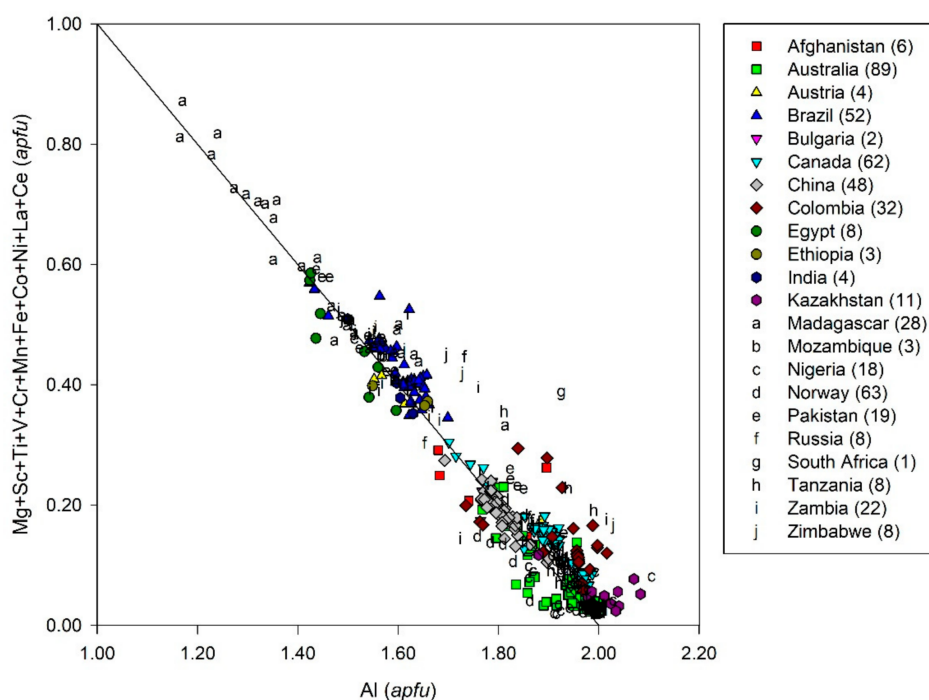




Table 1. Cont.

Elementss	1	2	3	4	5	6	7	8	9	10	11	12	13	14	15	16
Be <sup>2+</sup>	3.000	3.000	2.894	2.989	3.000	3.000	3.000	3.000	3.000	3.000	2.960	2.993	2.996	2.996	2.996	3.000
Mg <sup>2+</sup>	0.485	0.465	0.081	0.129	0.005	0.004	0.008	0.020	0.121	0.309	0.119	0.359	0.007	0.022	0.117	0.331
Ca <sup>2+</sup>	0.021	0.017	0.000	0.000	0.000	0.000	0.001	0.001	0.002	0.002	0.000	0.006	0.000	0.000	0.000	0.004
Mn <sup>2+</sup>	0.008	0.000	0.000	0.002	0.000	0.001	0.001	0.000	0.000	0.001	0.000	0.001	0.000	0.000	0.001	0.001
Fe <sup>2+</sup>	0.000	0.000	0.029	0.013	0.016	0.014	0.009	0.011	0.020	0.050	0.025	0.074	0.054	0.030	0.011	0.049
Li <sup>+</sup>	0.000	0.000	0.106	0.011	0.000	0.000	0.000	0.000	0.000	0.000	0.040	0.007	0.004	0.004	0.004	0.000
Na <sup>+</sup>	0.150	0.160	0.205	0.110	0.009	0.010	0.014	0.048	0.147	0.316	0.145	0.327	0.007	0.018	0.123	0.337
K <sup>+</sup>	0.243	0.223	0.006	0.003	0.001	0.002	0.000	0.001	0.002	0.004	0.000	0.028	0.002	0.006	0.000	0.005
Rb <sup>+</sup>	0.000	0.000	0.000	0.000	0.000	0.000	0.000	0.000	0.000	0.008	0.000	0.000	0.000	0.000	0.000	0.000
Cs <sup>+</sup>	0.001	0.001	0.005	0.000	0.000	0.000	0.000	0.004	0.004	0.001	0.000	0.000	0.000	0.000	0.000	0.000

<sup>1</sup> Compositions renormalized on the basis of 3 (Be + Li) and 18 O per formula unit. H<sub>2</sub>O = 0.5401 ln Na<sub>2</sub>O + 2.1867 [16]. 1. Ianapera, Madagascar. Ultramafic host, Type-3 core [11]. 2. Ianapera, Madagascar. Ultramafic host, Type-3 rim [11]. 3. Taylor 2, Canada. Average of 51 analyses with Li = (Na + K + Cs) - (Mg + Fe), which assumes all Fe as Fe<sup>2+</sup> [17]. 4. Davdar, China. Average of 48 analyses; Ce<sub>2</sub>O<sub>3</sub> by neutron activation, LiO 0.03 wt.% by fusion with Na<sub>2</sub>O<sub>2</sub> [18]. 5. Emmaville-Torrington, Australia. "Line 1"; average of 27 analyses [19]. 6. Emmaville-Torrington, Australia. "Line 2"; average of 31 analyses [19]. 7. Byrud, Norway. Average of 38 analyses [20]. 8. Poona, Australia. Average of 37 analyses [16]. 9. Lened, Canada. Average of 88 analyses [21]. 10. Fazenda Bonfim, Brazil. Average of approximately 130 analyses [22]. 11. Malyshevsk, Russia. Average of five analyses [23]. 12. Alto Ligonha, Mozambique. Average of three analyses [23]. 13. Jos, Nigeria. Average of five analyses [23]. 14. Sumbawanga, Tanzania. Average of five analyses [23]. 15. Muzo, Colombia. Average of three analyses [23]. 16. Ethiopia [this study, average of 32 analyses].



**Figure 6.** Al versus the sum of other Y-site cations, in atoms per formula unit, for 499 emerald analyses from the literature. The number of analyses per country is given in parentheses in the legend. Sources of data: [11–15], [16] (average of 37 analyses), [17–20], [21] (average of 88 analyses), [22] (average of approximately 130 analyses), [23–43], [44] (Kazakhstan values are averages of 11 analyses), [45] (average of 10 analyses), [46], [47] (two averages of five analyses each), [48–51], [52] (average of 55 analyses), and this study.

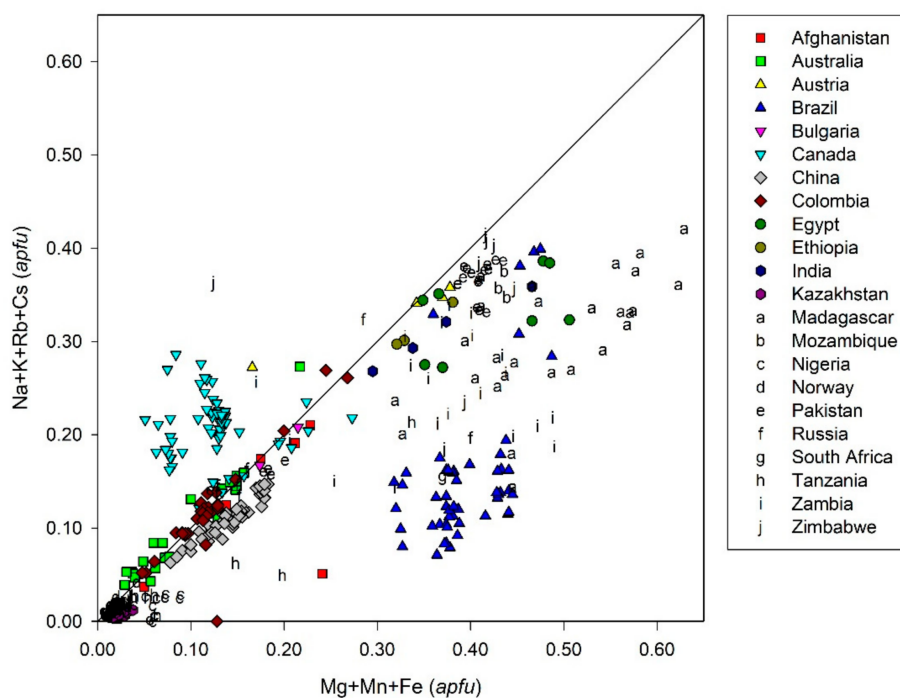
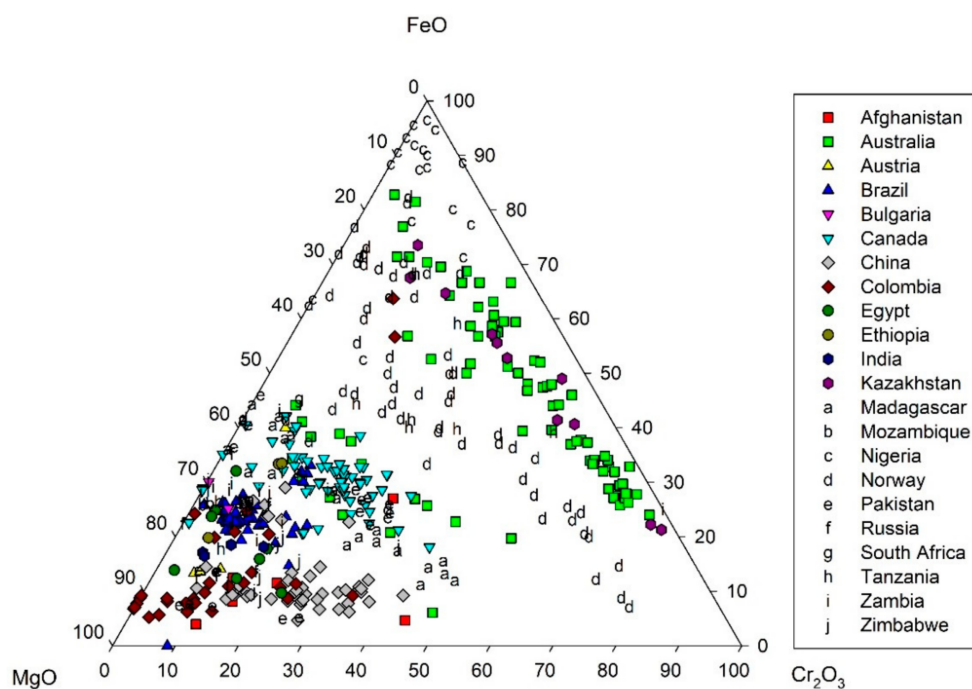


**Figure 7.** Mg + Mn + Fe vs. monovalent channel-site cations, in atoms per formula unit, for analyses from the literature. Sources of data are the same as in Figure 6.

Unfortunately, it is difficult to obtain accurate analyses of Be, Li, and ferric-ferrous ratios in beryl. Both Be and Li are too light to measure with the electron microprobe, which cannot distinguish between

$\text{Fe}^{3+}$  and  $\text{Fe}^{2+}$ . Thus, most published analyses of beryl are renormalized on the basis of 18 O and 3 Be atoms per formula unit and Fe is generally reported as exclusively ferric or ferrous. Points that lie to the right of the 1:1 line in Figure 6 indicate that some of the Fe in a given emerald is present as  $\text{Fe}^{3+}$ . Likewise, points that lie above the line could suggest the presence of  $\text{Li}^+$ , which may substitute for  $\text{Be}^{2+}$  at the Be site. Charge balance is maintained by adding a monovalent cation to a channel site. Beryllium can be analyzed with LA-ICP-MS (Laser Ablation–Inductively Coupled Plasma–Mass Spectrometry), SIMS (Secondary Ionisation Mass Spectrometry, or “ion microprobe” [23]), or by using wet chemical techniques. However, there is so much Be in the structure that the accuracy of such analyses is suspect. Lithium may be analyzed by the same techniques as Be, but because the concentrations are much lower, the accuracy would presumably be better. The amount of Li can also be estimated in Fe-free beryl from the number of monovalent cations at the channel sites.

The main substituents for Al at the Y site are plotted as oxides in Figure 8a. Magnesium is the main substituent in emeralds from most localities. The elements responsible for most of the variation in color in emerald crystals are plotted as oxides in Figure 8b. In most cases, the  $\text{Cr}_2\text{O}_3$  content is much greater than that of  $\text{V}_2\text{O}_5$ ; the main exceptions are for samples from the Lened occurrence in Canada [21,47], the Davdar occurrence in China [18], the Muzo mine in Colombia [1], the Mohmand district in Pakistan [1], and Eidsvoll in Norway [13]. The accuracy of data obtained by LA-ICP-MS is primarily dependent on the standards used for the analysis. Currently, the NIST 610 and 612 glasses are used for calibration standards, but it is likely that emerald standards are necessary to obtain accurate data for trace elements. Beryl has a wide stability field; the lower limit in the presence of water is between 200 °C and 350 °C, depending on the pressure and coexisting minerals [53]. However, the high-temperature stability and melting relationships remain unclear, partly because beryl may contain significant amounts of  $\text{H}_2\text{O}$  at the channel sites, and water has a significant effect on stability [52]. The effect of other channel constituents, such as Na, may be similar. Although thermodynamic data exist for beryl, the lack of experimental data for anything more complex than the BASH ( $\text{BeO}-\text{Al}_2\text{O}_3-\text{SiO}_2-\text{H}_2\text{O}$ ) system can be a barrier to understanding the formation of natural occurrences, such as those where Be-bearing minerals occur in metamorphic rocks [52].



(a)

Figure 8. Cont.

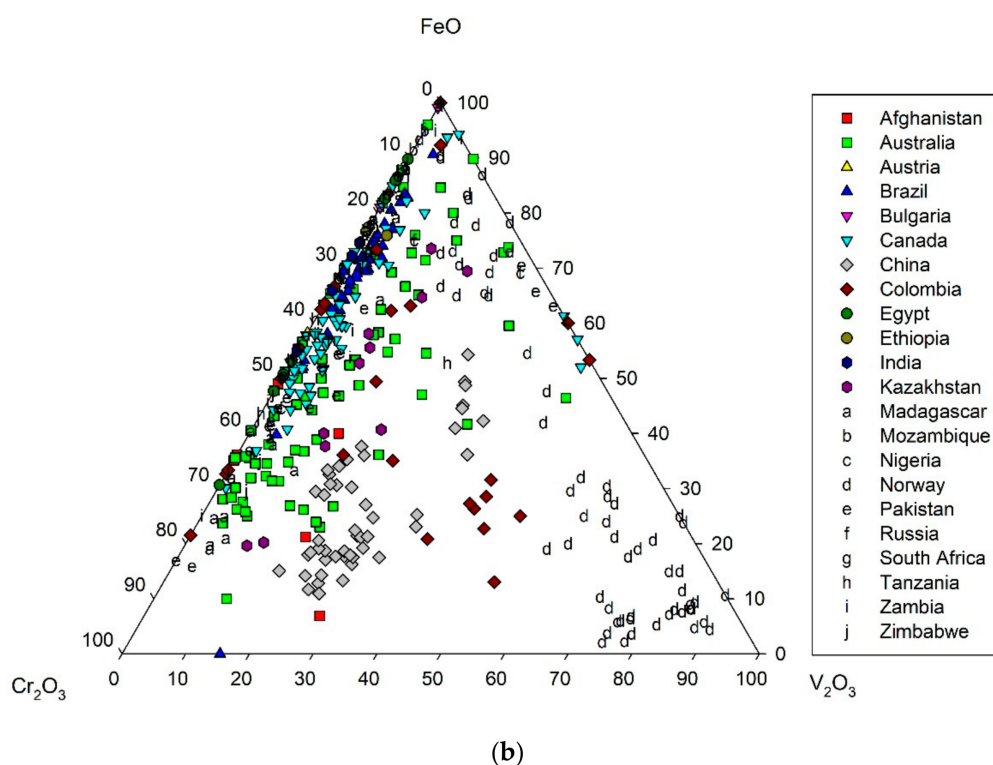


**Figure 8.** (a) Plot of emerald compositions in terms of FeO-MgO-Cr<sub>2</sub>O<sub>3</sub> (wt.%). Data from the literature (with all Fe as FeO). Sources of data are the same as in Figure 6. The diagram is after [39]. (b) Plot of emerald compositions in terms of FeO-Cr<sub>2</sub>O<sub>3</sub>-V<sub>2</sub>O<sub>3</sub> (wt.%). Data from the literature (with all Fe as FeO). Sources of data are the same as in Figure 6. The diagram is after [39].

#### 4. Sources of Be, Cr, and V: The Formation of Emerald

The sources of Be, Cr, and V of emerald. The Cr-V-bearing beryl is rare because (i) its constituent metals have opposite affinities and behavior in the continental and oceanic lithospheres, and (ii) there is only 2 ppm of Be in the upper continental crust. Beryllium is a lithophile element, which has a strong affinity for oxygen producing beryl and chrysoberyl (BeAlO<sub>4</sub>) at higher temperatures and at medium to low temperatures joins with silica to form silicate minerals, such as beryl, bertrandite [Be<sub>4</sub>Si<sub>2</sub>O<sub>7</sub>(OH)<sub>2</sub>], and/or Be-bearing micas. These minerals have a relatively low-density ( $\rho_{\text{beryl}} = 2.76$ ) and are concentrated in the crust ( $\rho_{\text{crust}} = 2.7$ ). Chromium and V are high-density transition metals that generally concentrate in the core and the mantle of the earth. Although Cr and V show both lithophile and siderophile affinities, they tend to form solid solutions with iron (Fe) to form, e.g., chromite (FeCr<sub>2</sub>O<sub>4</sub>) at high temperatures. Progressive changes in tectonic processes since the Archean preserved metamorphosed mafic-ultramafic rocks (M-UMR) and ancient mantle-related terranes in the upper continental crust. Consequently, Cr and V are more common than Be in the upper continental crust, with concentrations of ~100 ppm each.

Beryllium is present in crustal granites and associated dyke swarms of pegmatites, aplites, and quartz veins. The felsic rocks (FELSR), with more than 70% silica (SiO<sub>2</sub>), are intrusive into the continental lithosphere. The highest Be concentration occurs in granites and rhyolites (~5 ppm). The two-mica granites have concentrations between 5 and 10 ppm, while specialized granites have more than 200 ppm. Beryllium is carried by Be-minerals, but also by feldspar and micas. Chromium and V are more highly concentrated in M-UMR of the oceanic lithosphere that contain less than 50% SiO<sub>2</sub> (Figure 9a). These rocks, which are generally termed peridotites, are often metamorphosed into serpentinites containing up to 14 wt.% H<sub>2</sub>O (Figure 9a,b), or into talc-chlorite-carbonate schists. Chromium is dominantly sourced from chromite and V is sourced from V-bearing magnetite or coulsonite (Fe<sup>2+</sup>V<sup>3+</sup><sub>2</sub>O<sub>4</sub>). Nevertheless, Cr-V and Be can be present in sedimentary rocks and are highly

concentrated in shale (Figure 9c). Indeed, the weathering and erosion of M-UMR and FELSR on the continents delivers to the sea fine-grained clastic sediments composed of mud with Cr-V-Be-bearing grains and organic matter, as well as tiny fragments of quartz and calcite.

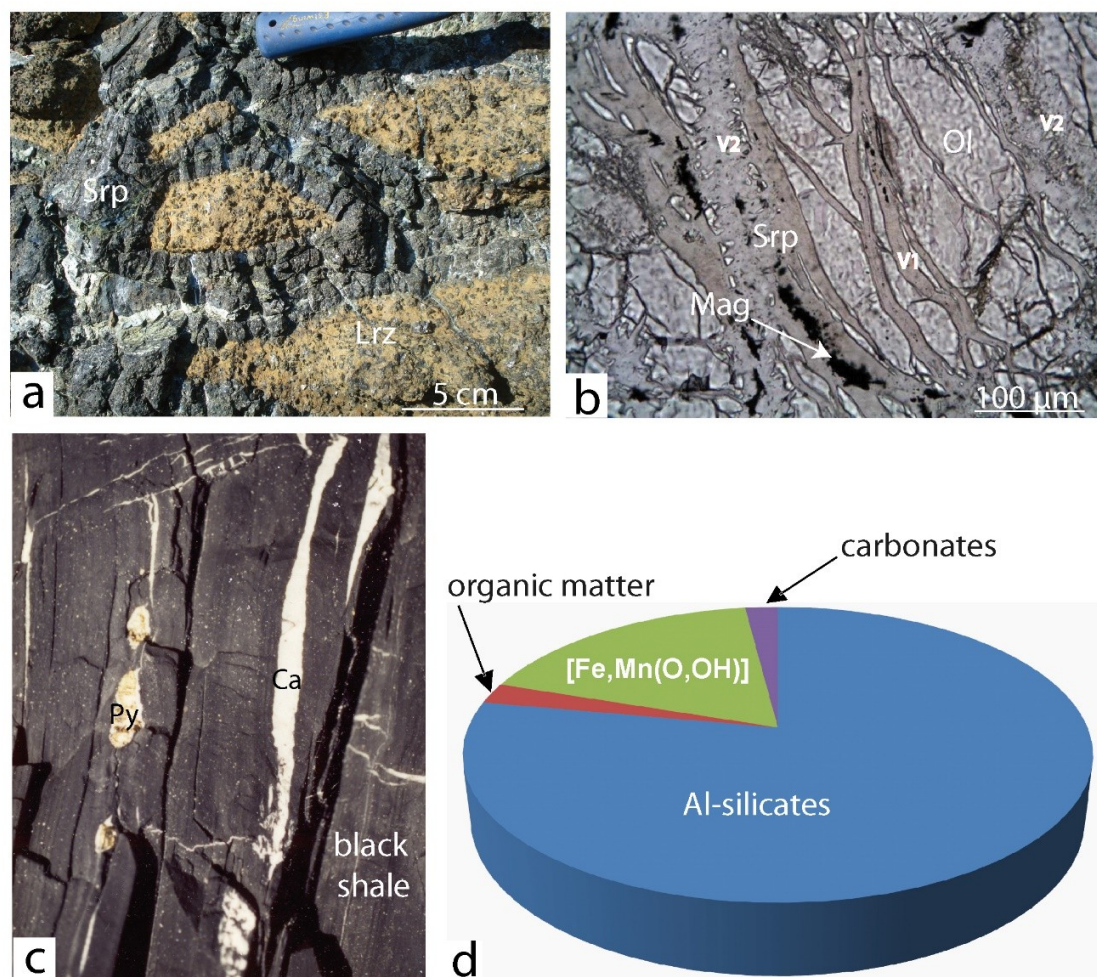


**Figure 9.** Potential geological sources of chromium (Cr) and vanadium (V) necessary for emerald formation in mafic-ultramafic rocks and black shales: (a) A lherzolite (Lrz) that is transformed into serpentinite (Srp), region of Montemaggiore on the Corsican cape, France; (b) Photomicrograph (plane polarized light) of an antigorite vein (V2) cross cutting lizardite veins (V1) and olivine (Ol). Fine-grained magnetite (Mag) is present in the centre of V1; V2 boundaries contain minute secondary olivine grains. Photo: B. Debret; (c) Colombian black shale crosscut by pyrite (Py) -bearing calcite (Ca) veinlets from the Coscuez mine. Photograph: G. Giuliani; (d) Pie diagram representation of the concentration (in %) and relative distribution of beryllium (Be) between the different phases extracted from a black shale containing 4 ppm of  $^9\text{Be}$ , Coscuez mine [54]. OM: Organic matter;  $[\text{Fe,Mn}(\text{O,OH})]$  = oxy-hydroxides of iron and manganese.

In anoxic and reducing environments, the un-oxidized organic matter imparts a dark colour to the black shale (BS). The Be contents of BS for Colombian deposits vary between 2 and 6 ppm, while Cr-V concentrations range between 100 and 1000 ppm. At the Coscuez emerald deposit (Figure 9d), the Be content of the BS is around 5 ppm. Beryllium mobility is principally associated with the breakdown of iron-manganese oxy-hydroxide phases. The amount of Be that can be mobilized ( $\sim 0.7$  ppm) may represent up to 18 wt.% of the total Be contained in the BS [54].

Emerald formation requires Be and Cr-V inter-reservoir circulation of fluids to mobilize these elements. Metasomatism and fluid/rock interaction is the main mechanism for element mobilization

in sedimentary (black shales) or granitic rocks for Be and metamorphosed-mafic-ultramafic rocks for Cr and V. These mineralizing fluids are trapped by emerald within the large channels parallel to the *c* axis (molecular components) or in fluid inclusions (several constituents in different systems, i.e., H<sub>2</sub>O-NaCl-CO<sub>2</sub>-(±H<sub>2</sub>S)-(±N<sub>2</sub>)-(±CH<sub>4</sub>)-(K, Mg, Be, F, B, Li, SO<sub>4</sub>, P, Cs)) within primary growth planes and secondary trails of fractures. Fluid inclusions are important fingerprints for emerald, and microthermometry, Raman spectrometry, and mass spectrometry for O-H isotope signatures make it possible to determine the nature and origin of the fluids [16,55].

## 5. Classification of Emerald Deposits

### 5.1. Genetic Classifications

The genetic classification schemes developed for emerald deposits in the 21st century were reviewed by [1]. The classification schemes are ambiguous and not particularly useful when it comes to understanding the mechanisms and conditions that led to the formation of an emerald deposit [52]. There is no ideal combination of mineralogical, chemical, geochemical, and physical parameters or combinations of these data with the age of the formation of the deposits and O-isotope composition of emerald [56].

Dereppe et al. [57] used artificial neural networks (ANN) to classify emerald deposits based on 450 electron microprobe analyses of emeralds from around the world. They defined five categories of deposits with “bad scores”. These important misclassifications affected essentially the shear zone and thrust-related deposits in mafic-ultramafic rocks and oceanic suture rocks, such as in Santa Terezinha de Goiás, Brazil, and either Panjsher valley (Afghanistan) or Swat valley (Pakistan).

Schwarz and Giuliani [58,59] recognized two main types of emerald deposit: Those related to granitic intrusions (type I) and those where mineralization is mainly controlled by tectonic structures, such as a fault or a shear zone (type II). Most emerald deposits fall into the first category and are subdivided based on the presence or absence of biotite schist at the contact. Type II deposits are subdivided into schist without pegmatite and black shale with veins and breccia. However, a number of emerald deposits of type I have been influenced by syntectonic events (e.g., Carnaíba, Brazil; Poona, Australia; Sandawana, Zimbabwe) or remain unclassified, such as the Gravelotte (Leydsdorp) deposit in South Africa [58].

Schwarz et al. [60] classified emerald deposits based upon their appearance in the field following several sketched geological profiles drawn by G. Grundmann: (i) Pegmatites without phlogopite schist; (ii) pegmatite and greisen with phlogopite schist; (iii) schist without pegmatite with (iiia) phlogopite schists, (iiib) carbonate-talc schist and quartz lens, (iiic) phlogopite schist and carbonate-talc schist; and (iv) black shale with breccia and veins.

Barton and Young [53] divided emerald deposits into those with a direct igneous connection and those where such a connection was indirect or absent. Further subdivisions were done based on the chemistry of the magma and/or the nature of the emerald-bearing metasomatic rocks (greisen and vein-like, skarn type, biotite schist, and vein-related). However, a number of emerald deposits cannot be unambiguously classified using this scheme (Kaduna in Nigeria, Swat valley in Pakistan and Eastern desert deposits in Egypt).

Schwarz and Klemm [61] used LA-ICP-MS to obtain approximately 2600 spot analyses of 40 major and trace elements from ca. 650 emerald samples from 21 different occurrences worldwide. The classification of the deposits was “non-genetic descriptive”, but was used instead as a geographic fingerprint. Nowadays, the gemological laboratories routinely use LA-ICP-MS for deciphering the geographic origin of individual stones [12,62–65], which is important for provenance and international trade certification. New standards and protocols for emerald analysis are being applied in gem testing laboratories for geographic and geological applications [66].

Aurisicchio et al. [23] obtained major and trace element data for emerald from several world deposits and reported important modifications regarding the origin of Be in some type II deposits (in

the classification proposed by Schwarz and Giuliani [58], i.e., type I granitic intrusions- and type II tectonic-related emerald deposits).

### 5.2. A Revised Classification for Emerald Deposits

We start by asking why a reclassification is desirable. Emerald deposits are relatively rare and form in a limited number of geological settings. Existing classification systems or models used to describe emerald formation are too restrictive and attempts at reclassification have proved inadequate to date.

Emerald is a medium to high temperature by-product of the Earth system and is hosted by diverse rock types of different ages. The first task of a field geologist is to identify the emerald-bearing rocks and to define the geological environment as magmatic, sedimentary, or metamorphic. Then, each emerald occurrence worldwide is linked to a major geological and tectonic regime related to the movement of lithospheric plates. Regional stresses in the lithosphere generate deformation subsystems with characteristic geometry, chemistry, and geology. The systems are either (i) closed (diabatic) systems with an exchange of heat with the surrounding rock and with very limited or absent fluid-rock interaction, or (ii) open systems with the migration of material and fluids along shear-zones and faults, resulting in the mobilization and re-precipitation of elements and tectonic melange zones. The tectonic systems are then characterized as compressive or extensional sub-systems with variable amounts of vertical and strike-slip movement encompassing large areas within orogens. Consequently, a more inclusive classification system for emerald deposits should consider tectonic, magmatic, and metamorphic-related types, geological environment, magmatic/metamorphic/sedimentary host rocks, and metasomatic conditions.

So, what would an enhanced classification look like? Giuliani et al. [55] classified emerald deposits into three broad types based on worldwide production in 2005 (see Figure 3): (i) The magmatic-metasomatic type (Ma) accounting for about 65% of the production; and (ii) the sedimentary-metasomatic (Se) and metamorphic metasomatic (Me) types, for 28% and 7%, respectively.

Marshall et al. [16] proposed an enhanced classification for emerald deposits based on the Me, Ma, and Se models, but also including the temperature of formation. They examined the possibility, at deeper crustal levels and high grade metamorphism, of the possible remobilization of previous beryl or emerald occurrences and partial melting of metamorphic rocks blurring the distinction between Me and Ma types.

In this work, we propose classifying emerald occurrences into two main types (Table 2):

(Type I) Tectonic magmatic-related with sub-types hosted in:

- (IA) Mafic-ultramafic rocks (Brazil, Zambia, Russia, and others);
- (IB) Sedimentary rocks (China, Canada, Norway, Kazakhstan Australia);
- (IC) Granitic rocks (Nigeria).

(Type II) Tectonic metamorphic-related with sub-types hosted in:

- (IIA) M-UMR (Brazil, Austria);
- (IIB) Sedimentary rocks-black shale (Colombia, Canada, USA);
- (IIC) Metamorphic rocks (China, Afghanistan, USA);
- (IID) Metamorphosed type I deposits or hidden-granitic intrusion-related (Austria, Egypt, Australia, Pakistan), and some unclassified deposits.

## 6. Different Types of Emerald Deposits

We will now examine the main emerald deposits worldwide using the above classification.

**Table 2.** New typological classification of the emerald occurrences and deposits worldwide.

Type of Deposit	Tectonic-Metamorphic-Related					Tectonic-Magmatic-Related		
Geological Environment	SEDIMENTARY		Metamorphic			Granitic		
Metamorphic Conditions	Anchizone to Greenschist facies		Greenschist to granulite facies			Greenschist to granulite facies		
Host-rocks	<i>Sedimentary Rocks</i>		<i>Metamorphic rocks</i>			<i>Mafic-UltraMafic Rocks (M-UMR)</i>	<i>Sedimentary Rocks (SR)</i>	<i>Granitoids</i>
Type	<b>TYPE IIB</b> carbonate platform sediments	<b>TYPE IIC</b> Metamorphism of SR	Migmatites	<b>TYPE IIA</b> Metamorphism of M-UMR	<b>TYPE IID</b> Metamorphosed Type IA, Mixed IA and IIA in M-UMR, and unknown	<b>TYPE IA</b> pegmatite- aplite- quartz- greisen veins, pods, metasomatites	<b>TYPE IB</b>	<b>TYPE IC</b>
Mineralization Style	veins and/or metasomatites	veins	veins	shear zone	shear zone, metasomatites, veins, boudins, fault	veins and/or metasomatites, skarns		pods
Origin of the Fluid	Metasomatic-hydrothermal	Metasomatic-hydrothermal	Hydrothermal	Metamorphic-metasomatic	(Magmatic- Metasomatic) with a metamorphic remobilization	Metasomatic-hydrothermal		
<b>Deposits</b>	Colombia (Eastern and western emerald zones)	China (Davdar)		Austria (Habachtal)	Austria (Habachtal)?: Probably metamorphic remobilization of type IA deposit	Brazil (Carnaíba, Socotó, Itabira, Fazenda Bonfim, Pirenópolis, etc.)	Norway (Eidsvoll)	
	Canada (Mountain River)			Brazil (Itaberaí, Santa Terezinha de Goiás)			China (Dyakou)	
			USA (Heddenite)	Pakistan (Swat-Mingora-Gujar-Kili, Barang)	Brazil (Santa Terezinha de Goiás)?: Probably related to hidden granitic intrusive cut by thrust and emerald-bearing shear-zone	Canada (Tsa da Gliza, Taylor 2)	Canada (Lened)	
		Afghanistan (Panjsher)			Pakistan (Swat-Mingora)? Probably related to undeformed hidden $\gamma$ intrusives	Bulgaria (Rila)	Australia (Emmaville, Torrington)	Nigeria (Kaduna)
	USA (Uinta?): question about the presence of emerald)				Australia (Poona): Probably metamorphic remobilization of Tye IA deposit	Urals (Malysheva, etc.)		
					Egypt (Djebel Sikait, Zabara, Umm Kabu): Probably metamorphic remobilization of Type IA deposit	Pakistan (Khaltaro)		
					Zambia (Musakashi): Unknown genesis, vein style, fluid inclusion indicates affinities with Types IIB and IIC	Afghanistan (Tawak)		
						India (Rajasthan, Gubaranda)		
						South Africa (Gravelotte)		
						Zambia (Kafubu, etc.)	Kazakstan (Delgebetey)	
						Tanzania (Manyara, Sumbawanga)		
						Mozambique (Rio Maria, etc.)		
						Australia (Menzies, Wodgina, etc.)		
						Ethiopia (Kenticha)		
						Madagascar (Ilanpera, Mananjary)		
						Zimbabwe (Sandawana, Masvingo, Filibusi)		
						Somalia (Boorama)		
						Ukraine (Wolodarsk)		



6.1. Tectonic Magmatic-Related (Type I)

Type I deposits are found in all five continents (Figure 2). The main geological environment is characterized by the presence of aluminous to peraluminous granitoids formed in continental collision domains. The collision increases the continental lithosphere thickness, resulting in increased pressure and temperature, and producing a zone of higher grade of metamorphism and partial melting of rocks, forming felsic magmas. These continental collisions have occurred at different geological times throughout the Wilson cycles of the supercontinents, with the formation of emerald deposits (Figure 10; [67]) during the following orogenies: Eburnean or Transamazonian (2.0 Ga (giga-annum)), Pan-African/Brasiliano (490–520 Ma (mega-annum)), Hercynian (300 Ma), Uralian (299–251 Ma), Yenshan (125–110 Ma), and Himalayan (25–9 Ma). In contrast, the emerald deposit at Kaduna in Nigeria is associated with Mesozoic (213–141 Ma) ring complexes with peralkaline granites formed in a volcanic to subvolcanic continental environment [68]. In the case of the Byrud mine in Norway, the emerald is related to Permo-Triassic intrusions associated with the evolution of the Oslo Paleorift. This rift was characterized by a succession of volcanic rocks and the emplacement of batholiths and the intrusion of syenitic dykes and sills [69].

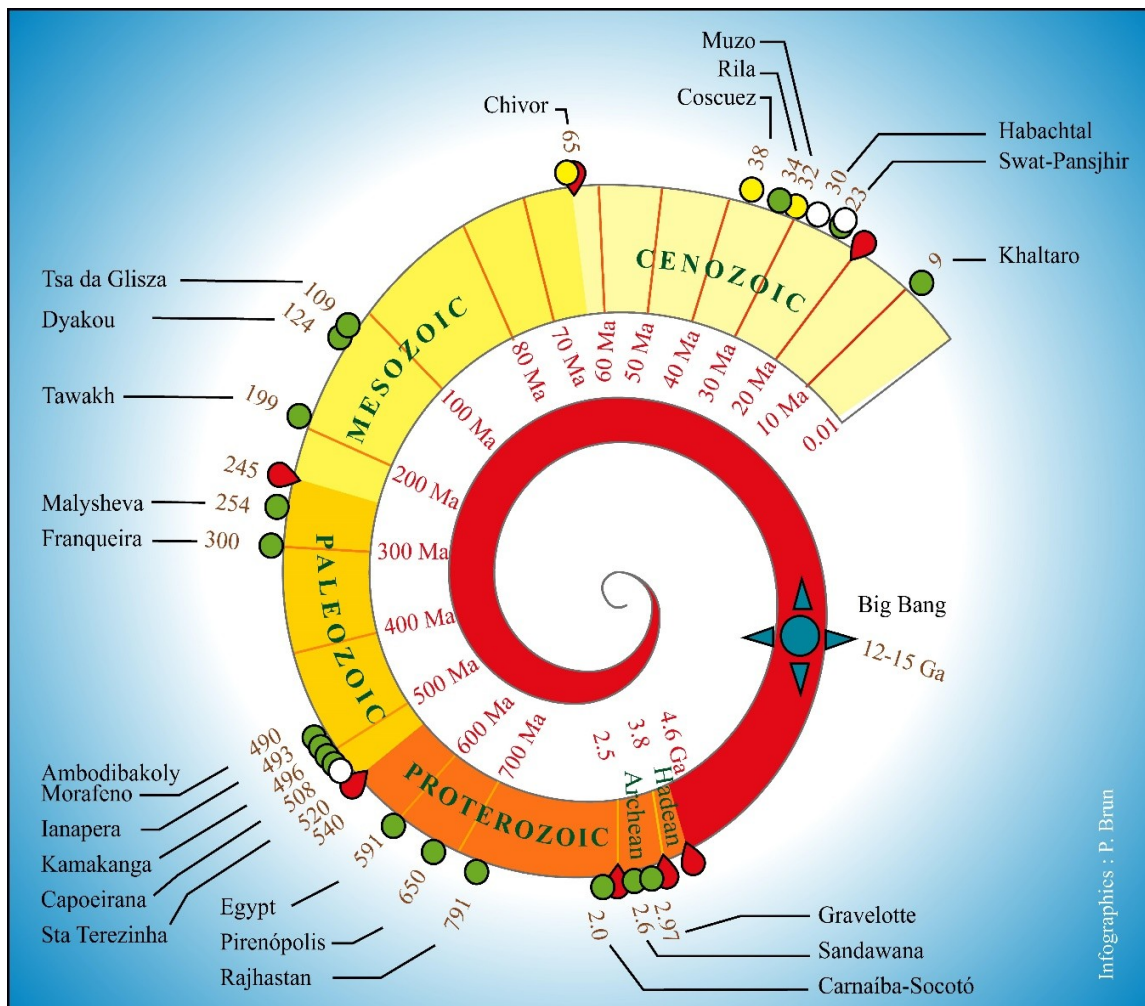


**Figure 10.** The spiral time of emerald. The oldest emerald formed during Archean times (2.97 Ga) in South Africa (Gravelotte deposit) and the youngest during Cenozoic times (9 Ma) in Pakistan (Kaltharo deposit). Nomenclature of the circles: Red = limit of geological era, green circle = emerald deposits related to the Tectonic magmatic-related types (types IA, IB, and IC); yellow and white circles = Tectonic metamorphic-related types (types IIA, IIB, IIC, and IID) with deposits hosted either in mafic-ultramafic rocks (white circle) or in sedimentary rocks (yellow circle).

Infographics : P. Brun

Type I emerald deposits, in terms of quantity and gem quality, remain the world's most important emerald deposits. Three sub-types are distinguished according to the emerald host-rocks.

#### 6.1.1. Sub-Type IA: Tectonic Magmatic-Related Emerald Deposits Hosted in M-UMR (Brazil, Zambia, Russia, and Others; See Table 2 and Figure 2)

These deposits produce high volumes of emerald. Why?

There are numerous Be- and/or Be-Ta-Nb-Sn-W-bearing granites of different ages accompanied by subordinate amounts of M-UMR in the continental crust.

There are large volumes of metamorphosed M-UMR in the Precambrian series of the continental crust, such as the recently discovered southern Ethiopian emerald deposit (Halo-Shakiso) hosted in the Archean and Proterozoic volcano-sedimentary series. It is associated with pegmatites and quartz veins similar to the proximal Ta-Nb-Be-bearing pegmatites from the nearby Kenticha mine.

At the regional scale and in several emerald mining districts, there are extended and continuous zones of mineralization related to granites, pegmatites, and quartz veins, as in the Kafubu mining area in Zambia where the mining licences extend for approximately 15 km of the strike length [50,70]. The development of modern mining on a large scale, as done by the company, Gemfields Group Ltd., through underground and huge open-cast mining, allows for the production of large quantities of high-quality commercial-grade gems.

Another example is the mining district of Itabira-Nova Era in Minas Gerais, located in Quadrilátero Ferrífero, Brazil (Figure 11). In 1978, the future deposit of Itabira was discovered on a private property called the "Itabira farm" [71]. After three years of development, the mine was mechanized and named the Belmont mine [72]. In 1988, emeralds were discovered at Capoeirana near Nova Era, 10 km southeast of the Belmont mine [73]. In 1998, the deposit of Piteiras was officially discovered. The emerald deposit is located 15 km southeast of Itabira city, between the Belmont and Capoeirana mines. The mineralized zone extends for over 5 km and the mines are located on two thrust zones (Brasiliano orogenesis) juxtaposing ultramafic rocks and highly deformed granites called "Borrachudos". At the regional scale, an extended emerald mining district was defined based on the geological continuity of the thrusts [74]; this district accounts for the majority of the Brazilian production.

In this type of deposit, granitic magmas have intruded M-UMR within volcano-sedimentary sequences or greenstone belts (Figure 12) and fluids expelled from the granite circulated within the thermal aureole, sometimes mixing with metamorphic fluids, and reacted with the pegmatite or quartz veins and M-UMR, forming emerald. The deposits are associated with vast amounts of fluid-rock interactions producing intense K-Na-Mg metasomatism of M-UMR and granite. This genetic pathway is the most common ([1,16,22,75,76]) and is characterized by emeralds contained in magnesium-rich micaceous rocks known as phlogopite schists or phlogopitites, or "glimmerite" in the Russian literature, "black wall zones" in [77], or "sludite" in Brazil. Generally, the pegmatite and the M-UMR experienced intense fluid infiltration and metasomatism where: (i) The M-UMR is converted into the emerald-bearing micaceous-host rock; (ii) the granitic rock itself is transformed into a feldspar-rich rock called plagioclase comprised of albite-andesine feldspar. Quartz is dissolved and the pegmatite becomes a desilicated pegmatite (Figure 13). The metasomatic processes are highly variable and dependent upon P-T conditions, the extent of fluid circulation, and the timing between granitic intrusions and regional deformation.

At Carnaíba, the vein-like metasomatic rocks, in which phlogopite is by far the most abundant mineral, have a longitudinal extension that may extend several hundreds of meters, whereas their thickness does not exceed a few metres. They display a clear zoning and are organized, in many places in the M-UMR, symmetrically around intrusive aplite-pegmatite dikelets, which channel the fluids [78].

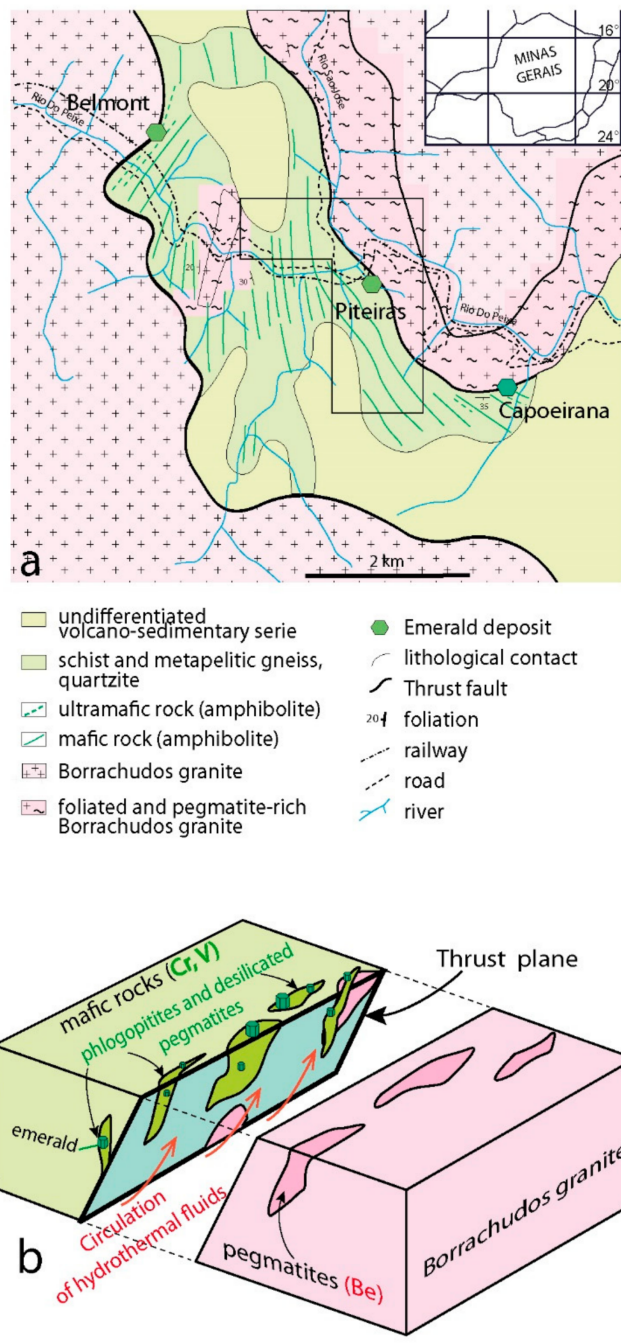


**Figure 11.** The emerald mining district of Itabira-Nova Era in Minas Gerais, Brazil, with the mines of Belmont, Piteiras, and Capoeirana: (a) Geological map of the extended regional mining district. The mining concession of Piteiras is bounded by the polygon area plotted in the figure. Three deposits are currently mined. All occur in the same geological context. Ultramafic bodies (chromium—Cr, vanadium—V, and magnesium-rich-bearing rocks) are in contact with the deformed granites of Borrachudos (beryllium—Be, aluminium-silica-rich pegmatites), modified after [73]; (b) schematic diagram representing the probable formation of the Piteiras-Capoeirana-Belmont emerald deposits. During the Brasiliano orogenesis (508 Ma), the hydrothermal fluid (red arrows) circulated along the thrust planes, altering granites and associated Be-bearing pegmatites and Cr-V-bearing mafic-ultramafics. The hydrothermal fluids interacted with both rocks and were enriched in all the elements necessary for emerald crystallization. Emerald crystallized in plagioclase (desilicated pegmatite) and phlogopite.

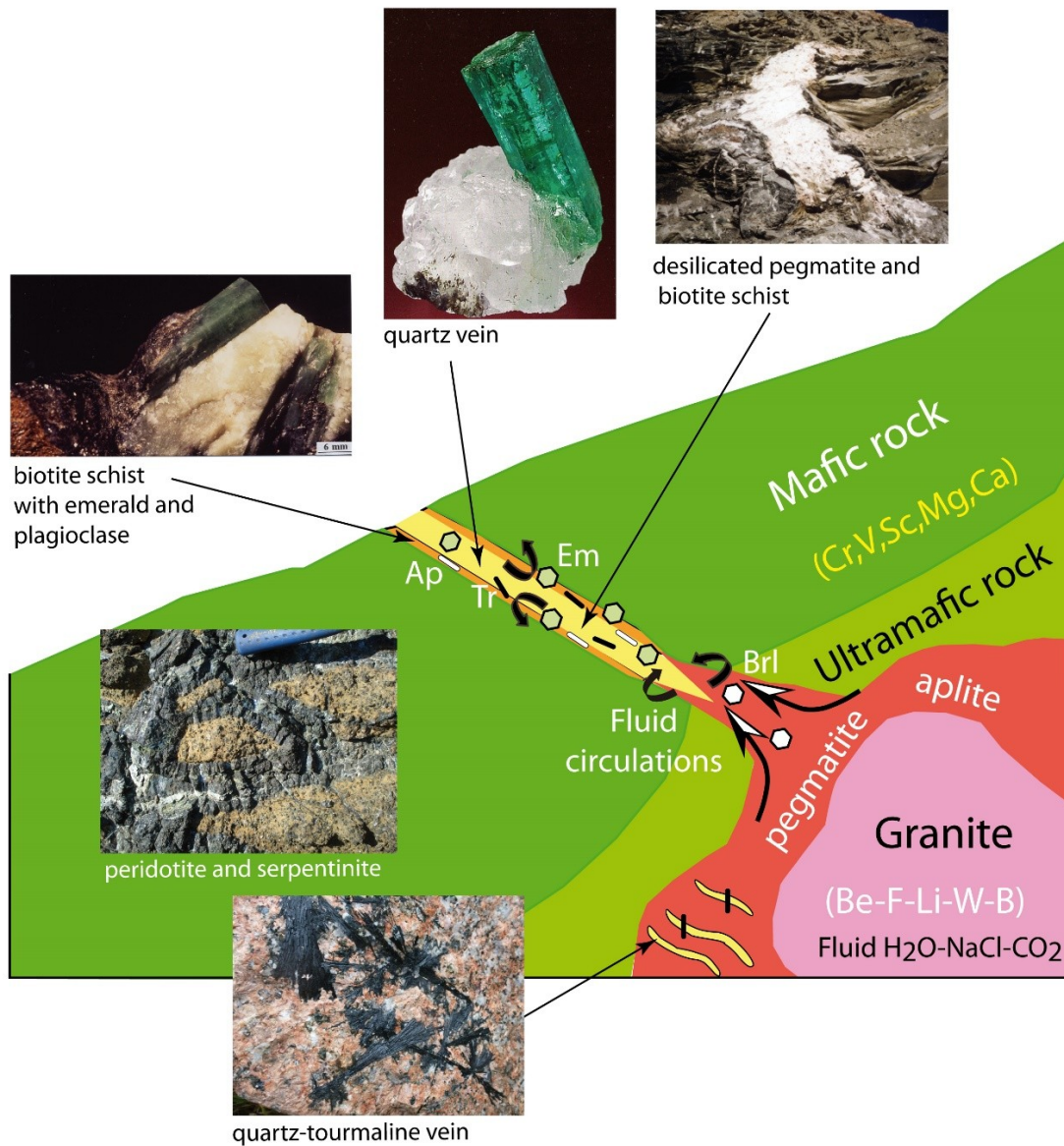


**Figure 12.** Idealized model for the Tectonic magmatic-related emerald type. The model is based on the emplacement in the crust of a granitic massif, with its pegmatite and aplite dikes and their tourmaline- (Tr) or beryl- (Brl) bearing quartz veins, intruding mafic (metabasalt) and/or ultramafic rocks (metaperidotite, serpentinite). The fluid circulations from the granite into the surrounding rocks and granitic dykes (arrows), preferentially along the contacts between the pegmatite or aplite or quartz veins and the regional rocks, transform the mafic rocks into a magnesium-rich biotite schist and the pegmatite into an albite-rich plagioclase. Emerald (Em) and apatite (Ap) precipitates in the rocks affected by the fluid/rock interaction. It can precipitate in the pegmatite, aplite, plagioclase, and quartz veins and their adjacent phlogopite schist zones.

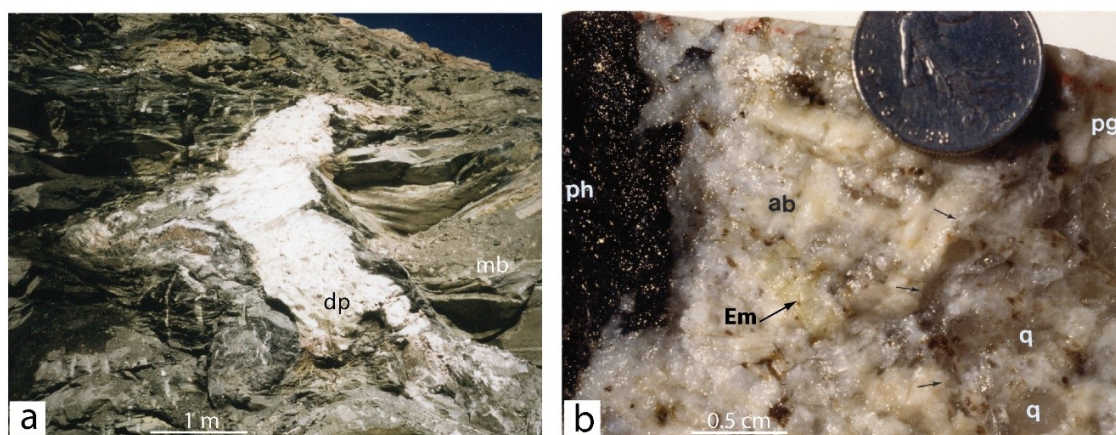


**Figure 13.** Desilicated emerald-bearing pegmatites: (a) Desilicated pegmatites crosscutting metabasites (mb) from the Kafubu mine (Zambia). Photograph: Dietmar Schwarz; (b) desilicated pegmatite from the Carnaíba mine, Brazil. At the contact of a pegmatite (pg) and a serpentinite, the metasomatic fluid dissolved quartz, mobilized Cr and V from the chromite-bearing serpentinite, and Be from the beryl-bearing pegmatite to form emerald (Em). The fluid transformed the serpentinite into a phlogopitite (ph) and the pegmatite in an albite-rich rock (ab). The three arrows indicate the limit of the dissolution of quartz (q) from the pegmatite. Photograph: Gaston Giuliani.

These metasomatic rocks, called exo-F-phlogopitites (1.3 to 4 wt.% F), formed a metasomatic column that consists of seven zones, from the central desilicated granitic vein (zone 7) to the enclosing serpentinite (Figure 14):

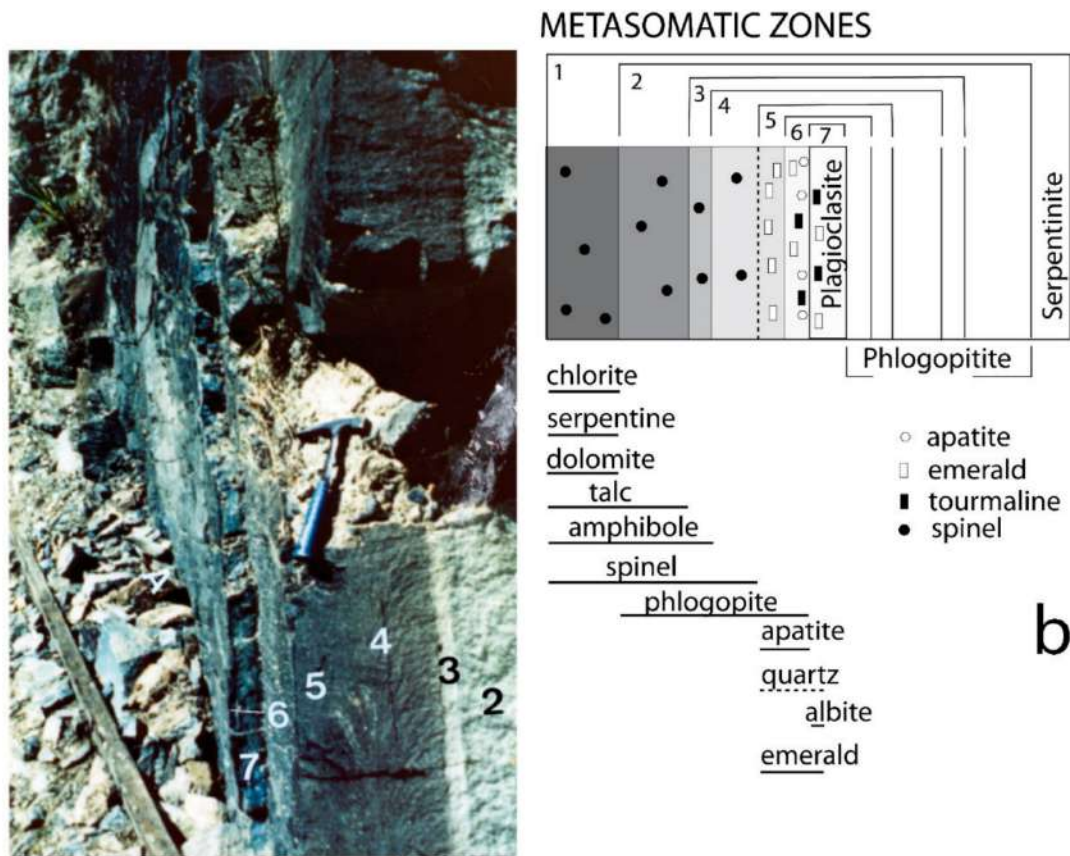
- Zone 6: Coarse-grained F-phlogopite + apatite + emerald + quartz;
- Zone 5: Fine-grained F-phlogopite + apatite + emerald;
- Zone 4: F-phlogopite + spinel (chromite + magnetite);
- Zone 3: F-phlogopite + spinel + amphibole (actinolite + tremolite);
- Zone 2: F-phlogopite + spinel + amphibole + talc; and
- Zone 1: spinel + amphibole (or dolomite) + talc + serpentine + chlorite.

From the inner to the outer zones, (i) phlogopite composition evolves with continuous or discontinuous decrease in the Al and Fe contents with an increase in the Si and Mg contents and K/Al ratio; (ii) amphibole evolves from actinolite to tremolite; and (iii) spinel from Al-chromite to Cr-magnetite.

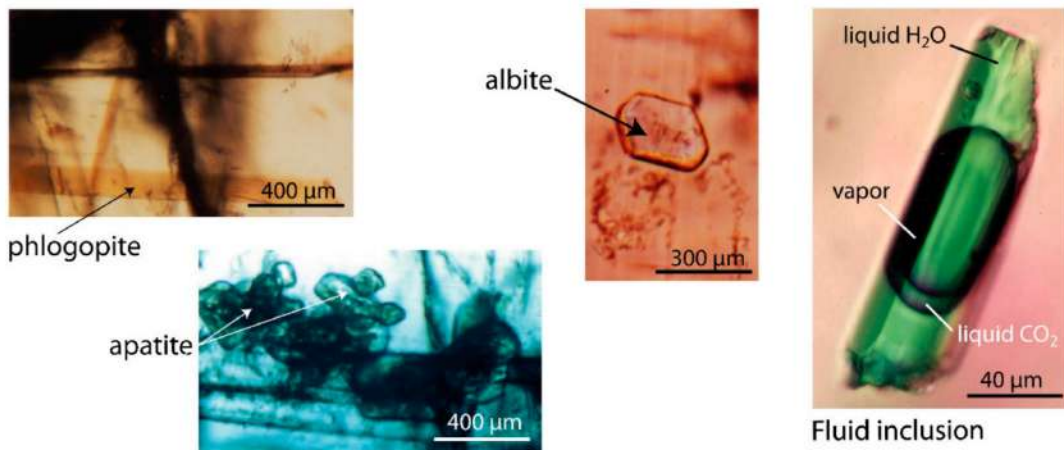
The aplopegmatite dikelets were transformed into plagioclases (with disseminated phlogopite and little hornblende) with irregular commonly centimeter-thick phlogopite rims, embayments, and veinlets called endo-phlogopitites by analogy with the endo-skarns [78].

The strong chemical gradients in the different zones of the metasomatic column are characterized by a change in the composition of phlogopite (Figure 15; [78,79]). From zone 6 to zone 2, the Al and Fe contents decrease while Si and Mg increase. This evolution is discontinuous and two abrupt changes are observed, one at the front of zones 6/5, where the evolution corresponds to an increase in Si and Mg and a decrease in the Al, Fe, and Na contents and the other within zone 4. Such pattern of evolution are coherent with infiltration metasomatism. The potassium content remains constant in zones 6 and 5, suddenly decreases within zone 4, and remains constant up to zone 2.

Over the whole column, the F content of phlogopite is in the range of 1.3 to 4 wt.% and the highest values are observed in the phlogopite of the outer zone that has the highest Mg/(Fe + Mg) ratios, in agreement with the so-called “Fe-F avoidance effect” [80].



**a** METASOMATIC ZONING AROUND A PEGMATITE VEIN



**C** INCLUSIONS IN EMERALD FROM ZONES 6 and 7

**Figure 14.** The metasomatism related to fluid circulation between aplopegmatite dikes and mafic-ultramafic rocks: (a) Metasomatic column formed by different mineralogical zones (zones 7 to 2) developed around a central pegmatite vein crosscutting serpentinites, Braúlia prospecting pit, Carnaíba; (b) vein-like metasomatic rocks and their mineralogical composition. The pegmatite is transformed into plagioclase (zone 7) and the metasomatic rocks consist of six zones, from the desilicated pegmatite to the enclosing serpentinite (zones 6 to 2). Emerald is found in the plagioclase and in zones 6 (coarse-grained phlogopite) and 5 (fine-grained phlogopite). Zone 1 is the protolith formed by the serpentinite (not seen on the photograph); (c) solids and fluid inclusion in emeralds from zones 7 and 6 (Photographs: Dietmar Schwarz and Gaston Giuliani).

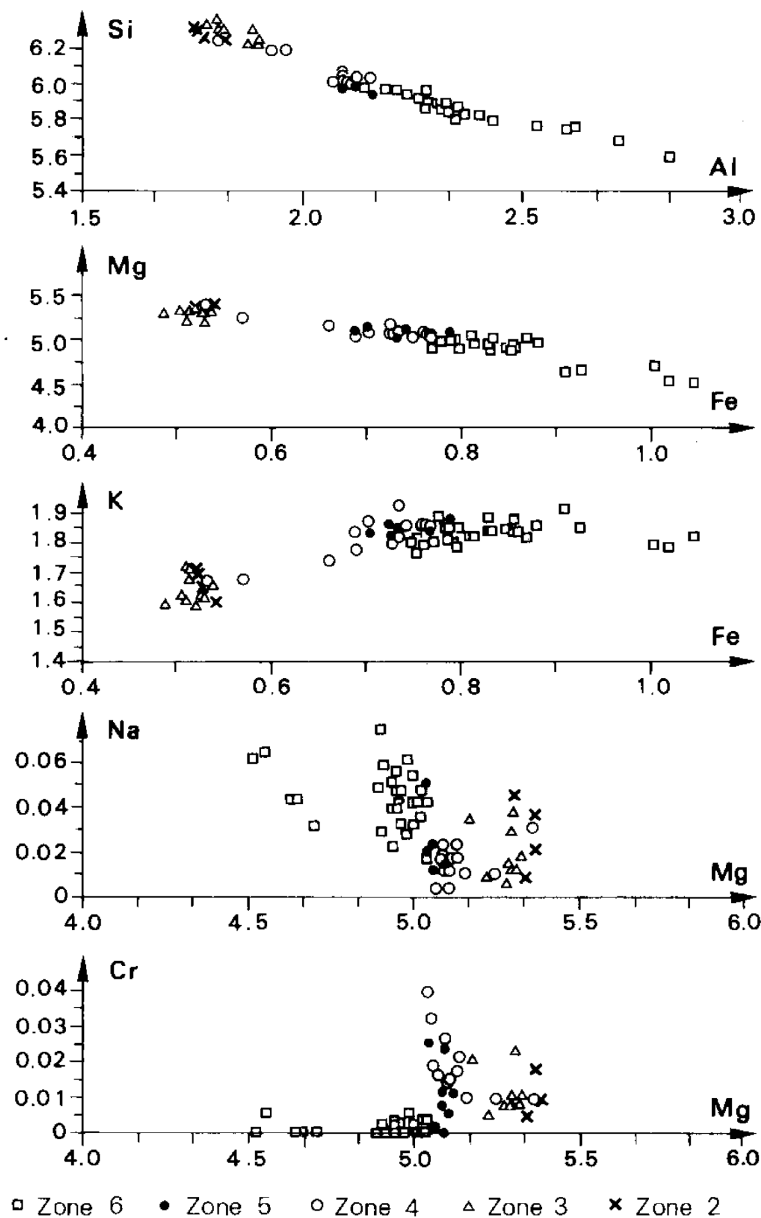


**Figure 15.** Evolution of the phlogopite composition in the phlogopitites of the different metamorphic zones (zones 6 to 2, see Figure 14 for the repartition of the different zones from the plagioclase to the serpentinite) at Braúlia prospecting pit, Carnaíba mine, Brazil. Composition calculated in atom per formula (electron microprobe data from [79]). From the inner to the outer zones, phlogopite composition evolves with a continuous or discontinuous decrease in the Al and Fe contents and an increase of the Si and Mg contents and K/Al ratio, corresponding to changes in the petrographic habitus of the phlogopite.

Chromium contents are usually very low (<0.05 wt.%) in zones 6 and 5 and present a peak (up to 0.7 wt.%) at the front of zones 5/4, at the place where the first crystals of chromite are observed. In the outer zones 4 to 2, the Cr contents of phlogopite are nearly constant (0.25 wt.%). Chromium dispersed in the original rock can be concentrated at the front advancing outwards, like a “sweep effect” [81]. The almost uniform Cr content of phlogopite in the outer zones, 4 to 2, may result from the establishment of an exchange equilibrium between mica and chromite, Cr behaving as an inert component.

Mass transfer calculations show that the infiltration metasomatism in serpentinites is accompanied by important transfers of material, concerning mainly Al, K, F, Si, Mg, Ca, and H<sub>2</sub>O (Figure 16). The strong enrichment in K, Rb, Li, Be, Nb, P, and F suggests that the metasomatic fluids have a magmatic origin, since some of these elements (including Rb, Nb, and Be) behave incompatibly during magmatic differentiation.

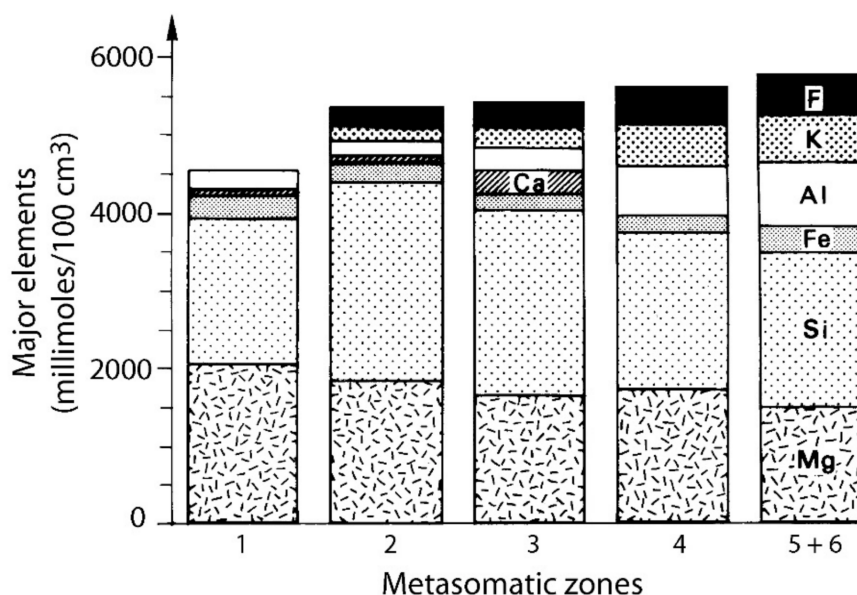


**Figure 16.** Mass balance calculations realized on the metasomatic column at Bode prospecting pit, Carnaíba mine, Bahia, Brazil (modified from [79]). Chemical mass balance was realized on major elements' molar composition (in millimoles/100 cm<sup>3</sup>) of the different metasomatic zones (1 to 5 + 6). It indicates the supply of many elements, such as K, Si, Al, and F, over the whole column, and Fe, in the inner most zones of 6 and 5, the leaching of Mg and Ca from the outer to the inner zones.

The association of phlogopitite–plagioclase corresponds to a “bimetasomatic system” in the sense given by [82]. The hydrothermal solutions that developed the potassic metasomatism in the serpentinites (phlogopitites) are alkaline, undersaturated with respect to microcline and quartz of the intrusive aplopegmatite, and albitizing.

The occurrence of emeralds is considered to be due to the efficiency of the metasomatic trap rather than a significant magmatic pre-enrichment in Be. The occurrence of strong chemical gradients in the zones of preferential circulation of the solutions (zones 6 and 5 of the exo-phlogopitites, plagioclases, and endo-phlogopitites) constitutes highly favorable conditions for the beryl formation.

Elevated temperature and alumina and silica activities are the main factors for emerald formation in the IA sub-type (Figure 17). At high temperatures ( $T > 600$  °C) and medium to high silica activity, beryl, phenakite (Be<sub>2</sub>SiO<sub>4</sub>), and chrysoberyl (BeAl<sub>2</sub>O<sub>4</sub>) are stable [53]. Emerald occurs in quartz veins, such as at the Kafubu deposits in Zambia [50,70], or greisens (an association of quartz and white micas), such as at the deposits of Delbegetey in Kazakhstan [51] and Khaltaro in Pakistan [83]. At lower silicate activities, albite is always stable and emerald is replaced by alexandrite (Cr-chrysoberyl) + phenakite. This is the case for emerald-bearing desilicated pegmatites in M-UMR, such as in Russia and Brazil. At higher Al<sub>2</sub>O<sub>3</sub> activities, corundum can crystallize, such as at the Poona emerald deposit in Australia [84].



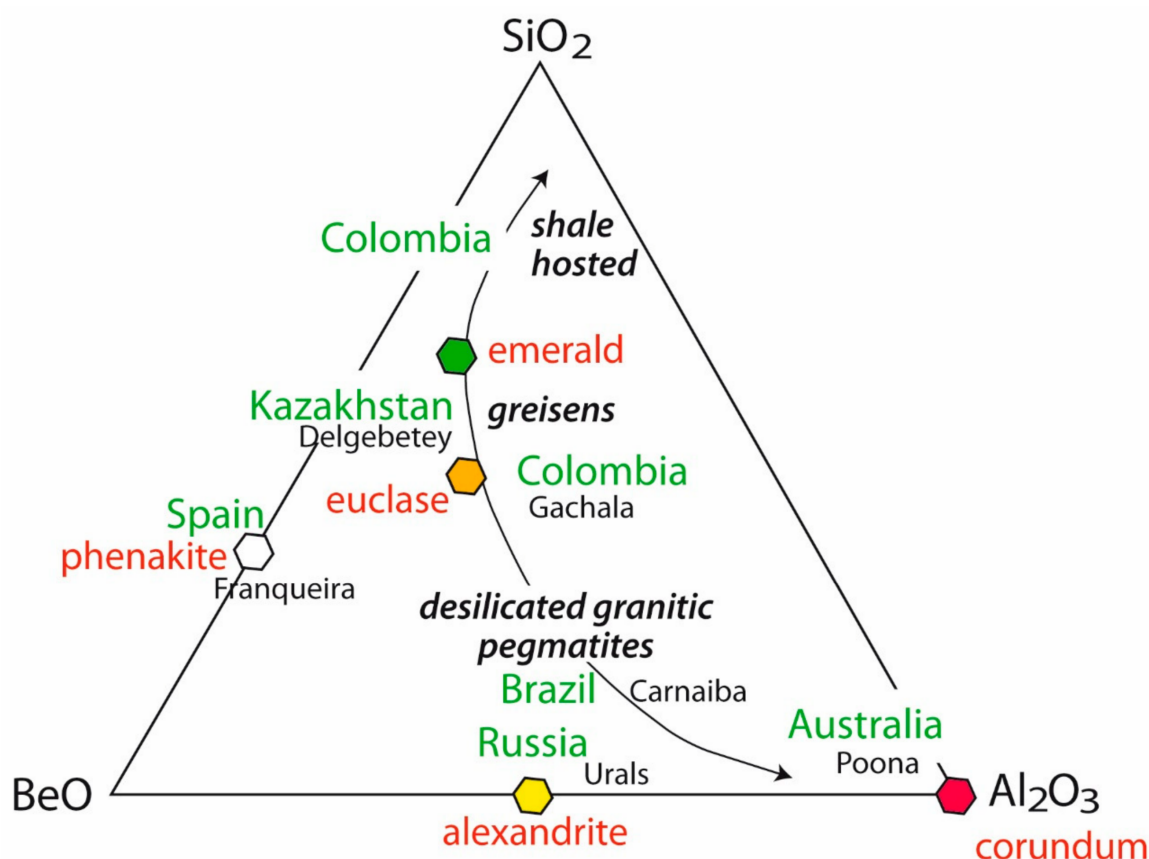


**Figure 17.** The ternary diagram of BeO-Al<sub>2</sub>O<sub>3</sub>-SiO<sub>2</sub> visualises the major types of emerald deposits as a function of their typical mineral assemblages, such as alexandrite, euclase, phenakite, and corundum ('BASH' system modified from [53]). Follow the discussion in the text.

The classic model of these granitic-metasomatic deposits presents much variability in terms of the geometry, chemical composition of the rocks, geological contacts, etc.:

1. At the Tsa da Gliza deposit in Canada, Be-bearing magmatic fluids from the neighboring granite reacted with the Cr- and V-bearing M-UMR [46]. Emeralds formed in aplite, pegmatite, and quartz veins surrounded by biotite schists. There is a continuum between the crystallization of granitic rocks, fluid rock-interaction, and emerald formation (Figure 18).
2. In the Kafubu area in Zambia (Figure 1c), emerald is found predominantly in metamorphosed M-UMR with phlogopite schist or in quartz-tourmaline veins adjacent to pegmatites.
3. At the Sandawana deposit in Zimbabwe, pegmatites intruded the M-UMR, but they are folded and fluid circulation in shear zones formed phlogopite schist. The fluid-rock interaction is coeval with the regional deformation [52]. Such phenomena are also found in the Carnaíba deposits in Brazil, where the dissolution of quartz from pegmatite is common [76].
4. At the Ianapera deposit in Madagascar, two coeval emerald deposits coexist (Figure 19; [11]): (1) A proximal one, formed at the contact between pegmatites and UMR; and (2) a distal one, hosted in biotite schist in fractures developed in mafic rocks with widespread fluid circulation affecting all the geological formations. Similarly, the Trecho Novo and Trecho Velho deposits at Carnaíba, Brazil [78] are also distal in nature.

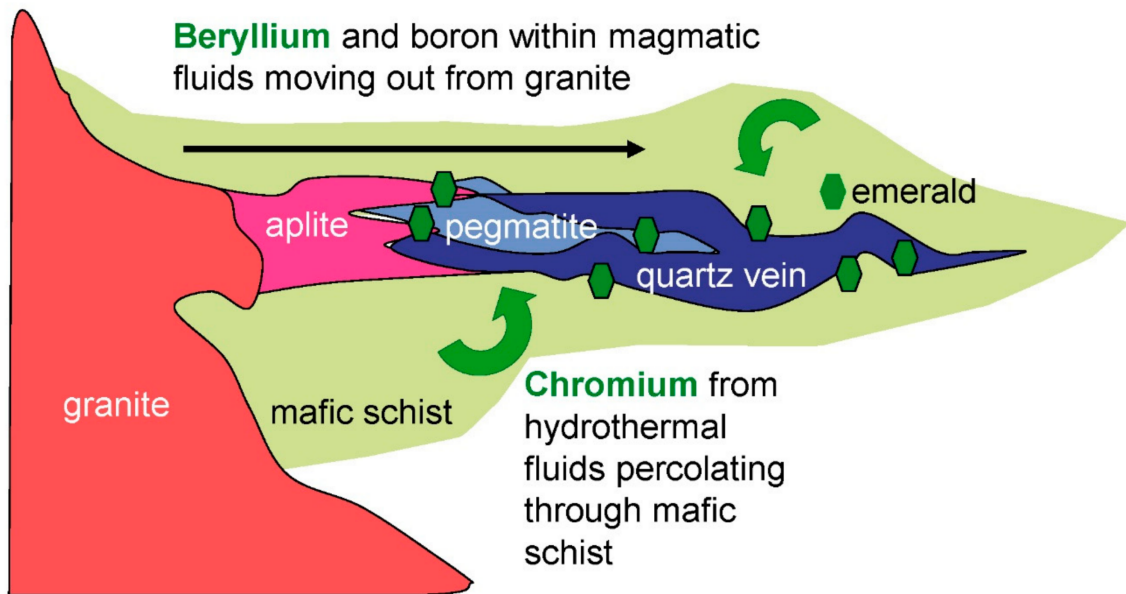


**Figure 18.** Genetic model proposed for the emerald mineralization at Tsa da Glisza, Yukon Territory, Canada.

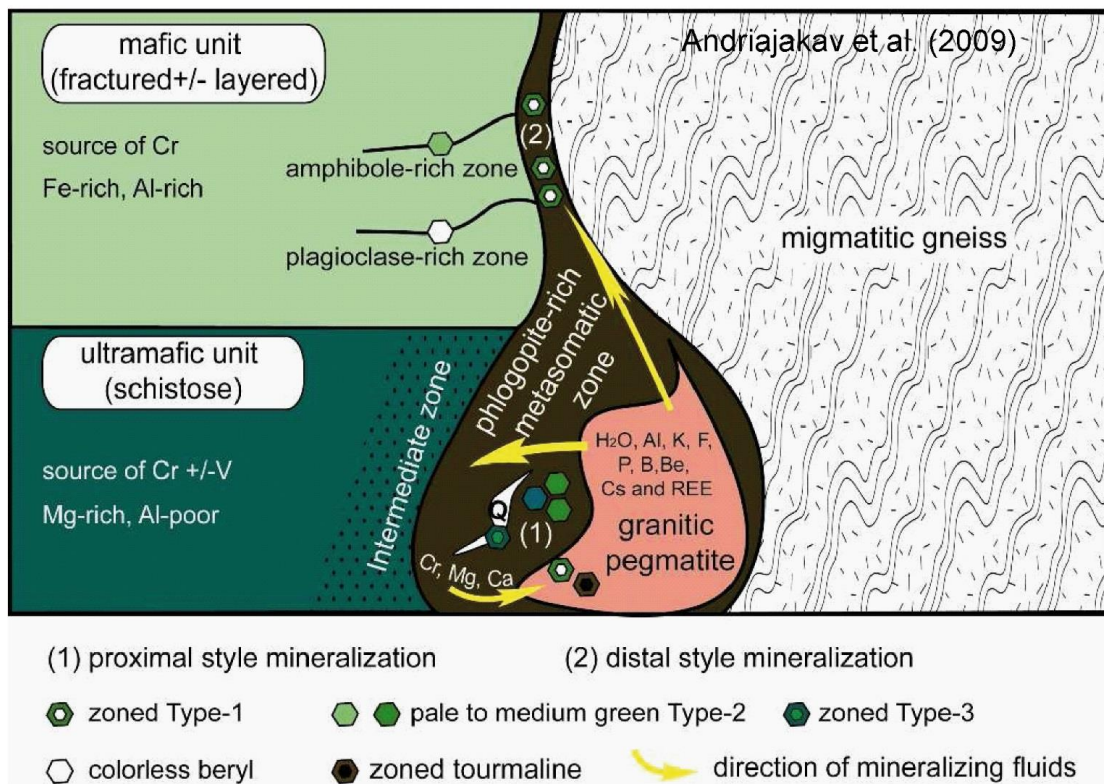


**Figure 19.** Schematic representation of the two styles of mineralization evidenced for the Ianapera emerald deposit, Madagascar: (1) Proximal mineralization occurs at the contact of pegmatite veins with ultramafic units. Emerald mineralization is hosted in metasomatic phlogopite and desilicated pegmatites or quartz-tourmaline veins, at the contact between migmatitic gneiss and garnet amphibolite; (2) distal style is formed by phlogopite veins crosscutting mafic rocks. In addition to phlogopite, these veins contain Mg-amphibole, apatite, and dolomite, and minor quartz, calcite, zircon, plagioclase, and chlorite.

### 6.1.2. Sub-Type IB: Tectonic Magmatic-Related Emerald Deposits Hosted in (Meta)-Sedimentary Rocks (China, Canada, Kazakhstan, Norway, Australia; See Table 2)

These emerald occurrences are associated with granites that intrude sedimentary or meta-sedimentary lithologies. These deposits are generally sub-economic and several variants are described, depending on the nature of the host-rocks and the mineralization styles.

1. At Dyakou (China), the Lower Cretaceous porphyritic granite intruded biotite granofels, quartzite, gneiss, and plagioclase amphibolite of Lower and Upper Neoproterozoic formations. The intrusion formed skarns and dyke swarms of quartz veins, which are crosscut by pegmatites [85]. Emerald in quartz veins is less abundant than in the pegmatites, but of higher quality (Figure 1b). Some pegmatites show a local zoning with an outer zone enriched in K-feldspar and an inner zone of emerald and quartz.
2. At the Lened V-rich emerald occurrence (Canada), Be and other incompatible elements (i.e., W, Sn, Li, B, and F) in the emerald, vein minerals, and surrounding skarn were derived during the terminal stages of crystallization of the proximal Lened pluton [21,47]. Decarbonation during pyroxene-garnet skarn formation in the host carbonate rocks probably caused local overpressuring and fracturing that allowed ingress of magma-derived fluids and formation of quartz-calcite-beryl-scheelite-tourmaline-pyrite veins. The vein fluid was largely igneous in origin, but the dominant emerald chromophore V was mobilized by metasomatism of V-rich sedimentary rocks (avg. 2000 ppm V) that underlie the emerald occurrence [21].
3. At Delbegetey (Kazakhstan), the emerald mineralization is confined to the granite that hornfelsed carboniferous sandstones. Emerald is found in muscovite greisen formed in the wall-rocks of muscovite-tourmaline-fluorite-bearing quartz veins [51].
4. At Eidswoll (Norway), the emerald Byrud Gård mine is related to Permo-Triassic alkaline intrusions. The V-bearing emerald occurs in Middle Triassic pegmatite veins that intruded Cambrian Alum shales and quartz syenite sills [20]. Vanadium and Cr were probably leached from the alum shales by the mineralizing fluids [13].
5. At Emmaville-Torrington (Australia), emerald is located in pegmatite, aplite, and quartz veins associated with the Mole granite. The granite intrudes a Permian metasedimentary sequence consisting of meta-siltstones, slates, and quartzites [19]. The emerald-bearing pegmatite veins contain quartz, topaz, K-feldspar, and mica. Emerald is embedded in cavities and surrounded by dickite in the quartz-topaz veins. In the quartz lodes, emerald is associated with Sn-W-F minerals. At the Heffernan's Wolfram mine, emerald occurs with wolframite in vugs in the pegmatites [86].

### 6.1.3. Sub-Type IC: Tectonic Magmatic-Related Emerald Deposits Hosted in Peralkaline Granites (Nigeria)

These emerald occurrences are located in the Jurassic younger granite ring complexes of the anorogenic magmatism of Nigeria [68]. These granites crystallized in a volcanic-subvolcanic environment. They are generally peralkaline with perthitic K-feldspar, sodic amphiboles, and alkaline pyroxene. The roof zone of the intrusions is characterized by disseminated tin, tungsten, niobium, tantalum, and zinc mineralization related to sodic or potassic metasomatism, sheeted quartz vein systems, pegmatite pods and veinlets, replacement bodies, and fissure-filling veins (Figure 20). The emerald mineralization is located in sporadic pegmatitic pods with quartz and feldspar, as well as topaz and gem quality aquamarine. The source of chromium for the emerald is debated, but it could be the consequence of the mode of emplacement of the granites, which involved mechanisms of underground cauldron subsidence. The caldera produced ignimbrite, rhyolite, and thin Cr-bearing basic flows, which collapsed during doming or swelling and intrusion of the younger granites. Assimilation of the previous basic volcanic rocks or local fluid interaction between the pegmatites and the basic flows could have enriched the metasomatic fluids in Cr and Fe, resulting in the formation of emerald-aquamarine beryls.

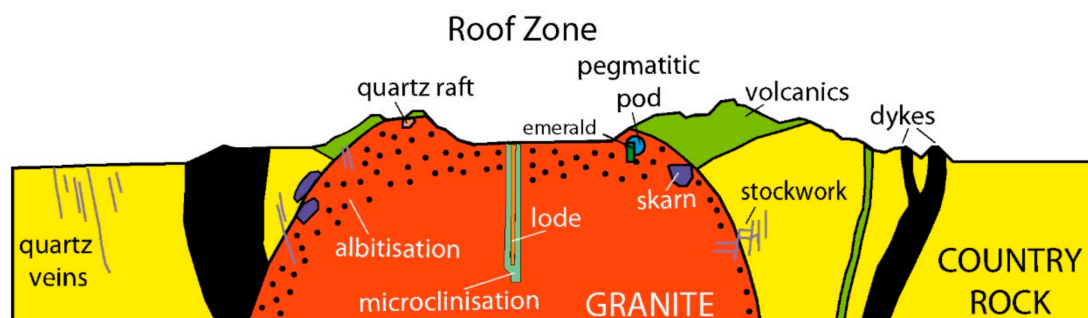


**Figure 20.** Ring complexes of Nigeria and emerald mineralization. Idealized cross-section showing structural setting and styles of mineralization.

## 6.2. Tectonic Metamorphic-Related (Type II)

Type II deposits are found in metamorphic environments with facies varying from high anchizone metamorphic illite crystallinity (Colombian black shales) to medium pressure conditions where the most exposed metamorphic rocks belong to the greenschist (ex: Swat talc-carbonate schist, Pakistan), amphibolite (ex: Habachtal metamorphic series, Austria), and up to granulite facies, with local partial melting of the rocks (migmatites of Hiddenite, USA). The majority of these deposits are characterized by the absence of granitic intrusions, and the deposits are linked to the circulation of fluids and metasomatism in thrusts, shear zones, or vein systems. Four sub-types are proposed in the new classification of emerald deposits (IIA, IIB, IIC, and IID).

### 6.2.1. Sub-Type IIA: Tectonic Metamorphic-Related Emerald Deposits Hosted in M-UMR (Brazil, Austria, Pakistan; See Table 1)

The Brazilian emerald deposits are partly associated with shear-zones cross-cutting M-UMR. The absence of a magmatic influence in their formation is constrained by field, geochemical, fluid inclusion, and stable isotope studies [15,76]. This is the case for the Santa Terezinha de Goiás deposit and the occurrence of Itaberaí. The economic importance of this deposit type is waning due to smaller emeralds, emerald dissemination, and higher artisanal mining cost and today represents only 4% of the total production of Brazil. The main Brazilian production is from type I deposits in Minas Gerais (74%) and Bahia (22%) [87]. Nevertheless, type IIA must be considered when prospecting in the Archean and Precambrian volcano-sedimentary series or greenstone belts.

1. The Santa Terezinha de Goiás deposit, located in central Goiás, produced 155 tons of emerald between 1981, date of the discovery, and 1988 [88]. The emerald grade was between 50 and 800 g/t. The infiltration of hydrothermal fluids is controlled by tectonic structures, such as the thrust and shear zones (Figure 21a). Pegmatite veins are absent and the mineralization is stratiform (Figure 21b). Emerald is disseminated within phlogopitites and phlogopitized carbonate-talc schists of the metavolcanic sedimentary sequence of Santa Terezinha [88–90]. Talc-schists provide the main sites for thrusting and the formation of sheath folds [91]. Emerald-rich zones are commonly found in the cores of sheath folds and along the foliation (Figure 21c). Two types of ore can be distinguished [88]: (i) A carbonate-rich ore composed of dolomite, talc, phlogopite, quartz, chlorite, tremolite, spinel, pyrite, and emerald; (ii) a phlogopite-rich ore composed of phlogopite, quartz, carbonates, chlorite, talc, pyrite, and emerald.

The distal São José two-micas granite, located 5 km from the emerald deposit, is a syntectonic foliated granite, which underwent a polyphase ductile deformation coeval to that observed in the emerald deposit [92]. C and S structures in the granite indicate shear deformation along a typical frontal thrust ramp and the granite overthrust the Santa Terezinha sequence where the emerald deposit is located. D'el-Rey Silva and Barros Neto [92] suggested that the granite most probably was the source of Be for the formation of emerald in the Santa Terezinha de Goiás deposit.

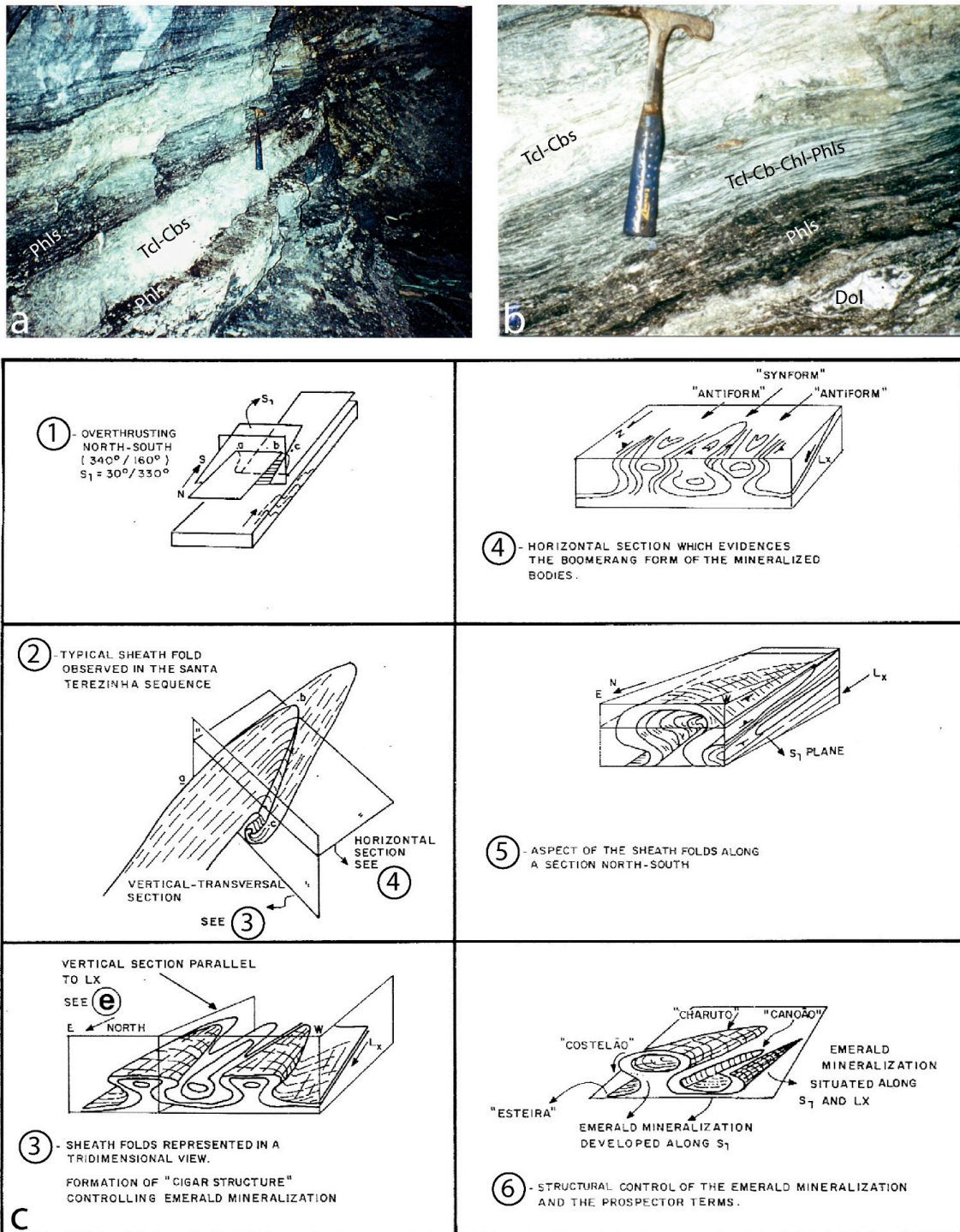


**Figure 21.** The Santa Terezinha de Goiás (Campos Verdes) emerald deposit, Goiás, Brazil: (a) Carbonated and phlogopite-rich emerald ores. The phlogopite schists (phls) underline the foliation of the talc-carbonate schists (Tcl-Cbs); (b) carbonates lenses (Dol) are observed within the talc-carbonate schists (Tcl-Cbs). The phlogopitisation affects the carbonated-talc-schists and the talc-carbonate-chlorite schist (Tcl-Cb-Chls) showing the “bed-by-bed” fluid injection along foliation planes; (c) structural evolution of the Santa Terezinha volcano-sedimentary sequence and the controls of the emerald mineralization on the basis of the structural study done on the Trecho Novo 167 underground mine (EMSA company property). Photographs: Gaston Giuliani.

2. The Habachtal deposit in the Austrian Alps has been studied in detail [77,93–97]. This alpine deposit is located in a contact zone, which overthrusts the volcano-sedimentary series of Habachtal (Habach Formation) on the ortho-augengneisses (central gneisses). The Paleozoic Habach formation is composed of a series of amphibolites, acid metavolcanics transformed in muscovite schists, and black pelites with interlayered serpentinites and talc series. Two metamorphic events, one occurring before the Alpine event ( $P < 3$  kb and  $T < 450$  °C) and one occurring during the Alpine event ( $4.5 < P < 6$  kb and  $500 < T < 550$  °C) were superimposed. The mineralized “blackwall zone”, the equivalent of a phlogopitite, is a tectonic or shear zone 100 m wide, formed from UMR (serpentinites) pinched between orthogneisses and amphibolites. Emerald is disseminated in the “blackwall zone” phlogopitites, talc-actinolite, and chlorite schists. The metasomatic process involves fluid percolation that extracted Be from the muscovite schists (average Be content = 36 ppm) and Cr from the serpentinites (Cr content = 304 ppm) to facilitate the crystallization of emerald (Figure 22). Fluid inclusions trapped by emerald belong to the  $H_2O-CO_2-NaCl$  system [96] with two generations of fluid inclusions: An early generation ( $XCO_2 < 4$  vol.%) and a late one ( $XCO_2$  up to 11 vol.%). Emerald-metasomatic fluids were related to hydration phenomena due to the alpine metamorphism [96].

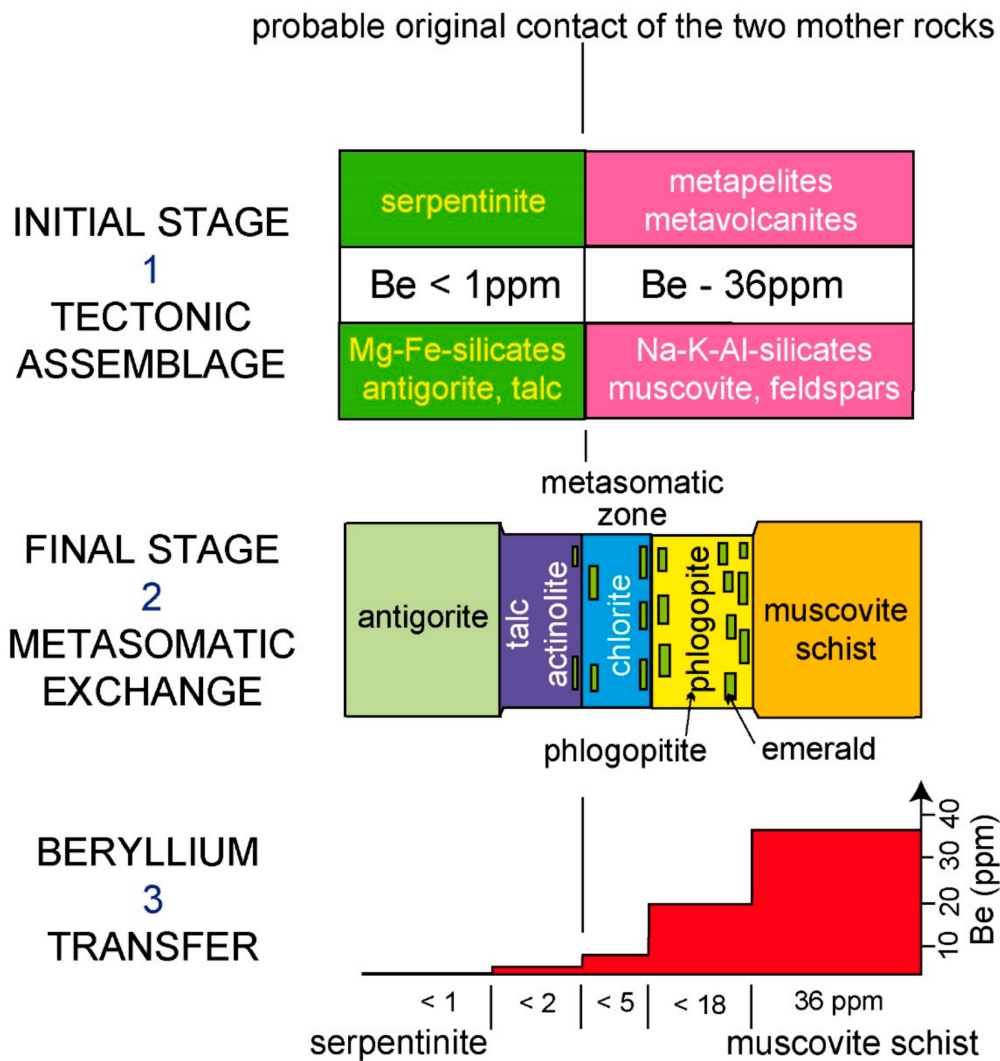


**Figure 22.** Model of formation of the Habachtal emerald deposit: (1) Initial stage showing the different lithologies with their respective Be contents; (2) final stage after regional metamorphism showing the final metasomatic rocks assemblages; (3) beryllium liberated from the muscovite schists is incorporated into the emerald crystals.

- The Swat-Mingora-Gujar Kili-Barang deposits are controlled by the Main Mantle Thrust [86,98–100]. The suture zone that marks the collision of the Indo-Pakistan plate with the Kohistan arc sequence is composed of a number of fault bounded rock melanges (blueschist, greenschist, and ophiolitic melanges).

The ophiolitic melange, which hosts the Pakistani emerald deposits, is composed mainly of altered ultramafic rocks with local cumulate, pillow lavas, and metasediments. Emerald occurs within hydrothermally altered serpentinites that show metasomatic zoning [100]: An outer zone composed of talc-magnesite  $\pm$  chlorite  $\pm$  micas; an intermediate zone consisting of talc-magnesite with dolomite veins; and an inner zone with dolomite-magnesite-talc schists and quartz-dolomite  $\pm$  tourmaline  $\pm$  fuschite veins. Emerald occurs disseminated in the inner and intermediate zones within or spatially associated with quartz-carbonate veins. Dilles et al. [100] obtained a  $^{40}\text{Ar}/^{39}\text{Ar}$  Oligocene age of  $23.7 \pm 0.1$  Ma for a fuchsite-quartz vein in the Swat emerald deposit.

Isotopic study of magnesite from the outer zone showed that the mineral association resulted from early metamorphic fluids [101], whereas the inner and intermediate zones resulted from the infiltration of hydrothermal fluids, which carried Si, Be, B, K, and Ca. Chromium came from the dissolution of chromite crystals in the serpentinites. Arif et al. [102] analysed Cr, Be, B, and other trace element contents in the ophiolitic rocks of the Indus suture zone in Swat. They showed that the Cr present in the Cr-bearing silicates (emerald, Cr-tourmaline, and Cr-muscovite) was derived from the original protolith. Beryllium and boron enrichments were found only in M-UMR affected by fractures and fluid circulation. In addition, analyses of small granitic dykes cutting granitic gneisses showed extreme B and Be enrichment. In consequence, Arif et al. [102] argued that the Be and B are sourced from a probable hidden leucogranite in depth.

#### 6.2.2. Sub-Type IIB: Tectonic Metamorphic-Related Emerald Deposits Hosted in Sedimentary Rocks: Black Shales (Colombia, Canada, USA; Table 2)

Colombian emerald deposits are unique. Why?

The Colombian emerald deposits are located on both sides of the Eastern Cordillera sedimentary basin, with an eastern zone comprising the mining districts of Gachalá, Chivor, and Macanal, and a western zone, including the mines of La Glorietta-Yacopi, Muzo, Coscuez, La Pita, Cunas, and Peñas Blancas (Figure 23). Their distribution along both sides of the basin ensures abundant production of high-quality emerald. These deposits are unique because there is no connection with granites in their formation [103,104].

The emerald mineralization is hosted in Lower Cretaceous (135–116 Ma) sedimentary rocks composed of a thick succession of sandstone, limestone, black shale, and evaporites. The salt and sulphate rocks were necessary for the formation of emerald. These intercalations of evaporites are found both in the Guavio (Figure 24) and Rosablanca formations, in the eastern and western emerald zones, respectively. The evaporites are responsible for the high salinity of the basinal brines (~40 wt.% equivalent NaCl) and the circulation of  $\text{H}_2\text{O-NaCl-CO}_2\text{-(Ca-K-Mg-Fe-Li-SO}_4\text{)}$  fluids trapped by emerald during its growth ([105]; Figure 25).

The tectonic-sedimentary evolution of the Eastern Cordillera basin is unique (Figure 26). The formation of the emerald deposits is related to changes in the acceleration and convergence of the Nazca and South American plates that took place at: (1) 65 Ma, forming the emerald deposits on the eastern side of the basin [106]; and at (2) 38–32 Ma, generating the Muzo and Coscuez deposits on the western side [103]. Formation at different ages and conditions resulted in two drastically different styles of mineralization in the eastern and western emerald zones [107,108].

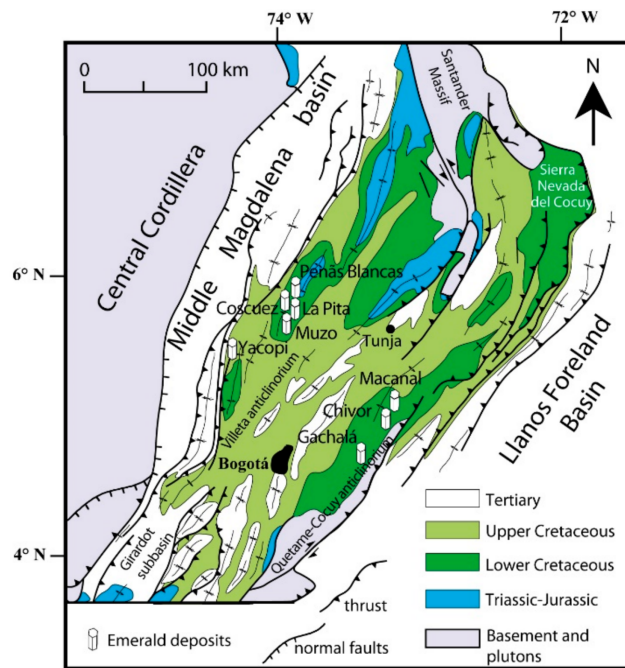


**Figure 23.** Simplified geological map of the basin from the Eastern Colombian Cordillera. The emerald deposits are hosted by Lower Cretaceous sedimentary rocks forming two mineralized zones located, respectively, on the eastern and western borders of the basin. On the western border, with the mining districts of La Glorietta-Yacopi, Muzo, Coscuez, La Pita, Cunas, and Peñas Blancas, and on the eastern border are Gachalá, Chivor, and Macanal.

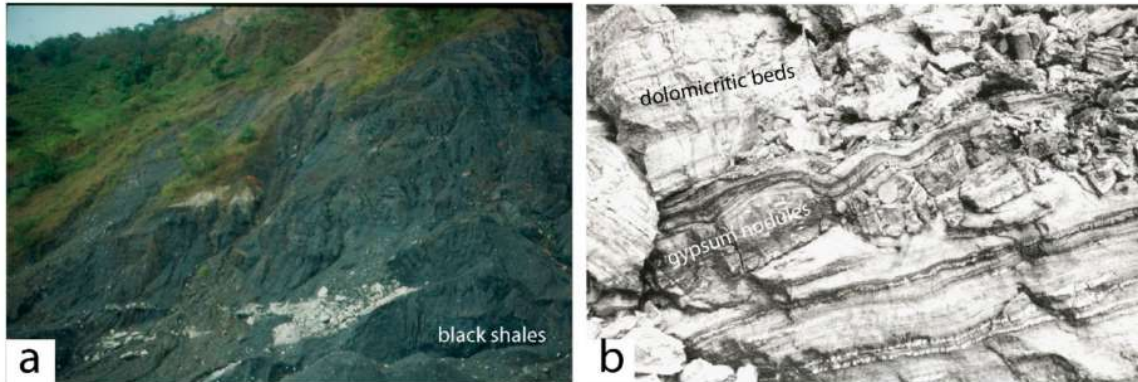


**Figure 24.** Evaporites in the the Chivor mining area: (a) The gypsum deposits present decametric lenses of white gypsum/dolostone alternations hosted in a black matrix made of crushed and dismembered black shales similar to the main evaporitic regional breccia level in emerald deposits; (b) Dolomitic beds are in alternation with nodulated beds of gypsum. Photographs: Yannick Branquet.

In the eastern emerald deposits, the Chivor mining district presents extensional structures extending from a brecciated regional evaporitic level (Figure 27), which acted as a local, gravity-driven detachment [107,108]. The brecciated rock unit in the Chivor area, which is in excess of 10 km long and 10 m thick (Figure 28a,b), is stratabound, i.e., parallel to the sedimentary strata, and dominantly composed of hydrothermal breccia (Figure 28c) made up of fragments of the hanging wall (carbonated carbon-rich BS, limestone, and whitish albitite (albitized black shale)) cemented by carbonates and pyrite (Figure 28d).



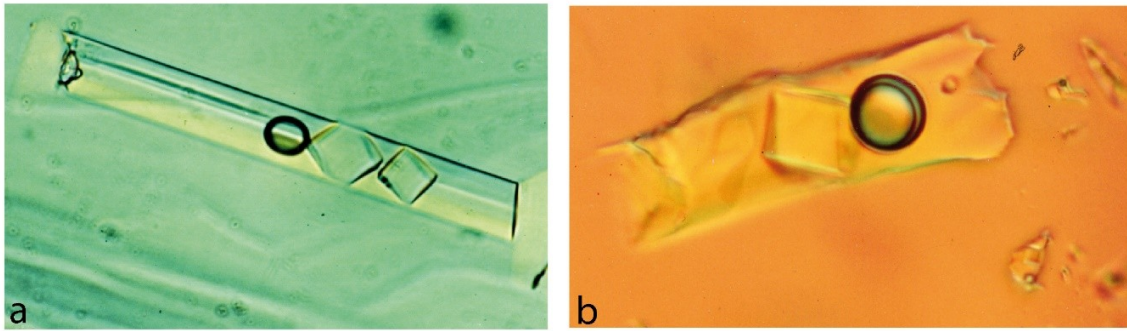


**Figure 25.** Highly saline basinal fluids trapped by fluid inclusions in Colombian emerald is strong evidence for the evaporitic origin of the mineralizing fluid: (a) Emerald from Oriente mine in Chivor (Eastern emerald zone). Primary multi-phase fluid inclusion trapped in an emerald. The cavity, 180 µm long, contains from the right to the left, two cubes of sodium chloride (halite), a rounded gas bubble, and two minute crystals of calcite all of which are wetted by a salty water occupying 75 vol.% of the cavity; (b) emerald from Coscuez (western emerald zone). The cavity, 40 µm long, contains 75 vol.% of salt water solution, 10 vol.% of gas corresponding to the vapour bubble, 15 vol.% of cubic halite crystal (NaCl), and a rounded crystal of carbonate (on the right of the cavity). The vapour phase is rimmed by liquid carbon dioxide. Photographs: Hervé Conge.

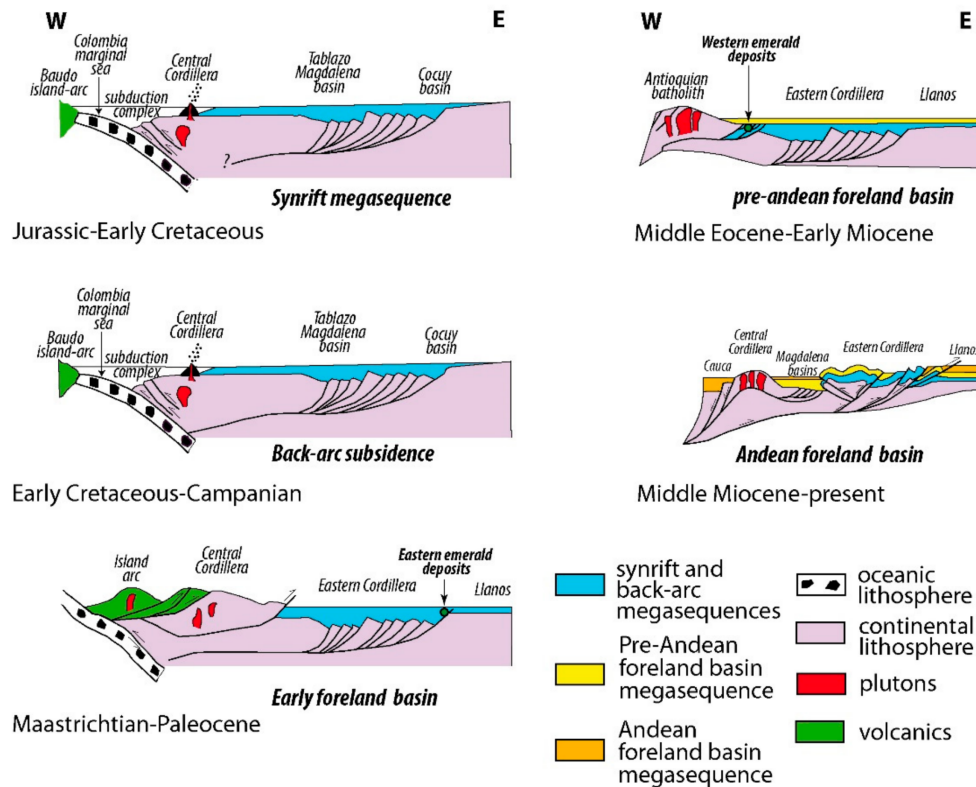


**Figure 26.** Basin development and tectonic history of the Llanos and Eastern Cordillera basins, and Middle Magdalena Valley in Colombia (modified from [109]). Four episodes of deformation have been recognized in the Tertiary of central Colombia: (1) Late Cretaceous–early Paleocene, with the formation at 65 Ma of the emerald deposits from the eastern zone; (2) middle Eocene with the creation of folds and thrusts in the Middle Magdalena valley and western border of the Eastern Cordillera basin, and with the formation, between 38–32 Ma, of the emerald deposits from the western; (3) late Oligocene–early Miocene; and (4) late Miocene–Pliocene at 10.5 Ma where the Eastern Cordillera was uplifted and eroded, with the outcropping of the emerald deposits from the eastern and western emerald zones.

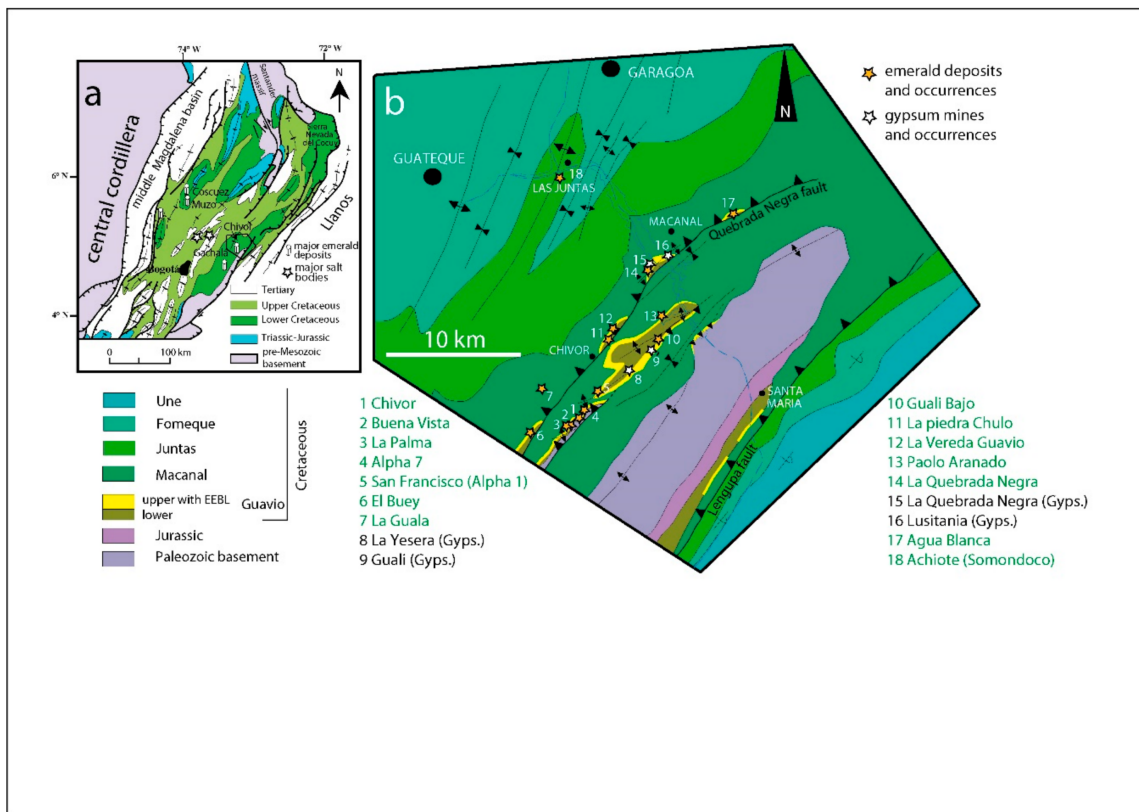


**Figure 27.** Deposits from the eastern emerald zone in Colombia:(a) Simplified geological map of the Eastern Cordillera with the location of the main emerald deposits. Inset is the location of Figure 27b; (b) geological map of the Chivor area. All emerald and gypsum deposits and occurrences are hosted within the Berriasian Upper Guavio Formation.

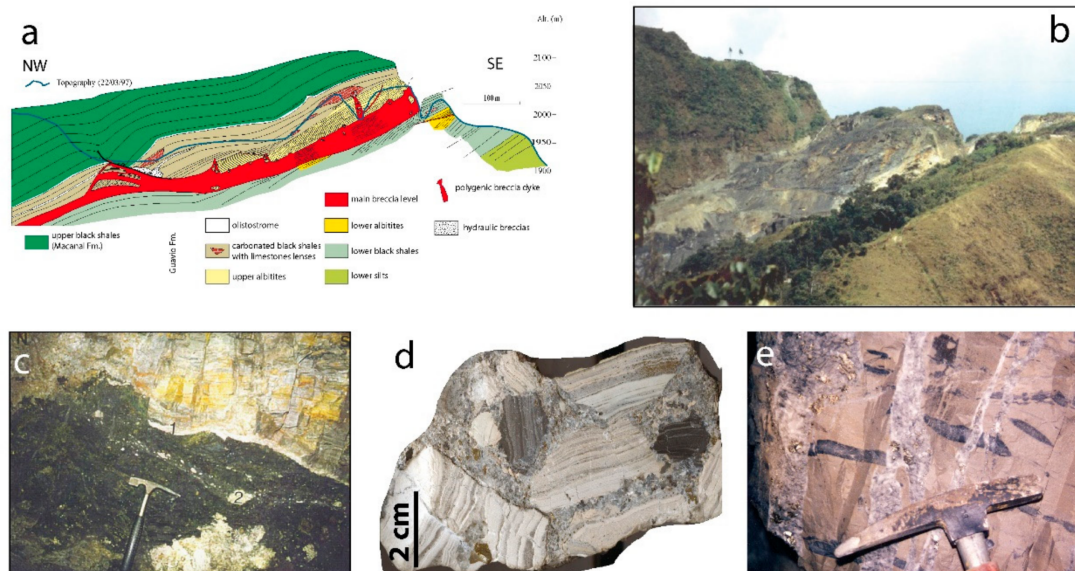


**Figure 28.** The Chivor mining area: (a) Geological cross-section through the Chivor emerald deposits; (b) south-eastern field view of the cross-section; (c) Chivor Klein pit. Upper contact of the main breccia level (in black) with albitites (1). The transport of clasts of albitite (2) within the breccia is marked by tails; (d) Oriente deposit. Polygenic breccia formed by clasts of albitite and black shales, cemented by pyrite, carbonates, and albite; (e) Oriente deposit. Carbonate-pyrite-emerald-bearing veins crosscutting albitite showing some remnants of black shale. Photographs b to d: Yannick Branquet; Photograph e: Gaston Giuliani.

All the mineralized structures, i.e., sub-vertical veins, extending from the roof of the brecciated level (Figure 28e), are mineralized listric faults that attest of the bulk extensional structures extending from the brecciated regional evaporitic level. At 65 Ma, to a small amount of horizontal stretching a large flow of hydrothermal fluids responsible for emerald deposition occurred through the regional evaporitic level. The observed structures of the breccia are diagnostic of hydraulic fracturing associated with the evaporite solution within the salt-bearing main breccia level. At the Cretaceous–Tertiary boundary, the overburden of the Guavio Formation in the Chivor area was about 5–6 km [110]. At that time, the area was slightly uplifted in an incipient foreland bulge [111]. This was [111] interpreted as extensional structures observed in the emerald deposits, resulting from flexural extension. Following this model, the emerald-related hydrothermal event recorded an abrupt change in the thermal and dynamic conditions of the Eastern Cordillera basin, which triggered regional-scale hot, deep, and over-pressured brines migration [110].

The western emerald deposits, such as Muzo (Figure 29a) and Coscuez (Figure 30), are characterized by compressive fold and thrust structures formed along tear faults. These tectonic structures are synchronous with the circulation of the hydrothermal fluids and emerald deposition. The deposits are hectometre-sized at most and display numerous folds, thrusts, and tear faults [112]. In the Muzo deposit, thrusts are marked by the calcareous BS, which overly siliceous BS (Figure 29b). All the tectonic contacts are marked by cm- to m-thick hydrothermal breccia called “cenicero”, i.e., ashtray, by the local miners (Figure 29c,d). These white- or red-coloured breccias outline the thrust planes, which are associated with intense hydraulic fracturing due to overpressured fluids [113]. Multistage brecciation corresponds to successive fault-fluid flow pulses and dilatant sites resulting from shear-fracturing synchronous to the thrust fault propagation.

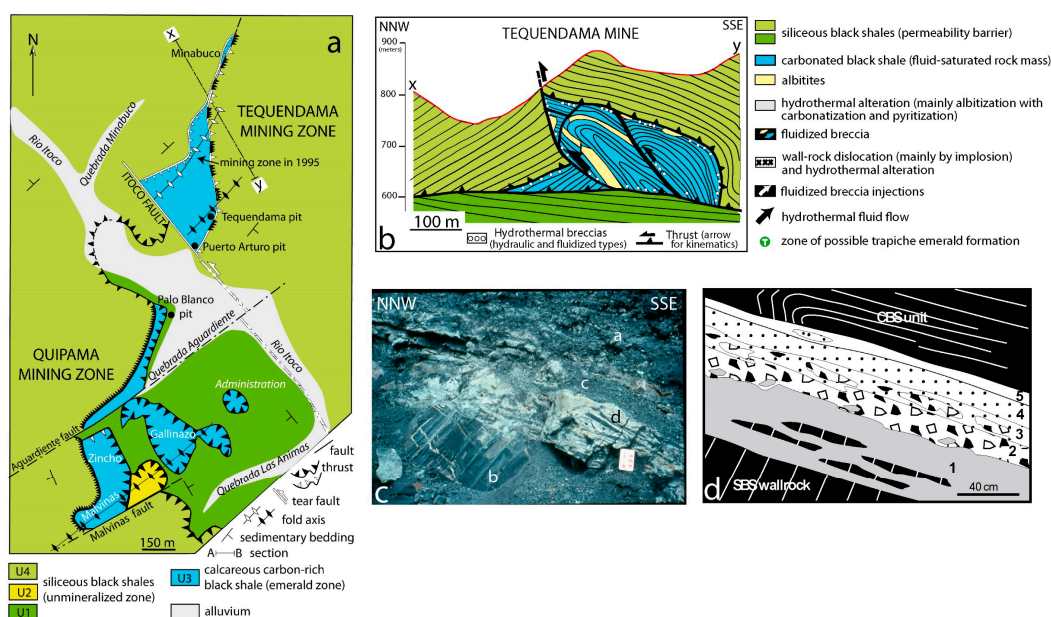


**Figure 29.** Tectonic style and lithologies of the Muzo emerald mining district, western emerald zone: (a) Geological map produced between 1994 and 1996. U1 through U4 represent the different tectonic units. The units, U1, U2, and U4, are comprised of barren siliceous black shales (cambiado), while U3 is composed of emerald-bearing calcareous carbon-rich black shale; (b) Tequendama mine cross-section along x-y (see Figure 29a). The cross-section shows the different lithologies and tectonic structures described by [112] and [107,113]. The thrusts and tear faults are associated with the presence of breccia, extensional veins, and related potential zones for trapiche emerald in the wall-rock dislocations and hydrothermal alteration [114]; (c) thrust verging NNW at Tequendama mine. The SSE dipping calcareous black shale unit (a) thrusts over the NNW dipping siliceous black shale unit (b). The siliceous beds are truncated at high angles by the thrust plane characterized by a hydrothermal breccia (c) and a thrust-parallel vein (d). Photograph: Gaston Giuliani; (d) texture and mineralogy of a thrust-parallel

and layered breccia called “cenicero” by the miners, outcrops of Puerto Arturo in 1994–95, Tequendama mine [107,113]. Layering of the breccia zoning: 1 = carbonate thrust vein; 2 = cemented breccia with pyrite and calcite crystals; 3 = tectonically reworked breccia with a red melange cemented by pyrite and ankerite; 4 = red layer totally cemented by pyrite and ankerite (“cenicero rojo”); 5 = pure pyrite layer (“cordón piritoso”). CBS = calcareous black shale; SBS = siliceous black shale.

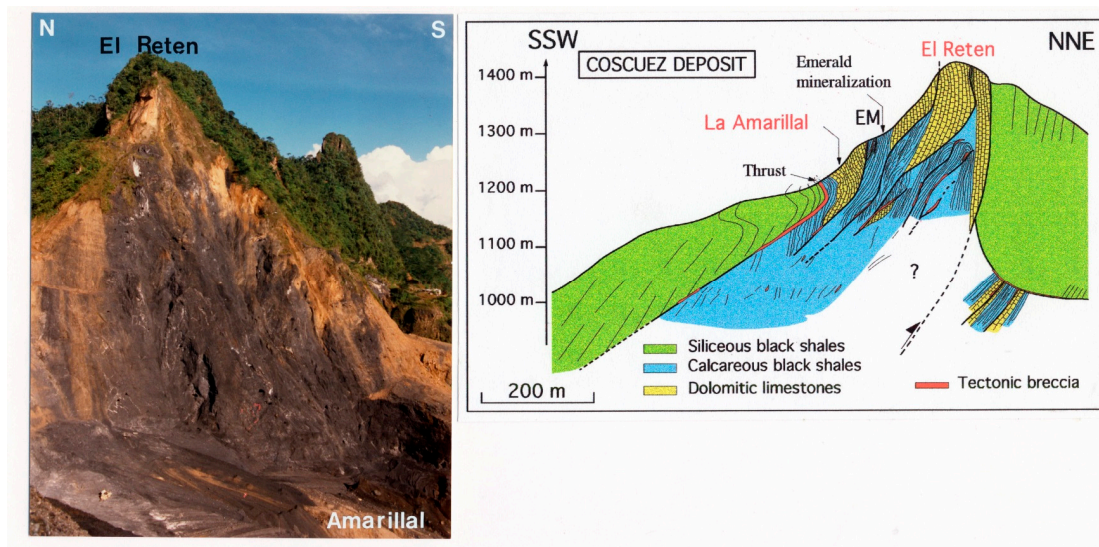
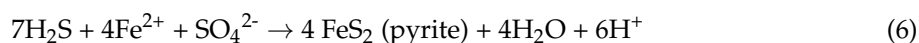
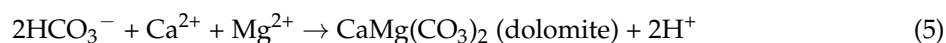
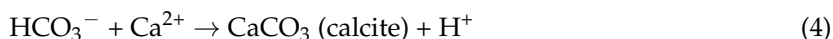
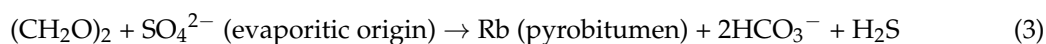


**Figure 30.** Tectonic style and lithologies of the Coscuez emerald mining district, western emerald zone: (a) General view of the Coscuez deposit in 1996. Photograph: Gaston Giuliani; (b) geological cross-section of the Coscuez deposit showing the lithostratigraphic column of the formations and the tectonic style marked by thrusts and faults. The emerald mineralization is linked to tectonic hydrothermal breccia zones, faults, thrusts, and stockwork veins [107,113].

The thermal-reduction of sulphate, at 300–330 °C, in the presence of organic matter in the black shale during the formation of the emerald-bearing veins is unique for Be-bearing mineralization [104,115]. Sulphates ( $\text{SO}_4^{2-}$ ) in minerals of evaporitic origin are reduced by the organic matter of the BS to form hydrogen sulphide ( $\text{H}_2\text{S}$ ) and hydrogen carbonate bounding ( $\text{HCO}_3^-$ ), which are responsible for the precipitation of pyrite, carbonates, and bitumen in the veins via the following reactions:



The consequence of pyrite precipitation is the depletion of iron in the fluid prior to emerald precipitation. This impacted the gemmological features of the emerald as follows: (i) Iron-free absorption spectra with sharp Cr-V bands; (ii) iron-poor chemical fingerprinting; and (iii) optical properties that correlate with the low trace elements content [116].

Although, as noted above, the emerald deposits in Colombia are unique, two minor occurrences that show similar recipes for emerald formation have been reported:

1. An emerald occurrence was described near Mountain River in the northern Canadian Cordillera [117]. These emerald veins are hosted within siliciclastic strata in the hanging wall of the Shale Lake thrust fault. The emerald formed as a result of inorganic thermal-chemical sulphate reduction via the circulation of deep-seated hydrothermal carbonic brines through basal

siliciclastic, carbonate, and evaporitic rocks (Figure 31). The deep-seated  $H_2O$ - $NaCl$ - $CO_2$ - $N_2$  brines, with a salinity up to 24 wt.% equivalent  $NaCl$ , were driven along deep basement structures and reactivated normal faults related to tectonic activity associated with the development of a back-arc basin during the Late Devonian to Middle Mississippian (385–329 Ma). The Mountain River emerald occurrence thus represents a similar and small-scale variation of the Colombian-type emerald deposit model [117].

2. Three emeralds were reported in the Uinta Mountains in Utah, USA [118,119]. The discovery was realized in the Neoproterozoic Red Pine shale, which is overlain by Paleozoic carbonate rocks. Based on the study of fibrous calcite hosted by the Mississippian carbonate units, subjacent to the hypothetical emerald-bearing shale, [120] proposed an amagmatic process for the formation of emeralds. The authors combined their chemical and isotope data on calcite, limestone, and the Red Pine shale using a model of formation similar to the Colombian type and involving thermal reduction of sulphates between 100 and 300 °C. Emeralds were not described [120] and one can question their existence in the Uinta Mountains. No one has described these emeralds since the discovery of [118].

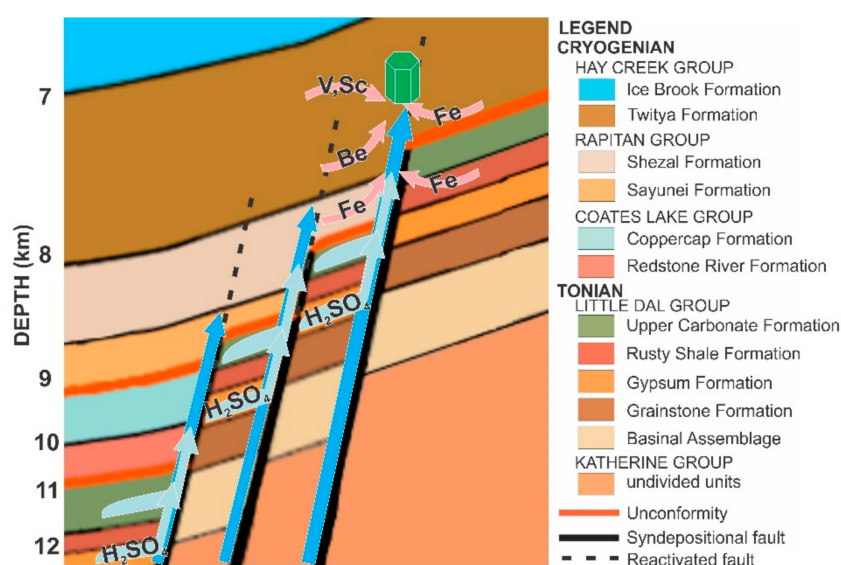


**Figure 31.** Idealized schematic model for the emerald mineralization of the Mountain River emerald occurrence located in Devonian to Mississippian platform sediments [117]. Emerald resulted from inorganic thermochemical sulphate reduction (light blue arrow) via the circulation of brines along a reactivated normal fault (dark blue arrow). The high-salinity brines result from the dissolution of evaporites lenses in the sediments. Be, V, Sc, and Fe were mobilized from the sedimentary formations (pinkish arrows).

### 6.2.3. Sub-Type IIC: Tectonic Metamorphic-Related Emerald Deposits Hosted in Metamorphic Rocks Other than M-UMR and Black Shales (Afghanistan, China, USA; Table 2)

This sub-type includes emerald-bearing quartz vein and veinlet deposits located in medium pressure metamorphic rocks from the greenschist to granulite facies:

1. The Panjsher emerald deposits in Afghanistan (Figure 1a) are located in the Herat-Panjsher suture zone along the Panjsher Valley. The suture zone, which marks the collision of the Indo-Pakistan plate with the Kohistan arc sequence, contains a number of faults, such as the Herat-Panjsher strike-slip fault, which was mainly active during the Oligocene-Miocene [121]. The emerald deposits lie southeast of the Herat-Panjsher Fault in the Khendj, Saifitchir, and Dest-e-rewat Valleys. The deposits are hosted in the Proterozoic metamorphic basement formed by migmatite, gneiss, schist, marble, and amphibolite. The basement is overlain to

the northwest by a Paleozoic metasedimentary sequence crosscut by Triassic granodiorite [86]. During the Oligocene, the Proterozoic rocks of the Panjsher valley were affected by the intrusion of granitoids [86] 20 km north and south of the emerald mining district [122]. The emerald deposits are hosted by metamorphic schists that have been affected by intense fracturing, fluid circulation, and hydrothermal alteration, resulting in intense albitization and muscovite-tourmaline replacements [122]. Emerald is found in vugs and quartz veins associated with muscovite, tourmaline, albite, pyrite, rutile, dolomite, and Cl-apatite [122]. Ar-Ar dating on a muscovite from the emerald-bearing quartz veins at the Khendj mine gave an Oligocene age of  $23 \pm 1$  Ma [123]. At the moment, the sources of Cr and Be remain unclear.

2. The Davdar emerald deposit is located in the western part of Xinjiang Province, China. The deposit is formed by emerald-bearing quartz-carbonate veins associated with a major northwest-southeast trending fault zone [18]. The deposit is hosted by lower Permian meta-sedimentary rocks, including sandstone, dolomitic limestone, siltstone, and shale, which have been metamorphosed at upper greenschist conditions [124] to produce metasedimentary host rocks, which include quartzite, marble, schist, and phyllite, prior to the emplacement of the emerald-bearing veins. Basaltic dykes of an unknown age, which are up to 10 m wide and crop out along strike lengths of up to 200 m, are the only intrusive igneous rocks known in the area. The dykes are emplaced along the northwest-southeast fault zone; no visible contacts are exposed between the dykes and the emerald-bearing veins. The emerald-bearing veins, which are up to about 20 cm wide, contain epidote, K-feldspar, tourmaline group minerals, carbonates, and iron oxides. Quartz and emerald crystals up to a few centimeters long are found in the veins. Alteration haloes up to a few cm wide occur around the veins. In the sandstone and dolomitic limestone, the alteration halo is barely visible, but it is conspicuous as a bleached white halo in the phyllite. The alteration halo is generally enriched in fine-grained silica with variable amounts of quartz, biotite, muscovite, feldspar, carbonate, and tourmaline. It is representative of a retrograde metamorphic assemblage typical of greenschist facies minerals (epidote, plagioclase, potassic feldspar, quartz, biotite, and chlorite). Emerald typically occurs in the quartz veins and not in the host rocks or the alteration haloes.
3. Hiddenite emerald was discovered in North Carolina northeast of the community of Hiddenite in 1875. Since then, a number of notable samples have been discovered, primarily from the Rist and North American Gem mines [125]. Over 3500 carats of emerald were extracted from the latter in the 1980s, including the 858 ct (uncut) "Empress Caroline" crystal [126]. At the Rist property the emeralds occur in quartz veins and open cavities (50% of the veins) that occupy NE-trending sub-vertical fractures in folded metamorphic rocks [126,127]. The hiddenite area is underlain by Precambrian migmatitic schists, gneisses, and interlayered calc-silicate rocks, metamorphosed in the upper amphibolite facies. The area is locally intruded by the Rocky face leucogranite. The quartz veins range in size from 2 to 100 cm wide, 30 cm to 7 m long, and 10 cm to 5 m high. Most of the veins are not interconnected and represent tensional gash fractures that sharply crosscut the prominent metamorphic fabric of the host rocks, suggesting that they formed during late or post metamorphic brittle-ductile deformation [126]. Wise and Anderson [127] identified four cavity assemblages: (1) An emerald-bearing assemblage composed of albite, beryl, calcite, dolomite, siderite, muscovite, cryptocrystalline quartz, rutile, and sulfides with clays; (2) a Cr-spodumene-bearing assemblage, which includes calcite, muscovite, and quartz. The green Cr-bearing spodumene, locally referred to as "hiddenite", occurs in only minor amounts; (3) a calcite assemblage dominated by calcite and quartz; and (4) an amethyst assemblage characterized by amethystine quartz, calcite, muscovite, and chabazite. Emerald and spodumene rarely occur together in the same vein or cavity. Within the emerald-bearing cavities, beryl crystals up to 20 cm in length are closely associated with dolomite, muscovite, and quartz. The crystals are typically color-zoned with a pale green to colorless core and an emerald-green rim. Speer [126] described the veins and reported that the emeralds occur as free-standing crystals attached to

cavity walls and as individual collapsed fragments. The collapsed crystals that have fallen from walls of the cavities show cementation phenomena, while the attached crystals exhibit dissolution, re-growth, and over-growth. Bleached wall-rock alteration halos up to 9 cm wide and rich in silica and chlorite are commonly peripheral to veins and crystal cavities. Wise and Anderson [127] pointed out that the emerald and Cr-spodumene mineralization in quartz veins and cavities is similar to what is seen in alpine-type fissures. In the absence of a pegmatitic or granitic body, the source of Be and Li remains in question; the source of Cr and V is also uncertain, given that M-UMR are unknown in the area. Speer [126] specified that the veins originated as hydrothermal filling of tensional sites during the waning ductile/brittle stages of metamorphism. Apparently, the geological setting and genesis of the Hiddenite emerald occurrences are unique.

#### 6.2.4. Sub-Type IID: Tectonic Metamorphosed or Remobilized Type IA Deposits, Tectonic Hidden Granitic Intrusion-Related Emerald Deposits, and Some Unclassified Deposits (Egypt, Australia, perhaps also Brazil, Austria, Pakistan, Zambia; Table 2)

This sub-type includes deposits probably genetically linked to hidden granitic intrusions (Swat valley) and those where metamorphism has blurred the distinction between metamorphic and magmatic origin (Habachtal, Eastern desert in Egypt). This sub-type permits reclassification and debate on the genesis of several deposits, including the following located in M-UMR:

1. Those for which the genesis is considered to be the consequence of regional metamorphism but with multi-stage emerald formation (Eastern desert of Egypt).
2. The sub-type IIA (Santa Terezinha de Goiás, Habachtal, and Swat Valley) where metamorphic-metasomatic deep crustal fluids circulated along faults or shear zones and interacted with M-UMR with apparently no magmatic intrusion.
3. The mineralization stages for the Poona deposit where emerald and ruby are associated.

It is also useful for considering deposits in meta-sedimentary rocks for which insufficient geological knowledge renders the genesis and classification uncertain (Panjsher Valley and Davdar deposits) and for the Hiddenite occurrences where the source of Be and origin of the mineralizing fluids are unknown.

The Egyptian emerald occurrences of Gebels Zabara, Wadi Umm Kabu, and Sikait occur in a N-W trending band circa 45 km long in the Nugrus thrust [128–130]. The deposits are located in a volcano-sedimentary sequence featuring an ophiolitic tectonic melange composed of metamorphosed M-UMR overlying biotite orthogneiss. Syntectonic intrusions of leucogranites and pegmatites occurred along the ductile shear-zone [43]. The study of [130] described three beryl-emerald generations that crystallized during magmatic, post-magmatic hydrothermal, and regional-metamorphic events. The genetic succession was based on chemical and microstructural studies. The original colorless Cr-poor beryl and phenakite of pegmatite origin has been partly replaced by the formation of Cr-rich beryl (emerald) through K-Mg metasomatism. At the Gebel Sikait, [130] described the occurrence of emerald in phlogopitites (i) at the contact between meta-pegmatite, meta-pelite, and meta-greisen veinlets of up to 10 cm in thickness and (ii) in folded quartz layers. At Gebel Zabara, the emerald is either in phlogopitites and talc-carbonate-chlorite-actinolite schists present in the serpentinite bodies, or in quartz veins. At Gebel Umm Kabo, emerald is within phlogopitites in contact with small lenses of quartz. The dating of phlogopite by K-Ar returned ages of 520 to 580 Ma [131] and by Rb/Sr returned ages of  $591 \pm 5.4$  Ma, confirming the Panafrican orogen.

Based on microtextures, [128,129] suggested that emerald formation occurred during low-grade regional metamorphism. The emerald formation was controlled in detail by the local availability of Be present in the beryl-bearing meta-pegmatite and quartz veins, Cr in the meta-M-UMR, and the metamorphic fluids, all in the context of the late Pan-African tectonic-thermal event. This genetic model has been challenged [43], who pointed to the intrusions of syntectonic leucogranites with the presence of greisens and beryl-emerald-bearing pegmatites and quartz veins along the shear zones. Fluid inclusion studies have shown the presence of H<sub>2</sub>O-NaCl-CO<sub>2</sub>-CH<sub>4</sub> fluids with a salinity between 8 to 22

wt.% equivalent NaCl and a temperature of homogenization between 260 and 390 °C [43]. The oxygen isotope data for emeralds were consistent with both magmatic and metamorphic origins for the source of the mineralizing fluid [132]. Grundmann and Morteani [130] confirmed the existing  $\delta^{18}\text{O}$  values with new isotopic data in the range of 9.9 to 10.7‰. They concluded that the complex interplay of magmatic and regional magmatic events during the genesis of the emeralds makes it impossible to relate their genesis to a particular event. The Pan-African regional metamorphic model is consistent with the remobilization of syntectonic Cr-poor beryl quartz veins and beryl-phenakite-bearing pegmatites.

The Egyptian emerald occurrence is a good example of the proposed sub-type IID emerald deposit: Magmatism, deformation, and remobilization by metamorphic-metasomatic fluids of the mixed Be and Cr reservoirs. The formation of emerald occurred during a regional tectonic event with the syntectonic intrusion of leucogranites and the injection of pegmatites, thrust and shear zone deformation accompanied by fluid circulation (with probable mixing of magmatic and metamorphic fluids), and reaction with rocks of different composition. The remobilization of Be, Cr, and V occurred at the same time through continuing regional tectonic activity. The oxygen isotopic composition of emerald with  $\delta^{18}\text{O}$  values around 10‰ is similar to the oxygen magmatic signatures found for other worldwide type IA emerald deposits [132].

With the proposed sub-type IID, the genesis of the Santa Terezinha de Goiás, Habachtal, Swat Valley, and Poona deposits can be discussed and finally classified using the chemistry of the emerald and O-H stable isotopes.

At the Santa Terezinha de Goiás deposit, the ductile-fragile deformation coeval with the mineralization was strongly assisted by fluids migrating along shear planes under lithostatic fluid pressure at 500 °C [15]. The O-H isotopic composition of phlogopite and emerald is consistent with both magmatic (evolved crustal granites) and metamorphic fluids. This hypothesis was also proposed [133] based on fluid inclusion studies showing the mixing between carbonic and aqueous fluids. Nevertheless, considering the absence of granites and pegmatites in the underground mine, which reaches depths of up to 400 m [134], the low beryllium concentration in the Santa Terezinha volcano-sedimentary series (Be < 2 ppm), the lack of tourmaline in the metasomatic rocks, the control of the mineralization by shear zone structures, and the  $\text{CO}_2\text{-H}_2\text{O-NaCl-(}\pm\text{N}_2\text{)}$  composition of the fluids, a metamorphic origin was preferred for the parental fluids of the emeralds [15,76]. The metamorphic hypothesis involves some input of Be-bearing metamorphic fluids released at the greenschist-amphibolite transition ( $T = 400\text{--}500$  °C) or fluids generated at higher grades of metamorphism and channeled along transcrustal structures at the brittle-ductile transition. Such specific features are similar to those found for gold deposits in the vicinity of the emerald deposit in the Goiás metallogenic province. The mineralizing fluids are channeled along lineaments and second order structures where  $\text{CO}_2$  unmixing, wall-rock interaction, and concomitant ore precipitation are promoted during temperature and pressure fluctuations.

Chemical analyses of Santa Terezinha de Goiás emeralds led [65] and [23] to question the proposed metamorphic origin [76]. The emeralds have the highest Cs contents ever reported for emerald, with values between 907 and 980 ppm, and with Li contents between 142 and 155 ppm. The high content of Cs supports another hypothesis that magmatic fluids mixed with metamorphic fluids [23]. Following this genetic scheme, despite the absence of pegmatites and granites up to a 400 m depth in the mine and along the metamorphic strike, the influence of the magmatic fluids is evidenced by the chemistry of emerald. In such a ductile shear zone environment, the intrusion of felsic granitoids into the volcano-sedimentary sequences along thrusts is common [135] and could have happened at the Santa Terezinha deposit. This new chemical result confirms the hypothesis proposed by D'el-Rey Silva and Barros Neto [92] that the probable source of Be for emerald was the intrusion of syntectonic two-mica granite at São José do Alegre, located 5 km to the southwest of the emerald deposit. Whole rock Sm/Nd data from the granite and the volcano-sedimentary sequence at Santa Terezinha yielded ages of  $510 \pm 110$  Ma ( $n = 6$ ) and  $556 \pm 77$  Ma, respectively [92,136].  $^{40}\text{Ar}/^{39}\text{Ar}$  ages on phlogopite grains from



the emerald-bearing phlogopitites yielded ages of  $550 \pm 4$  and  $522 \pm 1$  Ma, respectively [137]. These ages show considerable overlap in a large window, which characterizes the Brasiliano orogenesis [138].

At the Habachtal deposit, the emerald-bearing phlogopitites called the “blackwall zone” are located at the tectonic contact between the orthogneisses and amphibolites of the Habach group. The metasomatic “blackwall zone” is formed in sheared melange zones surrounding tectonic lenses of the serpentinite-talc series at the contact with the tourmaline-garnet-mica-bearing metapelitic unit of the Habach Group.

Detailed textural studies on emerald-tourmaline and plagioclase porphyroblasts [77,93,95] recorded three metamorphic episodes and crystallization for these minerals. Deformation enhanced fluid circulation and metasomatic reaction and produced the emerald-tourmaline-bearing phlogopitites. Fluid inclusions in the emerald show similar characteristics to those in syn-metamorphic Alpine fissures in the Habach Formation. Grundmann and Morteani [77] proposed the genesis of emerald through syntectonic growth during regional metamorphism.

Trumbull et al. [97] used B isotopes of coexisting tourmaline in the metapelites and phlogopitites. The  $\delta^{11}\text{B}$  isotope values suggest that two separate fluids were channelled and partially mixed in the shear zone during the formation of the metasomatic rocks. A regional metamorphic fluid carried isotopically light B as observed in the metapelite ( $-14 < \delta^{11}\text{B} < -10\text{‰}$ ) and a fluid derived from the serpentinite association carried isotopically heavier B ( $-9 < \delta^{11}\text{B} < -5\text{‰}$ ) typical for Middle Oceanic Ridge Basalt or an altered oceanic crust.

Grundmann and Morteani [77] pointed out that the source of Be was either the Be-rich garnet-mica schist series or the biotite-plagioclase gneisses (Be up to 36 ppm). Zwaan [52] was critical of this interpretation and warned that, in cases where pegmatitic sources of Be are not apparent, one must proceed with caution since fluids can travel far from granites and pegmatites. He pointed out that pegmatites do occur in the Zentral gneiss and the Habachtal emeralds contain up to 370 ppm of Cs [139], which suggest a pegmatitic source. However, the Cs data produced [23] are very different ( $79 < \text{Cs} < 157$  ppm). The possibility of metamorphism of a pre-existing Be-bearing felsic rock occurrence cannot be excluded and must be considered when constructing a model in a medium- to high-grade metamorphic regime [16]. The question is similar to what has been reported for the origin of tungsten for the Felbertal scheelite deposit [139], which is located in the same metamorphic series as the Habachtal emeralds and is now considered to represent metamorphic remobilization of a Be-W-enriched Variscan granite [140]. This hypothesis is likely correct for emerald because (1) Hercynian aquamarine-bearing pegmatites were found in the Habach series [141] and (2) scheelite disseminations with chalcopyrite and molybdenite in the banded gneiss series of the Habachtal emerald deposit are drawn in the lithologic cross-section presented [77]. Following this hypothesis, the source of Be is magmatic.

The Swat-Mingora-Gujar Kili-Barang emerald deposits are thrust controlled and there is no magmatic or pegmatite intrusions visible in the field [86,101]. Emerald is either disseminated in carbonate-talc-fuchsite-tourmaline-quartz schists or in quartz veins and a network of fractures in magnesite rocks. The mean oxygen isotopic composition of emerald is remarkably uniform at  $\delta^{18}\text{O} = 15.6 \pm 0.4\text{‰}$ . The mean hydrogen isotopic composition of the channel waters is  $\delta\text{D} = -42.2 \pm 6.6\text{‰}$  and that of the fluid calculated from hydrous minerals, such as tourmaline and fuchsite, is  $\delta\text{D} = -47 \pm 7.1\text{‰}$ . These O-H isotope data are consistent with both metamorphic and magmatic origins [101]. However, a magmatic origin is favored because the measured  $\delta\text{D}$  values of fuchsite and tourmaline are comparable to those found for muscovite and tourmaline from granites, such as the Makaland granitoid, exposed 45 km to the southwest of Mingora. The mineralization was probably caused by modified  $^{18}\text{O}$ -enriched hydrothermal solutions derived from an S-type granitic magma [101].

The magmatic model proposed for Pakistani emerald deposits can be constrained by the  $^{40}\text{Ar}/^{39}\text{Ar}$  ages obtained on the different rocks:  $83.5 \pm 2$  Ma for the Shangla blue-schist melange,  $22.8 \pm 2.2$  Ma for the tourmaline-beryl-fluorite-bearing Makaland Granite [142], and  $23.7 \pm 0.1$  Ma for a fuchsite mica

from a quartz vein in the Swat emerald deposit [100]. However, the chemical data for Swat emerald presented [23] show low Cs contents (61 to 74 ppm), which are unusual for granite-related emeralds.

Finally, the genesis of the Swat emerald deposits can result from both metamorphic and magmatic contributions, with up to now a magmatic source not identified in the emerald mining districts.

At the Poona deposit, three styles of emerald mineralization have been identified in M-UMR from the Precambrian series of the northern Murchinson Domain [143]: (a) Emerald in phlogopitites formed at the contact of beryl-granite-muscovite-bearing pegmatites and M-UMR; (b) emerald with ruby-sapphire, topaz, and alexandrite in banded fluorite-margarite-beryl-bearing banded greisens in phlogopitites; and (c) quartz-margarite-topaz-bearing veins in phlogopitites.

A multi-stage mineralizing episode was proposed [143] of: First, the intrusion of granites (probably between 2724–2690 Ma) and circulation of fluids in the M-UMR produced greisens and quartz veins with topaz, beryl, quartz, and muscovite. The first episode was affected by regional metamorphism of greenschist to lower amphibolite facies. Metasomatic reactions occurred at the borders of the greisen zones with the formation of ruby, alexandrite, and emerald. The third episode corresponded to the retrograde phase of metamorphism (probably between 2710–2660 Ma), where corundum and alexandrite were partially or totally replaced by margarite, muscovite, and/or emerald.

Fluid inclusions in emerald combined with the O-H isotope compositions of both lattice and channel fluids of emerald confirmed multiple origins yielding both igneous and metamorphic signatures [16]. This emerald-ruby association is unique worldwide and merits more petrologic and geochemical studies before proposing a coherent genetic scheme.

The genesis of the Panjsher Valley [98] and Davdar [18] emerald deposits is not well understood due to difficulties with access and poor exposure. The similar geographic and geologic environments indicate that these two deposits may share a similar genetic model. Both deposits are hosted in layered meta-sedimentary rocks, with metamorphic facies ranging up to lower amphibolite. Emerald occurs in both veins and host rocks. The veins are predominantly composed of quartz and carbonate, with minor amounts of albitic plagioclase, phlogopite, tourmaline, scheelite, and pyrite. The host rocks vary from shale to carbonate and are thought to be Paleozoic. Proximal to the veins, hydrothermal alteration is dominated by quartz and calcite with lesser amounts of albite, phlogopite, tourmaline, and pyrite. In both localities, there are mafic to felsic intrusions as stocks, dykes, or sills. However, no clear relationship between the intrusive rocks and emerald mineralization has been established. The high-salinity fluids [18,56,144] and meta-sedimentary host rocks combined with the lack of observed igneous association could also be compatible with a tectonic metamorphic-related (type IIB) formational model, but more field work needs to be carried out on these deposits to map the local geology to prove or disprove an igneous link.

Emeralds from the Musakashi deposit in Zambia are of high quality with a bluish color very different from that observed for emerald originating from the Kafubu mining district [63]. Discovered in 2002, the deposit is located ~150 km west of the Kafubu mines. The geology of the deposits is unknown, however, small fragments of emerald were discovered in eluvium adjacent to quartz veins [50]. The internal features, chemical composition, solids, and three-phase fluid inclusions are quite different from those of Kafubu emeralds. Saeseasaw et al. [63] examined three-phase fluid inclusions (halite + vapor + liquid) in emerald from Musakashi, Panjsher Valley, Davdar, and Colombia. They conclude that Musakashi fluid inclusions look like those from Colombia. Nevertheless, the photographs show that they are polyphase and contain a cube of halite and a rounded salt, which is probably sylvite (KCl). Such multiphase inclusions with both halite and sylvite are found in both Panjsher and Davdar emeralds [62]. In addition, the chemistry of these emeralds overlaps with those from Colombian, Panjsher, and Davdar [63]. The geological setting is not precisely known, but the emeralds are very different from those for type IA deposits as shown by their very low Cs contents ( $3 < Cs < 10$  ppm), which are similar to those found for Colombian and Davdar emeralds [63].

The genesis of the Hiddenite deposits remains obscure in terms of the sources of Be, Cr, and V, and the origin of the mineralizing fluids. Fluid inclusions are characterized as two populations of aqueous-carbonic fluids with two populations, those having high- and those having low-CO<sub>2</sub> contents, which underwent immiscibility between 230 and 290 °C, respectively [145]. The deposits are interpreted as late and low temperature metamorphic hydrothermal alpine-type quartz veins cutting meta-sedimentary and migmatitic biotite gneiss. The low temperature hydrothermal mineralization is confirmed by the association of quartz, carbonates, muscovite, and chabazite. The origin of the fluids must be clarified by the O-H isotopes' compositions of the different minerals associated with emerald, but a metamorphic origin has advanced [126,127].

## 7. Fluid Inclusions in Emerald

Emerald is one of the best hosts for fluid inclusions. It is commonly idiomorphic, well preserved, zoned, and displays growth zones optically, chemically, and especially via cathodoluminescence [20,85,117]. These growth zones facilitate the identification of primary vs. secondary fluid inclusions. Additionally, primary fluid inclusions often form during emerald precipitation and are elongated parallel to the host's *c* axis (Figure 32). The determination of fluid inclusion chemistry is generally limited to microthermometry [19,146,147], with more refined analyses performed via bulk leachate analyses or LA-ICP-MS or secondary ion mass spectrometry (SIMS) on quartz-hosted fluid inclusions petrographically determined as synchronous to emerald hosted inclusions [148,149]. In addition to fluid chemistry, fluid inclusions studies have proven most useful in determining the pressures and temperatures of emerald formation [47] and for determining if boiling is responsible for emerald colouration [19].

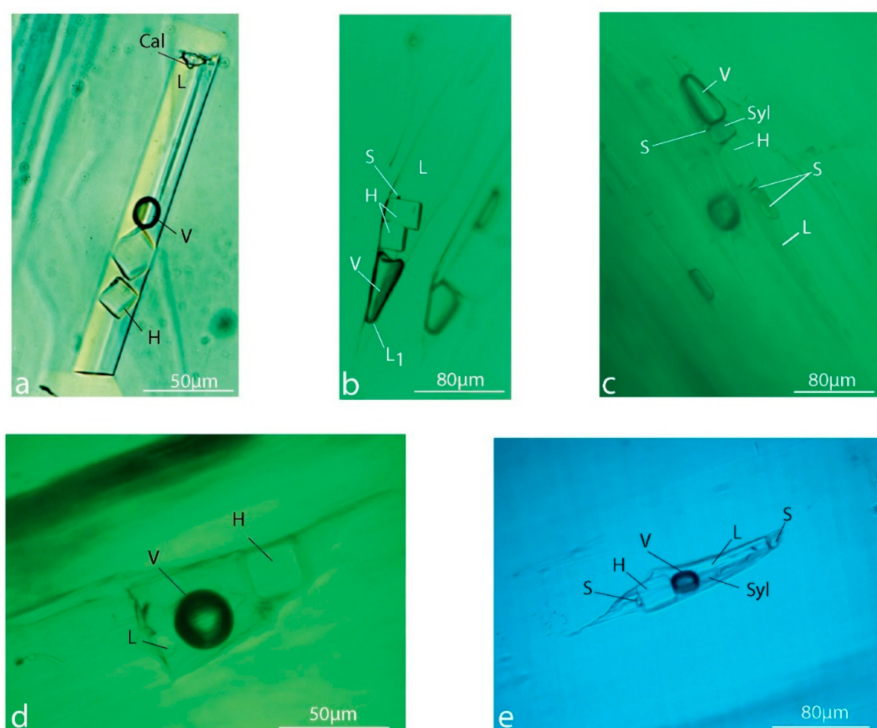


**Figure 32.** Primary fluid inclusions in emeralds: (a) Colombian fluid inclusion presenting a jagged and shredded outline. The cavity contains 75 vol.% of salted water solution (L), 10 vol.% of gas corresponding to the vapour bubble (V), 15 vol.% of halite (NaCl) daughter mineral, and a crystal of carbonate (Ca); (b) fluid inclusion in a Colombian emerald showing three cubes of halite (H), the liquid phase (L), the contracted vapour phase (V), a minute black phase (S), and a thin rim of liquid carbon dioxide (L<sub>1</sub>) rim visible at the bottom part of the vapour phase; (c) multiphase fluid inclusions from Panjsher emerald (Afghanistan). They contain vapour and liquid phases (V + L), a cube of halite (H),

usually a primary sometimes rounded salt of sylvite (Syl), and aggregates of several anisotropic grains (S). The volume and the concentration of NaCl and KCl are different from those observed in Colombia. The overall salinity is estimated to 30 to 33 wt.% eq. NaCl (Vapnik and Moroz, 2001; (d) three-phase fluid inclusion in emerald from Nigeria emerald showing halite (H), liquid (L), and vapour (V) phases. Generally, the primary halite-bearing fluid inclusions are associated with coeval monophasic or biphasic (V + L) fluid inclusions; (e) multiphase fluid inclusion from the Davdar emeralds (China). The cavities contain liquid (L) and vapour (V) phases with daughter minerals, like halite (H) and sometimes sylvite (syl), and aggregates or multiple solid inclusions (S). The morphology of the cavities and the infilling looks like those found in emeralds from Afghanistan. Photographs: Gaston Giuliani.

Emerald-hosted fluid inclusions are, in general, aqueous dominant, with a wide range of salinities from dilute to salt saturated (Table 3). Numerous emerald deposits also have gaseous species contained within the fluid inclusions; the gaseous phases are generally dominated by CO<sub>2</sub>, but other species, such as CH<sub>4</sub>, N<sub>2</sub>, and H<sub>2</sub>S, have been identified via Raman spectroscopy in a number of emerald studies [47,150,151]. Raman spectroscopy can also be used to identify accidental and daughter inclusions within fluid inclusions [152]. Raman analyses of emerald hosted inclusions often prove challenging, as beryl/emerald is generally fluorescent and thus the inclusion spectrum is lost in the fluorescence from the host. However, different laser wavelengths and confocal Raman spectrometers can be used to limit the effects of host fluorescence; these applications to gases and solid inclusions contained within fluid inclusions were reviewed [153–155].

Bulk leachate analyses of fluid inclusions by thermal decrepitation or crushing are limited by contamination via the emerald host. However, leachate analyses of fluid inclusions hosted in quartz precipitated synchronously with emerald have proven successful for general chemistry and especially for halogen sourcing [105]. A further limitation of the bulk methods is the presence of multiple fluid inclusion generations and careful detailed petrographic studies should be undertaken to determine if specific quartz and emerald-hosted fluid inclusions are amenable to bulk techniques.

Hydrogen isotopes [156] are generally determined from trapped channel fluids, which are analogous to primary fluid inclusions. The advantage of channel fluid extraction is that channel fluids are normally three (or more) orders of magnitude more abundant than fluids trapped in fluid inclusions. The oxygen isotope signature of fluids responsible for emerald precipitation is generally determined via the measurement of structural oxygen within emerald/beryl or from other synchronously precipitated silicates. The hydrogen isotope signature of the fluids may also be inferred from the analyses of synchronously precipitated hydrous silicates, such as mica or tourmaline [101]. Additionally, the extraction of the channel fluids may also yield a quantitative determination of the weight percent of H<sub>2</sub>O present in the emerald and this can be used to complement electron microprobe and LA-ICP-MS analyses to determine emerald chemistry.

Fluid fingerprinting to determine emerald provenance has proven incredibly useful. The pioneering studies [15,76] are consistently used to determine provenance and fluid sources, as done for the Biintal occurrence in Switzerland ([157]; Figure 33). Halogen bulk leachate analyses [105] can test for the presence of fluid interaction with evaporitic source rocks as well as providing more detailed information on the various dissolved salts present in the fluid inclusions. Although not yet routinely used, LA-ICP-MS, and to a lesser extent SIMS, can provide very detailed chemical analyses of formation fluids of emerald deposits, as they provide precise analyses of most of the elements of the periodic table and potentially their isotopes.

**Table 3.** Fluid inclusion data and oxygen isotope composition of several emerald deposits worldwide following the enhanced classification proposed for emerald deposits.

Type of Environment and Deposit	Tectonic	Tectonic Metamorphic-Related	
	Magmatic-Related Granitic Rocks in M-UM and SR (Type I)	(Meta) Sedimentary Rocks (Type IIB)	Metamorphic Rocks (Types IIA- IIC-IID)
Temperature	300-680°C	300-330°C*	350-400°C *1 260-550°C *2
Pressure	0.5 to 7 kbar	3 to 4 kbar	1.6 kbar *1D 4-4 to 5 kbar *2
Salinity	2 to 45 wt.% eq. NaCl	40 wt.% eq. NaCl	30 to 33 wt.% eq. NaCl *1P 35 to 41 wt.% eq. NaCl *1D 2 to 38 wt.% eq. NaCl *2
Composition	H <sub>2</sub> O-NaCl-(±CO <sub>2</sub> )-(±N <sub>2</sub> )-(±CH <sub>4</sub> )-(K,Be,FB,Li,P,Cs)	H <sub>2</sub> O-NaCl-(±CO <sub>2</sub> )-(±N <sub>2</sub> )-(±hydrocarbon liquid)-F15(K,Mg,Fe,Li,SO <sub>4</sub> ,Pb,Zn)	H <sub>2</sub> O-NaCl-(±CO <sub>2</sub> ) *1D H <sub>2</sub> O-NaCl-KCl-FeCl <sub>2</sub> -(±CO <sub>2</sub> ) *1P H <sub>2</sub> O-NaCl-(±CO <sub>2</sub> ) *2 CO <sub>2</sub> or CO <sub>2</sub> -H <sub>2</sub> O-NaCl-(±N <sub>2</sub> (±CH <sub>4</sub> ) *2 or H <sub>2</sub> O-CH <sub>4</sub> -CO <sub>2</sub> -NaCl *2
Oxygen isotopes	6.0 < δ <sup>18</sup> O < 15‰	16.2 < δ <sup>18</sup> O < 24.5‰	Panjsher: 13.25 < δ <sup>18</sup> O < 13.9‰ Davdar: 14.4 < δ <sup>18</sup> O < 15.8‰ Sta Terezinha: 12.0 < δ <sup>18</sup> O < 12.4‰ Gravelotte: 9.5 < δ <sup>18</sup> O < 9.7‰ Gebel Sikait: 9.8 < δ <sup>18</sup> O < 10.7‰ Habachtal: 6.5 < δ <sup>18</sup> O < 7.3‰
Origin of the fluid	Metasomatic-Hydrothermal	Basinal brines that have dissolved evaporites	Metamorphic-Metasomatic

Salinity in wt.% eq. NaCl = weigh per cent equivalent NaCl; kbar = kilobars; δ<sup>18</sup>O = ratio <sup>18</sup>O/<sup>16</sup>O in per mil (‰). Type IIB deposits: \* = Colombia. Some Types IIA, IIC, IID: \*1 = deposits of Panjsher (P) and Davdar (D); \*2 = deposits of Santa Terezinha de Goiás (Brazil), Gravelotte (South Africa), Gebel Sikait (Egypt), Habachtal (Austria)

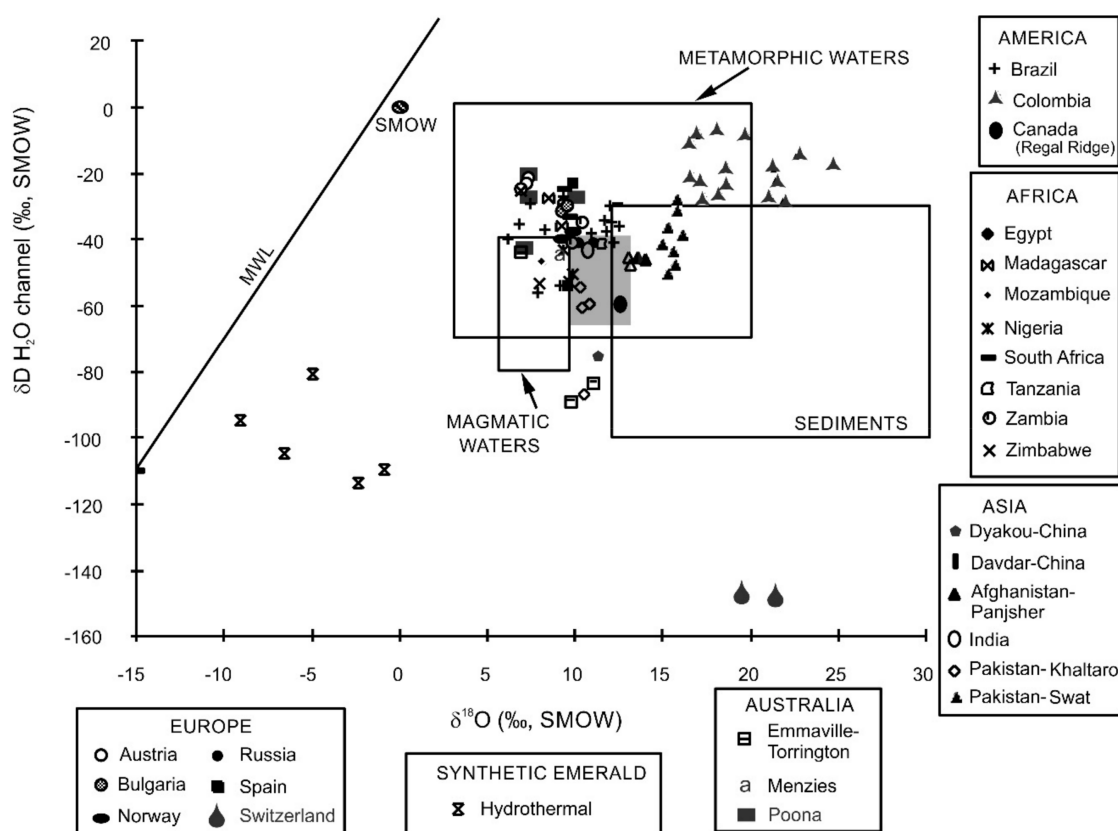


**Figure 33.** Channel δD H<sub>2</sub>O versus δ<sup>18</sup>O for emerald worldwide [15,76,157,158]. The isotopic compositional fields are from [159], including the extended (Cornubian) magmatic water box (grey). MWL = Meteoric Water Line, SMOW = standard mean ocean water.

The use of fluid inclusion petrography combined with microthermometry and halogen and cation bulk leachate analyses is useful for the discussion of the source of salts present in fluid inclusions [160]. The example of multi-phase halite-bearing fluid inclusions in emeralds (Figure 32) from Colombia (Eastern and Western emerald zones) and Afghanistan (Panjsher Valley) is very illustrative.

In Colombia, fluids trapped by emerald are commonly three-phase fluid inclusions (Figure 32a) characterized by the presence of a daughter mineral, i.e., halite (NaCl). At room temperature, the cavities contain 75 vol.% of salty water, i.e., aqueous brine (liquid H<sub>2</sub>O), 10 vol.% of gas corresponding to the vapor bubble (V), and 15 vol.% of halite daughter mineral (H). However, some Colombian emeralds have multiphase fluid inclusions presenting a liquid carbonic phase (CO<sub>2</sub>) forming up to 3 vol.% of the total cavity volume (Figures 25b and 32b), minute crystals of calcite (Figure 32a), very rare liquid and gaseous hydrocarbons [38], and sometimes two or three cubes of halite (Figure 32a,b), and sylvite (KCl).

The high Cl/Br ratio of the fluids (between 6300 and 18,900) indicates that the strong salinity of the brines is derived from the dissolution of halite of an evaporitic origin (Figure 34a; [105]). Cation exchanges, especially calcium, with the black shale host rocks are strong when compared to most basinal fluids (Figure 35; [161]) and are due to the relatively high temperature of the parent brines of emerald (T~300 °C). Indeed, these fluids are enriched in Ca (16,000 to 32,000 ppm), base metals (Fe ~5000 to 11,000 ppm; Pb ~125–230 ppm; Zn ~170–360 ppm), lithium (Li~400–4300 ppm), and sulfates (SO<sub>4</sub> ~400–500 ppm). In comparison, they have a composition and Fe/Cl and Cl/Br ratio similar to the fluids of the geothermal system of the Salton Sea in California (Figure 34b; [162]). The K/Na ratios confirm the Na-rich character of the fluids and the strong disequilibrium between K-feldspar and albite, as shown by the huge albitisation of the black shale (Figure 35).

In Afghanistan, primary multiphase halite-sylvite-bearing fluid inclusions (Figure 32c) are common for the Panjsher emeralds [15,86]. The fluids associated with emerald have total dissolved salts (TDS) between 300 and 370 g/L and the trapping temperature of the fluid is about 400 °C [144].

Crush-leach analyses of fluid inclusions indicate that the fluids are Cl-Na-rich and contain sulfates (140 < SO<sub>4</sub> < 4300 ppm) and lithium (170 < Li < 260 ppm), but very low to zero fluorine contents [160]. The K/Na ratio of the fluid inclusion confirms the disequilibrium, at ~400 °C, between K-feldspar and albite that drives the Na-metasomatism of the metamorphic schists and the deposition of albite in the veins (Figure 35). Crushing demonstrates that fluids are dominated by NaCl with Cl/Br ratios much greater than that of seawater (Figure 34a), indicating that the salinity was derived by the dissolution of halite. Thus, the high Cl/Br ratios are consistent with halite dissolution. The I/Cl versus Br/Cl ratios diagram (Figure 34b) also shows that the fluid inclusions have low I contents, which are also typical of brines derived from evaporite dissolution. They are comparable to the Hansonburg and contemporary fluids from the Salton Sea geothermal brines, both of which have dissolved evaporites [163,164].

Although it is not possible to unambiguously classify emerald deposits based solely on their fluid composition, there are some general observations that can prove useful: (1) The presence of salt cubes can limit possible modes of formation, as it is very unlikely that we can generate a salt saturated fluid in a purely metamorphic environment, hence the presence of salt cubes generally implies the input of igneous fluids or an interaction with evaporites and individual Ca/Na/K values may be specific to individual deposits; (2) compressible gases are seen in all types of emerald deposit, but gas ratios may also be used to identify individual deposits; and (3) specific daughter and accidental minerals contained within fluid inclusions cannot be used to identify specific deposit models within our classification system, but may again be used to fingerprint emeralds from specific deposits.

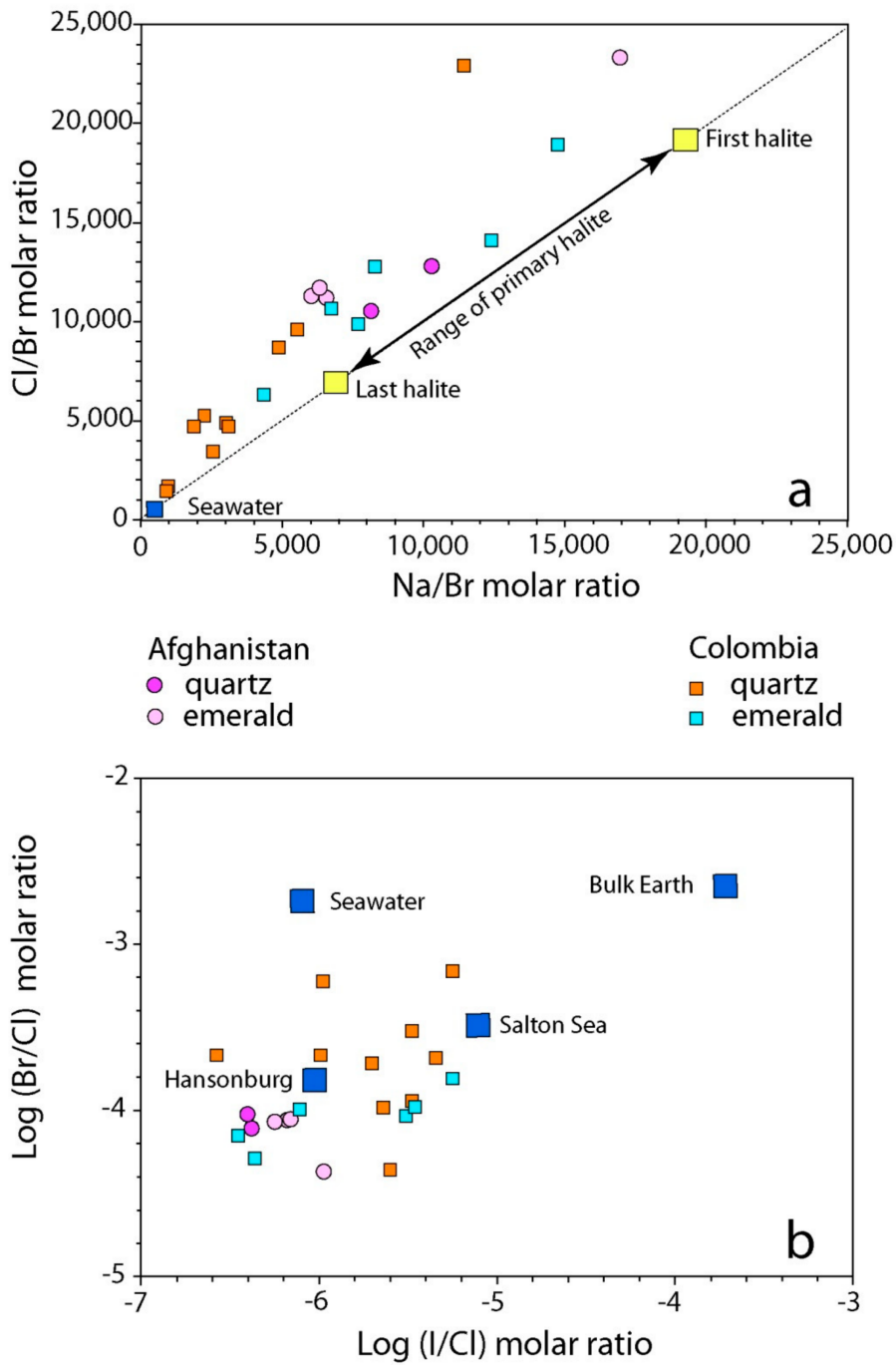


**Figure 34.** Origin of salinity in the emerald and quartz brines from Colombia and Afghanistan: (a) Analyses of the fluid inclusions from both emerald and quartz show a wide range of Na/Br and Cl/Br molar ratios that are much greater than those of primary halite and indicate a substantial loss of Br, typical of recrystallised halite for both emerald deposits; (b) log(I/Cl) versus log(Br/Cl) molar ratios of Afghan and Colombian fluid inclusions, which are depleted in both Br and I, indicative of evaporites contribution to the fluids in emerald and quartz. They are compared with the composition of fluids where evaporites are known to be involved, such as for the Salton Sea geothermal brines [163] and Hansonburg [164].

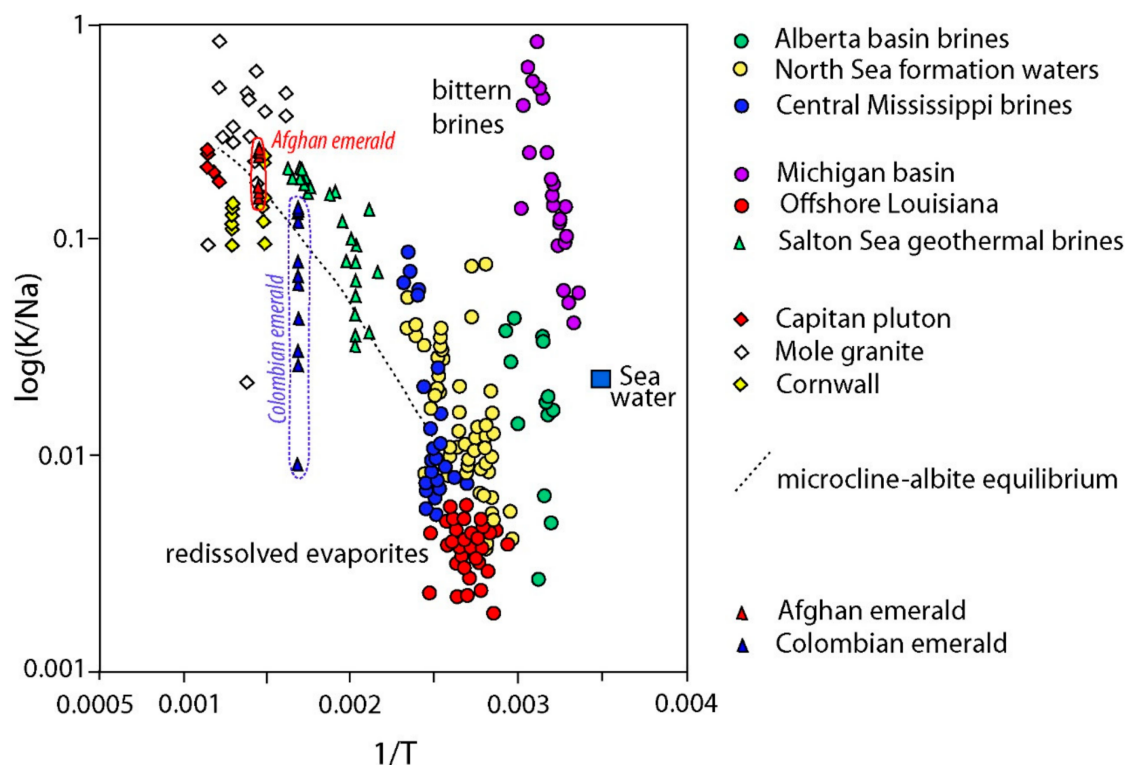


**Figure 35.** Diagram  $\log(K/Na)$  molar ratio versus  $1/T$  ( $^{\circ}K$ ) showing the evolution of the fluids associated with Colombian and Afghan emeralds relative to crustal fluids, including bittern brines, brines derived by dissolution of evaporites, and magmatic fluids. Sedimentary formation brines deviate significantly from the K-feldspar-albite equilibrium as well as for Afghan and Colombian brines, which are associated with a huge albitisation of their host-rock with the complete consumption of K-feldspar from, respectively, the schist and black shale.

## 8. Discussion of the Model of Formation of the Emerald Deposits Associated with M-UMR

The tectonic magmatic-related emerald deposits hosted in M-UMR (sub-type IA) occurred during orogenies from the end of the Archean (2.94 Ga) with the Gravelotte deposit in South Africa [165] to the Himalayan (9 Ma) with the Khaltaro deposit in Pakistan [83]. These deposits are related to plate tectonics over  $\sim 3.2$  billion years with stable convection cells initializing continental drifts and subduction zones, and are related either to continental collisions or continent-to-continent rifting.

The classical model of sub-type IA relates granites with their dyke swarms of aplopegmatites and quartz veins in metamorphosed M-UMR, fluid-rock interaction, and infiltrational metasomatism [15,58,166,167]. An alternative genetic model for the formation of these emeralds is a regional tectonic and metamorphic model [77,130,168–170]. This genetic controversy involving sub-type IA deposits shows that (i) they are possibly genetically different; (ii) that alternative models are always dependent on a school of thought, which we absolutely want to apply for all deposits; (iii) these deposits share many common denominators in terms of geological setting, age of formation, nomenclature of rocks, source of the elements, and source of the fluids; and finally, (iv) each deposit belongs to the same family, but with a wide range of genres and uncountable typological varieties that allow us to follow the evolution of a mountain range marked by magmatic events accompanied by metamorphic remobilizations, which sometimes erase the primary geological features of the emerald deposit.

The following discussion examines the possible genetic links existing between the different sub-type IA and sub-types IIA and IID hosted in M-UMR within the geological and dynamic evolution of a continental crust.



### 8.1. Sub-Type IA Emerald

This is the fruit of the fluid-rock interaction producing metasomatism in both pegmatite and M-UMR, whatever the origin of the fluid. The classical sub-type IA results from the fluid circulation at the contact between these two geochemically contrasting rocks. The most representative deposits described in the literature are those from Carnaíba [76,78], Franqueira [171,172], Khaltaro [83], and Kafubu [70]:

1. The granite emplacement is related to a tectonic event, but the pegmatites are not deformed and metamorphosed. They are clearly intruding the M-UMR of the volcano-sedimentary series, and sometimes roof pendants on the granite as observed in Bode mine at Carnaíba (Figure 36) or at Franqueira;
2. At Carnaíba, the granite and pegmatite intrusions and fluid circulation are coeval [67], and the pegmatite is transformed into plagioclase with disseminations of phlogopite (endo-phlogopite), and the M-UMR into phlogopite (exo-phlogopites). These exo-phlogopites display clear zonation with a very sharp metasomatic front, i.e., metasomatic columns formed by infiltrational processes [173]. The metasomatic fronts where an additional phase appears in the mineral association correspond to the change of one of the determinant components from mobile to inert: Ca is displaced from the serpentinites to the center of the column for the formation of actinolite-tremolite, but also apatite at the border of the endo-phlogopite. The occurrence of beryl is restricted to the most aluminous parts of the metasomatic zonation (plagioclase, endo-phlogopite, and exo-phlogopites proximal to the plagioclase). The inner part of the phlogopite zonation plays the role of a filter for the Be-bearing fluids and constitutes a very efficient “metasomatic trap” where the mobile behavior of Cr favored the formation of emerald. At Khaltaro in Pakistan, non-deformed pegmatites and quartz veins crosscut amphibolites, which were metasomatized on 20 cm-wide selvages that are symmetrically zoned around the veins [83], as found at Carnaíba (see Figure 14). Mass-balance calculations on the metasomatic column (Figure 37) have shown that (a) in the inner and intermediate metasomatic zones, K, F, H<sub>2</sub>O, B, Li, Rb, Cs, Be, Ta, Nb, As, Y, and Sr are gained and Si, Mg, Ca, Fe, Cr, V, and Sc are lost; and (b) in the outer zone, F, Li, Rb, Cs, and As are gained. The oxygen isotope composition of the hydrothermal minerals indicated the circulation of a single fluid of magmatic origin. At Kafubu, the regional metamorphic event pre-dates the emerald formation. The F-B-Li-rich phlogopites are located at the contact between tourmaline veins and pegmatites with Mg-metabasites. The pegmatites of the Lithium-Cesium-Tantalum family are linked to hidden fertile B-F-Nb-Ta-Li-Cs-rich granite.
3. These deposits sometimes exhibit multi-stage Be-mineralization, as observed at the Carnaíba deposit: A second minor stage of metasomatism affected in some areas the emerald-bearing phlogopites [15,90]. This stage is related to the intrusion of dyke swarms of quartz-muscovite veinlets with greisenisation of the granites, chloritisation, and muscovitisation of the phlogopites, general silicification, and muscovitisation of the plagioclases. This stage involves yellowish to whitish beryl, sometimes with molybdenite, scheelite, and schorlite.
4. These emerald mineralizations are interpreted to be due to the efficiency of the metasomatic trap rather than significant pre-enrichment in Be (5 to 11 ppm of Be in the Carnaíba granite). The occurrence of strong chemical gradients in the zone of preferential circulation of the solutions constitutes highly favorable conditions for the beryl crystallization.

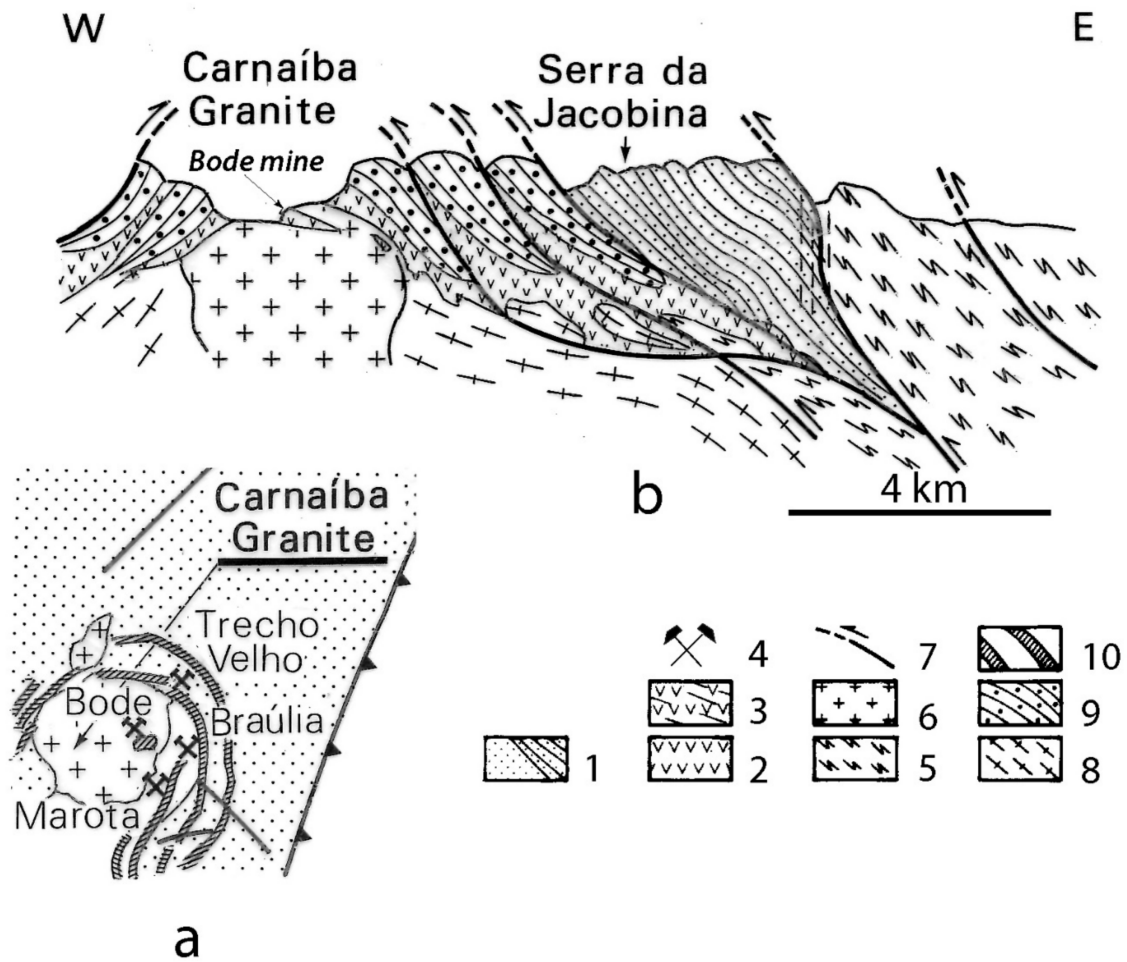


**Figure 36.** Schematic geological section of the emerald deposits of Carnaíba, Bahia state, Brazil: (a) The granite of Carnaíba and its emerald deposits cited in the present work. The Bode deposit is located in a roof-pendant of serpentinite present at the roof of the granite; (b) The Serra da Jacobina volcano-sedimentary sequence formed by intercalations of quartzite and serpentinite is crosscut by the Carnaíba granite. The pendants of serpentinite are present at the contact and on the roof of the granitic intrusion.

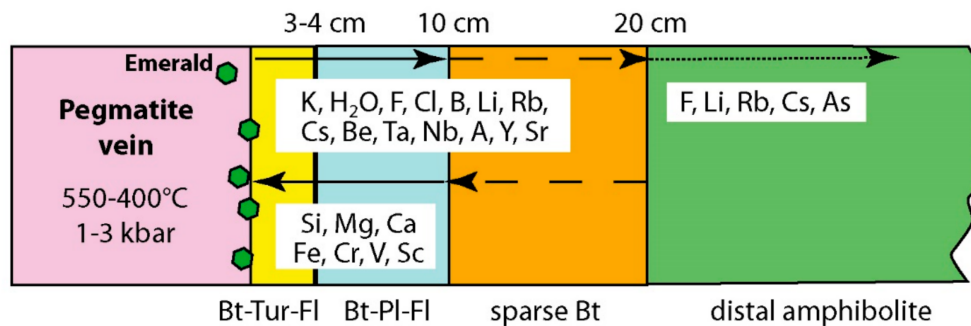


**Figure 37.** The Khaltaro emerald deposit, Nanga Parbat—Haramosh massif, Pakistan [83]. A symmetrically zoned metasomatic column is formed at the contact of the albitized pegmatites or hydrothermal quartz veins with amphibolite. The mass balance calculation in the metasomatized amphibolite indicates the gains and losses of components (see the transfers in the outer and inner zones). Emerald forms within the vein, near the contact with the altered amphibolite.

### 8.2. Multi-Stage Formation and Ages of Formation and Remobilization of Type IA Deposits

1. The Precambrian deposits located in the volcano-sedimentary series or greenstone belts are often folded and sheared, but metasomatic processes during emerald formation are generally coeval with the deformation, as in the deposits of Piteiras, Fazenda Bonfim, and Socotó (Brazil); Sumbawanga and Manyara (Tanzania); Kafubu (Zambia); and recently in the Gubaranda area from Eastern India [174].
2. The deposit at Sandawana in Zimbabwe [52,175] presents multi-stage formation; [169] advanced that the classical model of sub-Type IA cannot be applied. The Cs-Nb-Ta-bearing pegmatite veins that intruded UMR suffered the classical desilication with the formation of plagioclase. During folding, shearing, and regional metamorphism, after the albitisation of the pegmatites, a reactive F-P-Be-Li-rich fluid of pegmatitic origin circulated in a shear zone, affecting the albitites and reacting with the UMR, to form emerald-bearing phlogopites (Figure 38). Two generations of emerald are found: (i) Fine-grained crystals at the contact between albitite and phlogopite and (ii) euhedral gem crystals formed later in phlogopites either away from the albitite or in low-pressure zones next to the albitites. In that case, the albitites acted as incompetent levels, folded and sheared, and forming traps for euhedral emerald.

The syntectonic pegmatites yielded an age of  $2640 \pm 40$  Ma by U/Pb dating on monazite and an age of  $2600 \pm 100$  Ma by the Pb-Pb method on microlite [176]. The  $^{40}\text{Ar}/^{39}\text{Ar}$  dating on phlogopite and actinolite of the phlogopites yielded a very disturbed age spectra and variable total gas ages between 2225 and 2447 Ma, with relative plateau ages of 1903 Ma for the phlogopite and of 1936 Ma for the amphibole [52]. Two ages were proposed for the formation of emerald: (i) An Archean age at 2640 Ma, which is the age of the intrusion of the pegmatites, or (ii) a Proterozoic age at around 2000 Ma, which corresponds to a major tectono-metamorphic episode that affected the Limpopo belt formed around the Zimbabwe craton. Zwaan [52] opted for the first hypothesis, considering that the deformation at circa 2000 Ma modified the isotopic argon clock of mica and amphibole, but these integrated Ar-ages between 2200 and 2500 Ma correlate with the Archean thermal event. The complexity of dating rocks that suffered deformational events and remobilization of material illustrates the complexity of classifying ore deposits. The Sandawana deposit belongs to sub-type IA and its genetic link with a magmatic source is obvious in terms of chemical elements, but it could be re-classified as sub-type IID if the age of the emerald is considered to be younger than 2400 Ma.

3. The possible genesis of sub-type IIA deposits, such as those of Swat Valley, Santa Terezinha de Goiás, and Habachtal [168], was discussed previously. The presence of meta-pegmatites can be suspected based on either chemical data or O-H isotope composition of emerald and associated minerals, but has not been found up to now due to the tectonic regime (thrust and shear zone) and the level of observation. These deposits are classified as sub-type IIC based on the geological environment and are considered to be metamorphic with probable mixing of magmatic fluids (high Cs content for the Santa Terezinha emeralds). This hypothesis is strengthened by the Na/Li vs. Cs/Ga chemical diagram presented by Schwarz [65]. Figure 39 shows that these emerald deposits are grouped in one chemical field very different from those of Colombia, Russia, and Nigeria. They are characterized by a high Cs/Ga ratio, indicating appreciable to high amounts of Cs (magmatic source), and a high Na/Li ratio. The high Na content of this emerald is correlated with a high mean  $\text{H}_2\text{O}$  content in the channels, as, determined for Santa Terezinha de Goiás (2.9 wt.%,  $n = 5$ ), Habachtal (3.1 wt.%,  $n = 3$ ), and Swat Valley (3.4 wt.%,  $n = 1$ ) [15,16]. This is not just a coincidence, but is probably a genetic proxy Be-Cs source for emerald in these three deposits, i.e., magmatic sources with huge fluid circulation and metasomatism in a metamorphic environment.

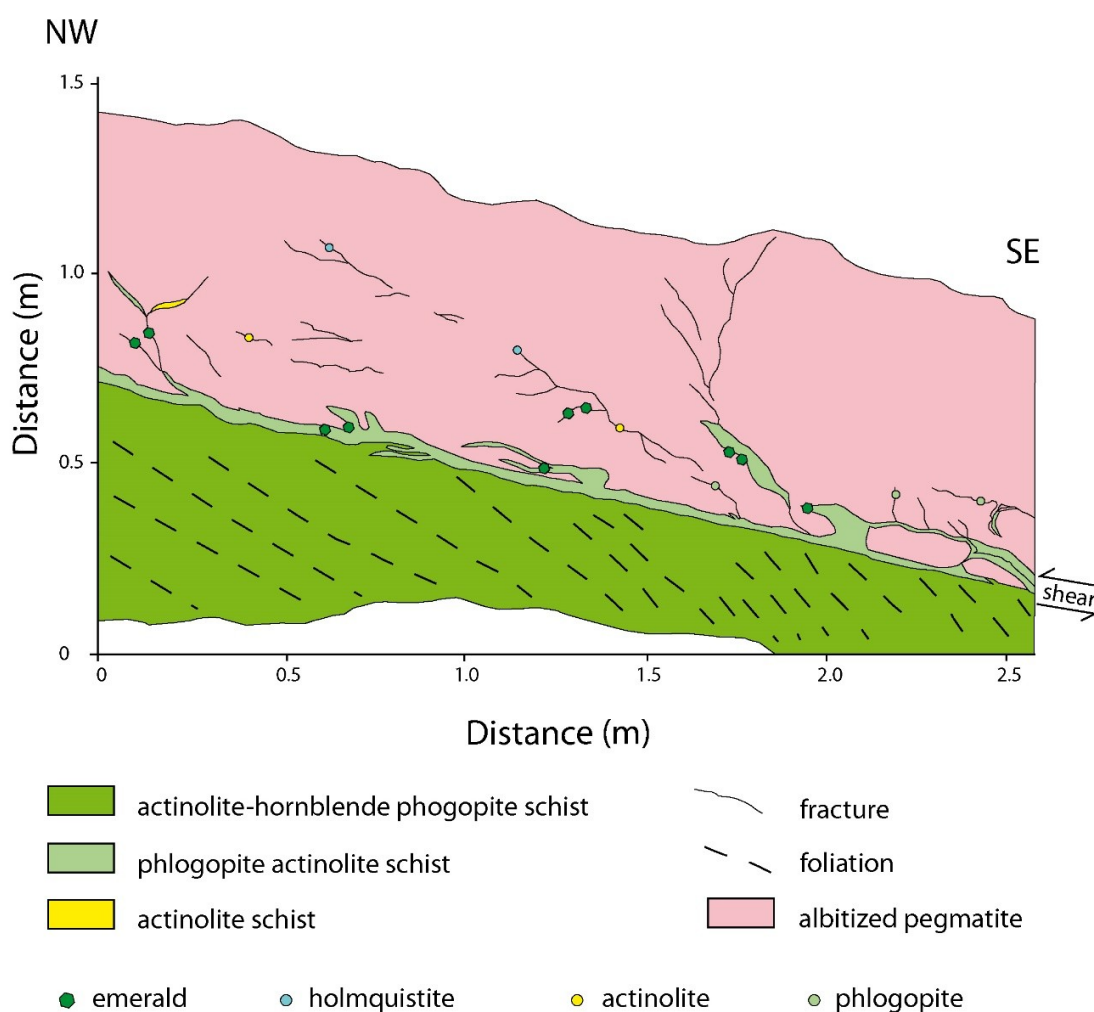


**Figure 38.** Cross-section of the mineralization at the Zeus underground mine, 200 ft. level, 26/28 stope, Sandawana deposit, Zimbabwe [167]. Fluids infiltrated along the schistosity of the actinolite-hornblende-phlogopite schist, and induced a metasomatic reaction with emerald formation at the foot wall of the pegmatite.

The Habachtal deposit is a complex deposit in terms of the genetic model and the previous discussion about the possible remobilization of Be-W enriched Hercynian pegmatites (possible sub-type IID deposit) by the regional metamorphism [168] opens the debate on the age of the formation of this deposit. The genesis of the emerald is metasomatic, but bound to the regional metamorphism of alpine age [77]. The K-Ar age obtained on phlogopite from the phlogopitites is 22 Ma, while the tracks of fission on apatite yielded ages of 9 Ma. The K-Ar age on muscovite from the muscovite schist is 27 Ma. The Rb/Sr dating realized on the zones of growth of garnets from the Schieferhülle formation, situated structurally above the Habach formation, indicated ages of crystallization between 62.0 and 30.2 Ma [177]. This age around 30 Ma is in agreement with the dates found for the end of the growth of garnet in the central Alps [178]. So, the best estimation established for the growth of the Habachtal emeralds would be situated around 30 Ma [179].

- The deposits of the Eastern desert in Egypt and Poona in Australia are good examples of sub-type IID, where sub-type IA deposits were remobilized by regional metamorphism with deformation and remobilization of older rocks, following the genetic model proposed by Grundmann and Morteani [77].

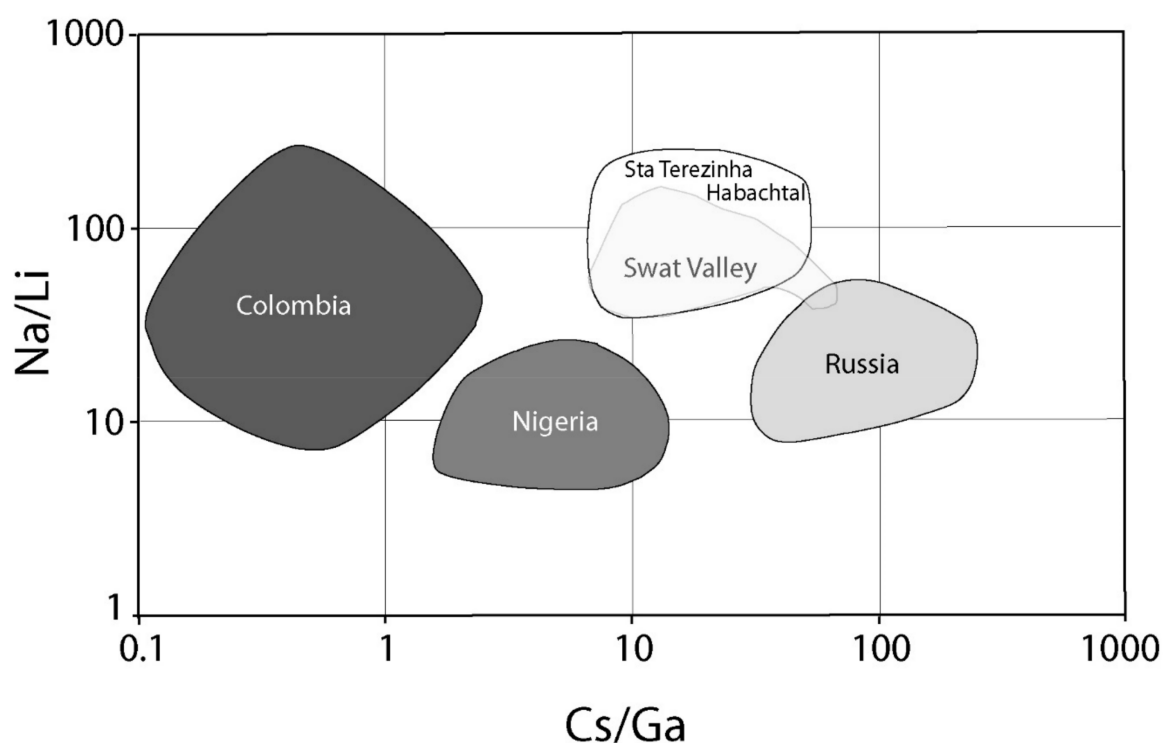


**Figure 39.** Cs/Ga versus Na/Li diagram of emeralds from Colombia, Nigeria, Russia, Pakistan, Austria, and Swat valley presented by Schwarz [65]. The diagram indicates that the chemical ratios of emerald from Santa Terezinha de Goiás (Brazil), Habachtal (Austria), and Swat valley (Pakistan) plot in the same population field. They are characterized by moderate to high Cs/Ga and very high Na/Li ratios. Discrepancies are observed for the concentrations of Cs and other elements when compared with the analysis presented by Aurisicchio et al. [23].

## 9. Exploration Now and in the Future

The majority of development of exploration methods for emerald has been for sub-type IIB deposits in Colombia. In Colombia, repeated washing of sediments is an effective and ubiquitous technique employed by local emerald-seeking “guaqueros” to reveal emerald in mineralized drainages. However, as pointed out by Lake [180], it is not effective to directly recover beryl by density separation because its specific gravity (~2.7) is similar to most rock-forming minerals. Geochemistry has also proven to be useful in Colombia. Escobar [181] studied the geology and geochemistry of the Gachalá area and found that Na enrichment and depletion of Li, K, Be, and Mo in the host rocks were very good indicators for locating mineralized areas. Beus [182] presented the results of a United Nations-sponsored geochemical survey of the streams draining emerald deposits in the Chivor and Muzo areas. The spatial distribution of areas with emerald mineralization was linked, on a regional scale, to intersections of the NNE- and NW-trending fault zones. The black shale units in those tectonic blocks that contain emerald mineralization were found to be enriched in CO<sub>2</sub>, Ca, Mg, Mn, and Na, and depleted in K, Si, and Al [182]. The results of this study were tested with a stream sediment sampling program in the Muzo area. The results showed that samples collected from emerald-bearing tectonic blocks had anomalously low K/Na ratios. Beus [182] also suggested using a “composite” geochemical ratio that takes into account the albitization and leaching phenomena:  $M = \text{Na}^3 / (\text{K} \times \text{Li} \times \text{Mo})$  (with Na and K in wt.% and Li and Mo in ppm) where *M* is an expression of the degree of metasomatic alteration. Other combinations, such as K, Li, Co or K, Li, Ba could be tried to determine the most contrasting value of *M* [182]. Subsequently, it was discovered that the Na content of the sediments was the best indicator of the mineralized zones in the drainage basins. Several new emerald occurrences were discovered by U.N. teams using the results of this study [183].

More recently, Ringsrud [183] reported that Colombian geologists were analyzing soil samples collected from altered tectonic blocks for Li, Na, and Pb to delineate emerald mineralization. Cheilletz et al. [103] showed that the Be content of black shale outside of the leached mineralized areas ranges from 2 to 6 ppm. Beryllium concentrations in the leached areas were found to range from 0.1 to 3.0 ppm [182]. Cheilletz and Giuliani [184] observed that the spatial coexistence of emerald districts and gypsum and anhydrite deposits could be used to prospect for new deposits.

Branquet et al. [107,113] observed that discovering new deposits will necessitate prospecting that is structurally oriented and focused on finding (1) the stratiform brecciated level in the eastern zone and (2) structural traps along regional tear faults in the western zone.

Geophysical techniques, such as induced polarization (IP) and magnetic surveys, have been used at Chivor and Muzo to delineate pyrite mineralization that is abundant and often associated with emerald-bearing veins [185]. Gutiérrez [186] tested several radiometric and magnetometric techniques at Chivor and Macanal deposits with some success.

Escobar [177] applied the criteria for emerald exploration in Colombia to stream sediment geochemical data for the Yukon and Northwest Territories in Canada. The criteria had to be adjusted for a number of factors, including the absence of Be in the Northwest Territories data and elevated Na due to plutonic alkali feldspar weathering into black shale drainages. Escobar [181] also noted that Colombian-type emerald deposits have relatively small footprints, and regional-scale geochemical surveys with data points 5–10 km apart may not be sufficient to show an emerald occurrence. Despite these constraints, Escobar [181] was able to identify several regions of interest.

With respect to other type II deposits, Arif et al. [187] observed that in the Swat valley in Pakistan, the emerald deposits occur in carbonate-altered ultramafic rocks, which also host Cr-rich dravite and “oxy-dravite”. They suggested that the presence of high-Cr magnesian tourmaline, particularly in magnesite–talc-altered ultramafic rocks, can represent a criterion for further emerald exploration in the lower Swat region of Pakistan and in other ultramafic-hosted emerald-producing regions worldwide.

Wise [188] suggested that the morphology of quartz, calcite, pyrite, and rutile crystals may serve as potential exploration guides for the discovery of hidden emerald deposits in the Hiddenite district of North Carolina. Emerald-bearing veins are characterized by: (1) quartz with multiple generations, including fine-grained doubly terminated crystals and very coarse-grained prismatic crystals; (2) calcite with largely rhombohedral habit, commonly accompanied by dolomite and siderite; (3) pyrite crystals dominated by octahedral faces; and (4) rutile that varies from single untwinned crystals to highly reticulated aggregates.

Some work has also been done in northwestern Canada to explore for type I deposits. Murphy et al. [189] plotted potential Be reservoirs and Cr and V reservoirs in the Yukon Territory and suggested that the best place to look is where the two come together. Lewis et al. [190] noted that all beryl occurrences in the Yukon Territory are intrusion-related, but for an intrusion to become enriched enough to reach Be-saturation to form beryl, it must be “ultrafractionated”.

Future efforts will move towards the development of more effective exploration guidelines that consider the geological factors responsible for emerald formation. For type I deposits, this could involve exploring continental collision domains and considering the overlaps of Be and Cr-V reservoirs, mineralogical and geochemical anomalies (F, K, Li, P, B) linked to high intensity fluid/rock interaction, and deposit location, e.g., proximal or distal to the granitic intrusive. This last point is an important one as illustrated by the Ianapera deposit in Madagascar [11,135] where emerald occurs in two different, but coeval settings: (1) A proximal one, formed classically at the contact between pegmatites (and quartz veins) and M-UMR; and (2) a distal one formed outside the roof of the granite, with emerald-bearing phlogopites in fractures and faults. The fluid percolation affected all the geological formations and different M-UMR, resulting in several types of zoned and un-zoned emerald habits with contrasting Cr-V chemistry.

## 10. Conclusions and Perspectives

The elaboration of a new classification proposed for emerald occurrences and deposits is the first step to building a new scheme for studying Be-mineralization from the field to the laboratory. The economic emerald deposits, in terms of volume and quality, are the Tectonic magmatic-related type hosted in M-UMR (Brazil, Zambia, Russia) or the Tectonic metamorphic-related type hosted in either low- (Colombia) to medium- (Afghanistan, China) temperature metamorphosed sedimentary rocks or medium-temperature metamorphosed M-UMR (Brazil, Pakistan).

The enhanced classification proposed in the present paper, based on objective geological criteria, takes into account the question of genesis of a number of deposits, which has been brought to the fore by research using new analytical facilities in the 21st century: The following topics were discussed: (i) Magmatic intrusives in M-UMR from classical intrusion to multi-stage formation through fluid circulation, metasomatism, and emerald formation synchronous with folding and shearing of regional metamorphic sequences; (ii) the presence of hidden intrusives that are probably the source of Be and Cs for emerald, such as in the Swat valley and Santa Terezinha de Goiás deposits; and (iii) metamorphic remobilization of previous Be-magmatic mineralization over several orogenic episodes, such as for the Habachtal and Egyptian emerald occurrences. All these cases reflect the mixing of magmatic and metamorphic fluids.

The present work, which connects geological knowledge of the formation of gem deposits to studies of the properties and features of individual gems, is a step forward in the great challenge of geographic origin determination. The enhanced classification typology for emerald deposits opens a new framework for mineral exploration guidelines.

**Author Contributions:** G.G., L.A.G., D.M., A.E.F., and Y.B. contributed with their field and laboratory work, and experience to the realization of this description of the state-of-the-art of the geology and genesis of emerald deposits and the proposal of the enhanced classification typology.

**Funding:** The present paper was realized without any direct funding. The work is based on the knowledge and funding obtained in the course of more than 20 years work on the geology of gems.

**Acknowledgments:** The authors acknowledge the three reviewers for their constructive comments. We thank very much the guest editors of the special issue “Mineralogy and Geochemistry of Gems”, namely Panagiotis Voudouris, Stefanos Karampelas, Vasilios Melfos, and Ian Graham for their invitation to present an extended review on emerald deposits. We acknowledge with thanks the editorial team of “Minerals” for their handling and the final layout. The authors want to thank Dietmar Schwarz, Vincent Pardieu, Victor Carillo, and Jean-Claude Michelou for their discussion and contribution of photographs. Gaston Giuliani wants to thank the Institut de Recherche pour le Développement (IRD, France) and the French CNRS and the Universities of Lorraine and Paul Sabatier (CRPG/CNRS-Université de Lorraine and GET/IRD-Université Paul Sabatier) for academic and financial support for research on the geology of gems over the past thirty years. The authors want to thank Mackenzie Parker for editing.

**Conflicts of Interest:** The authors declare no conflict of interest.

## References

1. Groat, L.; Giuliani, G.; Marshall, D.; Turner, D. Emerald. In *Geology of Gem Deposits*; Raeside, E.R., Ed.; Mineralogical Association of Canada, Short Course Series 44: Tucson, AZ, USA, 2014; pp. 135–174.
2. In the News. Gemfields’ October emerald auction: US\$21.5 million in sales. *Incolor* **2018**, *37*, 22.
3. Schmidt, S. Une des plus grandes émeraudes au monde a été découverte dans une mine en Zambie. Trust My Science, Nature. 2018. Available online: <https://trustmyscience.com> (accessed on 11 February 2019).
4. Ibbetson, R. Miner finds giant 5,655-carat emerald in Zambia worth up to £ 2m. *Daily Mail Online*, 30 October 2018.
5. Yager, Y.G.; Menzie, W.D.; Olson, D.W. *Weight of Production of Emeralds, Rubies, Sapphires, and Tanzanite from 1995 through 2005*; Open File Report 2008–1013; USGS Reston: Reston, VA, USA, 2008; 9p.
6. Wood, D.L.; Nassau, K. Characterization of beryl and emerald by visible and infrared absorption spectroscopy. *Am. Mineral.* **1968**, *53*, 777–800.
7. Damon, P.E.; Kulp, J.L. Excess helium and argon in beryl and other minerals. *Am. Mineral.* **1958**, *43*, 433–459.

8. Giuliani, G.; Marty, B.; Banks, D. Noble gases in fluid inclusions from emeralds: Implications for the origins of fluids and constraints on fluid-rock interactions. In Proceedings of the 18th Biennial Meeting of European Current Research on Fluid Inclusions, Siena, Italy, 4–5 July 2005. CD-ROM.
9. Charoy, B. Cristallogénèse du béryl: L'état des connaissances. In *L'Émeraude*; Giard, D., Giuliani, G., Cheilletz, A., Fritsch, E., Gonthier, E., Eds.; AFG-CNRS-ORSTOM Edition: Paris, France, 1998; pp. 47–54.
10. Schwarz, D.; Schmetzer, K. The definition of emerald: The green variety of beryl colored by chromium and/or vanadium. In *Emeralds of the World, (2002) ExtraLapis English No. 2: The Legendary Green Beryl*; Lapis International, LLC: East Hampton, CT, USA, 2002; pp. 74–78.
11. Andrianjakavah, P.R.; Salvi, S.; Béziat, D.; Rakotondrazafy, A.F.M.; Giuliani, G. Proximal and distal styles of pegmatite-related metasomatic emerald mineralization at Ianapera, southern Madagascar. *Miner. Deposita* **2009**, *44*, 817–835. [[CrossRef](#)]
12. Zwaan, J.C.; Jacob, D.E.; Häger, T.; Calvacanti Neto, M.T.O.; Kanis, J. Emeralds from the Fazenda Bonfim region, Rio Grande do Norte, Brazil. *Gems Gemol.* **2012**, *48*, 2–17. [[CrossRef](#)]
13. Rondeau, B.; Fritsch, E.; Peucat, J.J.; Nordru, F.S.; Groat, L.A. Characterization of emeralds from a historical deposit: Byrud (Eidsvoll), Norway. *Gems Gemol.* **2008**, *44*, 108–122. [[CrossRef](#)]
14. Artioli, G.; Rinaldi, R.; Stahl, K.; Zanazzi, P.F. Structure refinements of beryl by single-crystal neutron and X-ray diffraction. *Am. Mineral.* **1993**, *78*, 762–768.
15. Giuliani, G.; France-Lanord, C.; Zimmermann, J.-L.; Cheilletz, A.; Arboleda, C.; Charoy, B.; Coget, P.; Fontan, F.; Giard, D. Composition of fluids,  $\delta D$  of channel  $H_2O$  and  $\delta^{18}O$  of lattice oxygen in beryls: Genetic implications for Brazilian, Colombian and Afghanistani emerald deposits. *Int. Geol. Rev.* **1997**, *39*, 400–424. [[CrossRef](#)]
16. Marshall, D.; Downes, P.J.; Ellis, S.; Greene, R.; Loughrey, L.; Jones, P. Pressure–temperature–fluid constraints for the Poona emerald deposits, Western Australia: Fluid inclusion and stable isotope studies. *Minerals* **2016**, *6*, 130. [[CrossRef](#)]
17. Brand, A.A.; Groat, L.A.; Linnen, R.L.; Garland, M.I.; Breaks, F.W.; Giuliani, G. Emerald mineralization associated with the Mavis Lake Pegmatite Group, near Dryden, Ontario. *Can. Mineral.* **2009**, *47*, 315–336. [[CrossRef](#)]
18. Marshall, D.; Pardieu, V.; Loughrey, L.; Jones, P.; Xue, G. Conditions for emerald formation at Davdar, China: Fluid inclusion, trace element and stable isotope studies. *Mineral. Mag.* **2012**, *76*, 213–226. [[CrossRef](#)]
19. Loughrey, L.; Marshall, D.; Jones, P.; Millsted, P.; Main, A. Pressure–temperature–fluid constraints for the Emmaville–Torrington emerald deposit, New South Wales, Australia: Fluid inclusion and stable isotope studies. *Cent. Eur. J. Geosci.* **2012**, *4*, 287–299. [[CrossRef](#)]
20. Loughrey, L.; Marshall, D.; Ihlen, P.; Jones, P. Boiling as a mechanism for colour zonations observed at the Byrud emerald deposit, Eidsvoll, Norway: Fluid inclusion, stable isotope and Ar–Ar studies. *Geofluids* **2013**, *13*, 542–558. [[CrossRef](#)]
21. Lake, D.J.; Groat, L.; Falck, H.; Cempirek, J.; Kontak, D.; Marshall, D.; Giuliani, G.; Fayek, M. Genesis of emerald-bearing quartz veins associated with the Lened W-skarn mineralization, northwest territories, Canada. *Can. Mineral.* **2017**, *55*, 561–593. [[CrossRef](#)]
22. Santiago, J.S.; Souza, V.S.; Filgueiras de, B.C.; Jiménez, F.A.C. Emerald from the Fazenda Bonfim deposit, northeastern Brazil: Chemical, fluid inclusions and oxygen isotope data. *Braz. J. Geol.* **2018**, 1–16. [[CrossRef](#)]
23. Aurisicchio, C.; Conte, A.M.; Medeghini, L.; Ottolini, L.; De Vito, C. Major and trace element geochemistry of emerald from several deposits: Implications for genetic models and classification schemes. *Ore Geol. Rev.* **2018**, *94*, 351–366. [[CrossRef](#)]
24. Kovaloff, P. Geologist's report on Somerset emeralds. *S. Afr. Mining Eng. J.* **1928**, *39*, 101–103.
25. Zambonini, F.; Caglioto, V. Ricerche chimiche sulla roosterite di San Piero in Campo (Isola d'Elba) e sui berilli in generale. *Gazz. Chim. Ital.* **1928**, *58*, 131–152.
26. Leitmeier, H. Das Smaragdorkommen in Habachtal in Salzburg und seine Mineralien. *Tscher. Miner. Petrog.* **1937**, *49*, 245–368. [[CrossRef](#)]
27. Otero Muñoz, G.; Barriga Villalba, A.M. *Esmeraldas de Colombia*; Banco de la Republica: Bogotá, Colombia, 1948.
28. Simpson, E.S. *Minerals of Western Australia*; Government Printer: Perth, Australia, 1948; Volume 1, pp. 195–207.
29. Gübelin, E.J. Emeralds from Sandawana. *J. Gemmol.* **1958**, *6*, 340–354. [[CrossRef](#)]



30. Vlasov, K.A.; Kutakova, E.I. *Izumrudnye Kopi*; Moscow Akademiya Nauk SSSR: Moscow, Russia, 1960; 252p.
31. Martin, H.J. Some observations on southern Rhodesian emeralds and chrysoberyls. *Chamb. Mines J.* **1962**, *4*, 34–38.
32. Petrusenko, S.; Arnaudov, V.; Kostov, I. Emerald pegmatite from the Urdini Lakes, Rila Mountains. *Annuaire de l'Université de Sofia Faculté de Géologie et Géographie* **1966**, *59*, 247–268.
33. Beus, A.A.; Mineev, D.A. *Some Geological and Geochemical Features of the Muzo-Coscuez Emerald Zone, Cordillera Oriental, Colombia*; Empresa Colombiana de Minas, Biblioteca: Bogotá, Colombia, 1972; 55p.
34. Hickman, A.C.J. The Miku emerald deposit. *Geol. Surv. Zambia Econ. Rep.* **1972**, *27*, 35.
35. Garstone, J.D. The geological setting and origin of emeralds from Menzies, Western Australia. *J. R. Soc. West. Aust.* **1981**, *64*, 53–64.
36. Hanni, H.A.; Klein, H.H. Ein Smaragdorkommen in Madagaskar. *Zeitschrift der Deutschen Gemmologischen Gesellschaft* **1982**, *21*, 71–77.
37. Graziani, G.; Gübelin, E.; Lucchesi, S. The genesis of an emerald from the Kitwe District, Zambia. *Neues Jb. Miner. Monat.* **1983**, 175–186.
38. Kozłowski, A.; Metz, P.; Jaramillo, H.A.E. Emeralds from Sodomondoco, Colombia: Chemical composition, fluid inclusion and origin. *Neues Jb. Miner. Abh.* **1988**, *59*, 23–49.
39. Hammarstrom, J.M. Mineral chemistry of emeralds and some minerals from Pakistan and Afghanistan: An electron microprobe study. In *Emeralds of Pakistan*; Kazmi, A.H., Snee, L.W., Eds.; Van Nostrand Reinhold: New York, NY, USA, 1989; pp. 125–150.
40. Ottaway<sc>, T.L. The Geochemistry of the Muzo Emerald Deposit, Colombia. M.Sc. Thesis, University of Toronto, Toronto, ON, Canada, 1991.
41. Schwarz, D. Australian emeralds. *Austral. Gemmol.* **1991**, *17*, 488–497.
42. Schwarz, D.; Kanis, J.; Kinnaird, J. Emerald and green beryl from central Nigeria. *J. Gemmol.* **1996**, *25*, 117–141. [[CrossRef](#)]
43. Abdalla, H.M.; Mohamed, F.H. Mineralogical and geochemical investigations of beryl mineralizations, Pan-African belt of Egypt: Genetic and exploration aspects. *J. Afr. Earth Sci.* **1999**, *28*, 581–598. [[CrossRef](#)]
44. Gavrilenko, E.V.; Pérez, B.C. Characterisation of emeralds from the Delbegetey deposit, Kazakhstan. In *Mineral Deposits: Processes to Processing*; Stanley, C.J., Rankin, A.H., Bodnar, R.J., Naden, J., Yardley, B.W.D., Criddle, A.J., Hagni, R.D., Gize, A.P., Pasava, J., Eds.; Balkema: Rotterdam, The Netherlands, 1999; pp. 1097–1100.
45. Alexandrov, P.; Giuliani, G.; Zimmerman, J.L. Mineralogy, age and fluid geochemistry of the Rila Emerald deposits, Bulgaria. *Econ. Geol.* **2001**, *96*, 1469–1476. [[CrossRef](#)]
46. Groat, L.A.; Marshall, D.D.; Giuliani, G.; Murphy, D.C.; Piercey, S.J.; Jambor, J.L.; Mortensen, J.K.; Ercit, T.S.; Gault, R.A.; Mathey, D.P.; et al. Mineralogical and geochemical study of the Regal Ridge showing emeralds, southeastern Yukon. *Can. Mineral.* **2002**, *40*, 1313–1338. [[CrossRef](#)]
47. Marshall, D.D.; Groat, L.A.; Falck, H.; Douglas, H.L.; Giuliani, G. Fluid inclusions from the Lened emerald occurrence; Northwest Territories, Canada: Implications for Northern Cordilleran Emeralds. *Can. Mineral.* **2004**, *42*, 1523–1539. [[CrossRef](#)]
48. Vapnik, Y.; Sabot, B.; Moroz, I. Fluid inclusions in Ianapera emerald, Southern Madagascar. *Int. Geol. Rev.* **2005**, *47*, 647–662. [[CrossRef](#)]
49. Vapnik, Y.; Moroz, I.; Eliezri, I. Formation of emeralds at pegmatite-ultramafic contacts based on fluid inclusions in Kianjavato emerald, Mananjary deposits, Madagascar. *Mineral. Mag.* **2006**, *70*, 141–158. [[CrossRef](#)]
50. Zwaan, J.C.; Seifert, A.V.; Vrána, S.; Laurs, B.M.; Anckar, B.; Simons, W.B.S.; Falster, A.U.; Lustenhouwer, W.J.; Muhlmeister, S.; Koivula, J.K.; et al. Emeralds from the Kafubu area, Zambia. *Gems Gemol.* **2005**, *41*, 116–148. [[CrossRef](#)]
51. Gavrilenko, E.V.; Calvo Pérez, B.; Castroviejo Bolibar, R.; Garcia Del Amo, D. Emeralds from the Delbegetey deposit (Kazakhstan): Mineralogical characteristics and fluid-inclusion study. *Mineral. Mag.* **2006**, *70*, 159–173. [[CrossRef](#)]
52. Zwaan, J.C. Gemmology, geology and origin of the Sandawana emerald deposits, Zimbabwe. *Scr. Geol.* **2006**, *131*, 211.

53. Barton, M.D.; Young, S. Nonpegmatitic deposits of beryllium: Mineralogy, geology, phase equilibria and origin. In *Beryllium: Mineralogy, Petrology, and Geochemistry*; Grew, E.S., Ed.; Mineralogical Society of America: Washington, DC, USA, 2002; Volume 50, pp. 591–691.
54. Giuliani, G.; Bourlès, D.; Massot, J.; Siame, L.L. Colombian emerald reserves inferred from leached beryllium of their host black shale. *Explor. Min. Geol.* **1999**, *8*, 109–116.
55. Giuliani, G.; Branquet, Y.; Fallick, A.E.; Groat, L.; Marshall, D. Emerald deposits around the world, their similarities and differences. *InColor* **2015**, *special issue*, 56–69.
56. Sabot, B. Classification des gisements d'émeraude: Apports des études pétrographiques, minéralogiques et géochimiques. Thèse de Doctorat, Université de Nancy, Nancy, France, 2002.
57. Dereppe, J.M.; Moreaux, C.; Chauvaux, B.; Schwarz, D. Classification of emeralds by artificial neural networks. *J. Gemmol.* **2000**, *27*, 93–105. [[CrossRef](#)]
58. Schwarz, D.; Giuliani, G. Emerald deposits—A review. *Austral. Gemmol.* **2001**, *21*, 17–23.
59. Schwarz, D.; Giuliani, G.; Grundmann, G.; Glas, M. Die Entstehung der Smaragde, ein vieldiskutiertes Thema. In *Smaragd, der Kostbarste Beryll, der Teuerste Edelstein*; Schwarz, D., Hochlitner, R., Eds.; ExtraLapis: Charleston, SC, USA, 2001; pp. 68–73.
60. Schwarz, D.; Giuliani, G.; Grundmann, G.; Glas, M. The origin of emerald—A controversial topic. *ExtraLapis Engl.* **2002**, *2*, 18–21.
61. Schwarz, D.; Klemm, L. Chemical signature of emerald. *Int. Geol. Congr. Abstr.* **2012**, *34*, 2812.
62. Giuliani, G.; Groat, L.; Ohnenstetter, D.; Fallick, A.E.; Feneyrol, J. The geology of gems and their geographic origin. In *Geology of Gem Deposits*; Raeside, E.R., Ed.; Mineralogical Association of Canada, Short Course Series 44: Tucson, AZ, USA, 2014; pp. 113–134.
63. Saeseasaw, S.; Pardieu, V.; Sangsawong, S. Three-phase inclusions in emerald and their impact on origin determination. *Gems Gemol.* **2014**, *50*, 114–132.
64. Ochoa, C.J.C.; Daza, M.J.H.; Fortaleche, D.; Jiménez, J.F. Progress on the study of parameters related to the origin of Colombian emeralds. *InColor* **2015**, *special issue*, 88–97.
65. Schwarz, D. The geographic origin determination of emeralds. *InColor* **2015**, *special issue*, 98–105.
66. Hainschwang, T.; Notari, F. Standards and protocols for emerald analysis in gem testing laboratories. *InColor* **2015**, *special issue*, 106–114.
67. Giuliani, G. La spirale du temps de l'émeraude. *Règne Minéral* **2011**, *98*, 31–44.
68. Kinnaird, J.A. Hydrothermal alteration and mineralization of the alkaline anorogenic ring complexes of Nigeria. *J. Afr. Earth Sci.* **1985**, *3*, 229–251. [[CrossRef](#)]
69. Larsen, B.T.; Olaussen, S.; Sundvoll, B.; Heeremans, M. The Permo-Carboniferous Oslo Rift through six stages and 65 million years. *Episodes* **2008**, *31*, 52–58.
70. Seifert, A.V.; Žaček, V.; Vrána, S.; Pecina, V.; Zachariáš, J.; Zwaan, J.C. Emerald mineralization in the Kafubu area, Zambia. *Bull. Geosci.* **2004**, *79*, 1–40.
71. Bastos, F.M. Emeralds from Itabira, Minas Gerais, Brazil. *Lapid. J.* **1981**, *35*, 1842–1848.
72. Hänni, H.A.; Schwarz, D.; Fischer, M. The emeralds of the Belmont mine, Minas Gerais, Brazil. *J. Gemmol.* **1987**, *20*, 446–456. [[CrossRef](#)]
73. de Souza, J.L.; Mendes, J.C.; da Silveira Bello, R.M.; Svisero, D.P.; Valarelli, J.V. Petrographic and microthermometrical studies of emeralds in the “Garimpo” of Capoeirana, Nova Era, Minas Gerais State, Brazil. *Miner. Deposita* **1992**, *27*, 161–168. [[CrossRef](#)]
74. Rondeau, B.; Notari, F.; Giuliani, G.; Michelou, J.-C.; Martins, S.; Fritsch, E.; Respingier, A. La mine de Piteiras, Minas Gerais, nouvelle source d'émeraude de belle qualité au Brésil. *Rev. Gemmol. AFG* **2003**, *148*, 9–25.
75. Walton, L. *Exploration Criteria for Colored Gemstone Deposits in Yukon*; Open file 2004-10; Geological Survey of Canada: Ottawa, ON, Canada, 2004; 184p.
76. Giuliani, G.; Cheilletz, A.; Zimmermann, J.-L.; Ribeiro-Althoff, A.M.; France-Lanord, C.; Féraud, G. Les gisements d'émeraude du Brésil: Genèse et typologie. *Chron. Rech. Min. BRGM* **1997**, *526*, 17–60.
77. Grundmann, G.; Morteani, G. Emerald mineralization during regional metamorphism: The Habachtal (Austria) and Leydsdorp (Transvaal, South Africa) deposits. *Econ. Geol.* **1989**, *84*, 1835–1849. [[CrossRef](#)]
78. Rudowski, L.; Giuliani, G.; Sabaté, P. Les phlogopitites à émeraude au voisinage des granites de Campo Formoso et Carnaíba (Bahia, Brésil): Un exemple de minéralisation protérozoïque à Be, Wo et W dans les ultrabasiques métasomatisées. *C. R. Acad. Sci.* **1987**, *304*, 1129–1134.

79. Rudowski, L. Pétrologie et géochimie des granites transamazoniens de Campo Formoso et Carnaíba (Bahia, Brésil) et des phlogopitites à émeraude associées. Thèse de Doctorat, Université Paris VI, Paris, France, 1989.
80. Muñoz, J.L. F-OH and Cl-OH exchange in micas with applications to hydrothermal ore deposits. In *Micas*; Bailey, S.W., Ed.; Mineralogical Society of America: Washington, DC, USA, 1984; Volume 13, pp. 469–493.
81. Guy, B. Contribution à l'étude des skarns de Costabonne (Pyrénées orientales, France) et à la théorie de la zonation métasomatique. Ph.D. Thesis, Université de Paris VI, Paris, France, 1979.
82. Korzhinskii, D.S. The theory of systems with perfectly mobile components and processes of mineral formation. *Am. J. Sci.* **1965**, *263*, 193–205. [[CrossRef](#)]
83. Laurs, B.M.; Dilles, J.H.; Snee, L.W. Emerald mineralization and metasomatism of amphibolite, Khaltaro granitic pegmatite hydrothermal vein system, Haramosh mountains, northern Pakistan. *Can. Mineral.* **1996**, *34*, 1253–1286.
84. Grundmann, G.; Morteani, G. Ein neues Vorkommen von Smaragd, Alexandrit, Rubin und Saphir in einem Topas-führenden Phlogopit-felds von Poona, Cue District, West Australien. *Zeitschrift der Deutschen Gemmologischen Gesellschaft* **1995**, *44*, 11–31.
85. Xue, G.; Marshall, D.; Zhang, S.; Ullrich, T.D.; Bishop, T.; Groat, L.A.; Thorkelson, D.J.; Giuliani, G.; Fallick, A.E. Conditions for early Cretaceous emerald formation at Dyakou, China: Fluid inclusion, Ar-Ar, and stable isotope studies. *Econ. Geol.* **2010**, *105*, 339–349. [[CrossRef](#)]
86. Kazmi, A.H.; Snee, L.W. Geology of the world emerald deposits: A brief review. In *Emeralds of Pakistan: Geology, Gemology and Genesis*; Kazmi, A.H., Snee, L.W., Eds.; Van Nostrand Reinhold Company: New York, NY, USA, 1989; pp. 165–228.
87. Martins, S. Brazilian emeralds. In Proceedings of the Oral Communication, II World Emerald Symposium, Bogotá, Colombia, 12–14 October 2018.
88. Biondi, J.C. Depósitos de esmeralda de Santa Terezinha (GO). *Rev. Bras. Geociências* **1990**, *20*, 7–24. [[CrossRef](#)]
89. Gusmão Costa, S.A. de Correlação da seqüência encaixante das esmeraldas de Santa Terezinha de Goiás com os terrenos do tipo greenstone belt de Crixás e tipologia dos depósitos. In Proceedings of the Boletim de Resumos Expandidos XXXVIII Congresso Brasileiro de Geologia Goiânia, Goiás, Brazil, 1986; Volume 2, pp. 597–614.
90. Giuliani, G.; D'El-Rey Silva, L.J.; Couto, P.A. Origin of emerald deposits of Brazil. *Miner. Deposita* **1990**, *25*, 57–64. [[CrossRef](#)]
91. D'el-Rey Silva, L.J.H.; Giuliani, G. Controle estrutural da jazida de esmeraldas de Santa Terezinha de Goiás: Implicações na gênese, na tectônica regional e no planejamento de lavra. In Proceedings of the Boletim de Resumos Expandidos XXXV Congresso Brasileiro de Geologia, Belém, PA, Brazil; 1988; Volume 1, pp. 413–427.
92. D'el-Rey Silva, L.J.H.; de Barros Neto, L.S. The Santa Terezinha-Campos Verdes emerald district, central Brazil: Structural and Sm-Nd data to constrain the tectonic evolution of the Neoproterozoic Brasília belt. *J. S. Am. Earth Sci.* **2002**, *15*, 693–708. [[CrossRef](#)]
93. Morteani, G.; Grundmann, G. The emerald porphyroblasts in the penninic rocks of the central Tauern Window. *Neues Jb. Miner. Monat.* **1977**, *11*, 509–516.
94. Grundmann, G. Polymetamorphose und Abschätzung der Bildungsbedingungen der smaragd-führenden gesteinsserien der leckbachscharte, Habachtal, Österreich. *Fortschr. Mineral.* **1980**, *58*, 39–41.
95. Grundmann, G.; Morteani, G. Die geologie des smaragd-vorkommens im Habachtal (Land Salzburg, Österreich). *Archiv. Lagerstättenforsch. Geol. Bundesanst* **1982**, *2*, 71–107.
96. Nwe, Y.Y.; Grundmann, G. Evolution of metamorphic fluids in shear zones: The record from the emeralds of Habachtal, Tauern window, Austria. *Lithos* **1990**, *25*, 281–304. [[CrossRef](#)]
97. Trumbull, R.B.; Krienitz, M.-S.; Grundmann, G.; Wiedenbeck, M. Tourmaline geochemistry and  $\delta^{11}\text{B}$  variations as a guide to fluid-rock interaction in the Habachtal emerald deposit, Tauern window, Austria. *Contrib. Mineral. Petr.* **2009**, *157*, 411–427. [[CrossRef](#)]
98. Bowersox, G.; Snee, L.W.; Foord, E.E.; Seal, R.R., II. Emeralds of the Panjsher Valley, Afghanistan. *Gems Gemol.* **1991**, *27*, 26–39. [[CrossRef](#)]
99. Hussain, S.S.; Chaudhry, M.N.; Dawood, H. Emerald mineralization of Barang, Bajaur Agency, Pakistan. *J. Gemmol.* **1993**, *23*, 402–408. [[CrossRef](#)]

100. Dilles, J.H.; Snee, L.W.; Laurs, B.M. Geology, Ar-Ar age and stable isotopes geochemistry of suture-related emerald mineralization, Swat, Pakistan, Himalayas. In Proceedings of the Geological Society of America, Annual Meeting, Seattle, WA, USA, 1994; Abstracts. Volume 26, p. A-311.
101. Arif, M.; Fallick, A.E.; Moon, C.J. The genesis of emeralds and their host rocks from Swat, northwestern Pakistan: A stable-isotope investigation. *Miner. Deposita* **1996**, *31*, 255–268. [[CrossRef](#)]
102. Arif, M.; Henry, D.J.; Moon, C.J. Host rock characteristics and source of chromium and beryllium for emerald mineralization in the ophiolitic rocks of the Indus suture zone in Swat, NW Pakistan. *Ore Geol. Rev.* **2011**, *39*, 1–20. [[CrossRef](#)]
103. Cheilletz, A.; Féraud, G.; Giuliani, G.; Rodriguez, C.T. Time-pressure-temperature formation of Colombian emerald: An  $^{40}\text{Ar}/^{39}\text{Ar}$  laser-probe and fluid inclusion-microthermometry contribution. *Econ. Geol.* **1994**, *89*, 361–380. [[CrossRef](#)]
104. Ottaway, T.L.; Wicks, F.J.; Bryndzia, L.T.; Kyser, T.K.; Spooner, E.T.C. Formation of the Muzo hydrothermal emerald deposit in Colombia. *Nature* **1994**, *369*, 552–554. [[CrossRef](#)]
105. Banks, D.; Giuliani, G.; Yardley, B.W.D.; Cheilletz, A. Emerald mineralisation in Colombia: Fluid chemistry and the role of brine mixing. *Miner. Deposita* **2000**, *35*, 699–713. [[CrossRef](#)]
106. Cheilletz, A.; Giuliani, G.; Branquet, Y.; Laumonier, B.; Sanchez, A.J.M.; Féraud, G.; Arhan, T. Datation K-Ar et  $^{40}\text{Ar}/^{39}\text{Ar}$  à  $65 \pm 3$  Ma des gisements d'émeraude du district de Chivor-Macanal: Argument en faveur d'une déformation précoce dans la Cordillère Orientale de Colombie. *C. R. Acad. Sci.* **1997**, *324*, 369–377.
107. Branquet, Y.; Cheilletz, A.; Giuliani, G.; Laumonier, B. Fluidized hydrothermal breccia in dilatant faults during thrusting: The Colombian emerald deposits case. In *Fractures, Fluid Flow and Mineralization*; McCaffrey, K.J.W., Lonergan, L., Wilkinson, J.J., Eds.; Geological Society London: London, UK, 1999; Volume 155, pp. 183–195.
108. Branquet, Y.; Giuliani, G.; Cheilletz, A.; Laumonier, B. Colombian emeralds and evaporites: Tectono-stratigraphic significance of a regional emerald-bearing evaporitic breccia level. In Proceedings of the 13th SGA Biennial Meeting, Nancy, France, 24–27 August 2015; Volume 4, pp. 1291–1294.
109. Cooper, M.A.; Addison, F.T.; Alvarez, R.; Coral, M.; Graham, R.; Hayward, A.B.; Howe, S.; Martinez, J.; Naar, J.; Pena, R.; et al. Basin development and tectonic history of the Llanos basin, Eastern Cordillera, and Middle Magdalena valley, Colombia. *AAPG Bull.* **1995**, *79*, 1421–1443.
110. Branquet, Y.; Cheilletz, A.; Cobbold, P.R.; Baby, P.; Laumonier, B.; Giuliani, G. Andean deformation and rift inversion, eastern edge of Cordillera Oriental (Guatèque, Medina area), Colombia. *J. S. Am. Earth Sci.* **2002**, *15*, 391–407. [[CrossRef](#)]
111. Bayona, G.; Cortès, M.; Jaramillo, C.; Ojeda, G.; Aristizabal, J.J.; Harker, A.R. An integrated analysis of an orogen-sedimentary basin pair: Latest Cretaceous (Cenozoic evolution of the linked Eastern Cordillera orogen and the Llanos foreland basin of Colombia. *Geol. Soc. Am. Bull.* **2008**, *120*, 1171–1197. [[CrossRef](#)]
112. Laumonier, B.; Branquet, Y.; Lopès, B.; Cheilletz, A.; Giuliani, G.; Rueda, F. Mise en évidence d'une tectonique compressive Eocène-Oligocène dans l'Ouest de la Cordillère orientale de Colombie, d'après la structure en duplex des gisements d'émeraude de Muzo et de Coscuez. *C. R. Acad. Sci.* **1996**, *323*, 705–712.
113. Branquet, Y.; Laumonier, B.; Cheilletz, A.; Giuliani, G. Emeralds in the Eastern Cordillera of Colombia: Two tectonic settings for one mineralization. *Geology* **1999**, *27*, 597–600. [[CrossRef](#)]
114. Pignatelli, I.; Giuliani, G.; Ohnenstetter, D.; Agrosi, G.; Mathieu, S.; Morlot, C.; Branquet, Y. Colombian trapiche emeralds: Recent advances in understanding their formation. *Gems Gemol.* **2015**, *51*, 222–259. [[CrossRef](#)]
115. Giuliani, G.; France-Lanord, C.; Cheilletz, A.; Coget, P.; Branquet, Y.; Laumonier, B. Sulfate reduction by organic matter in Colombian emerald deposits: Chemical and stable isotope (C, O, H) evidence. *Econ. Geol.* **2000**, *95*, 1129–1153. [[CrossRef](#)]
116. Bosshart, G. Emeralds from Colombia. *J. Gemmol.* **1991**, *22*, 409–425. [[CrossRef](#)]
117. Hewton, M.L.; Marshall, D.D.; Ootes, L.; Loughrey, L.E.; Creaser, R.A. Colombian-style emerald mineralization in the northern Canadian Cordillera: Integration into a regional Paleozoic fluid flow regime. *Can. J. Earth Sci.* **2013**, *50*, 857–871. [[CrossRef](#)]
118. Keith, J.D.; Thompson, T.J.; Ivers, S. The Uinta emerald and the emerald-bearing potential of the Red Pine shale, Uinta Mountains, Utah. *Geol. Soc. Am. Abstr. Program* **1996**, *28*, 85.

119. Keith, J.D.; Nelson, S.T.; Thompson, T.J.; Dorais, M.J.; Olcott, J.; Duerichen, E.; Constenius, K.N. The genesis of fibrous calcite and shale-hosted emerald in a nonmagmatic hydrothermal system, Uinta mountains, Utah. *Geol. Soc. Am. Abstr. Program* **2002**, *34*, 55.
120. Nelson, S.T.; Keith, J.D.; Constenius, K.N.; Duerichen, E.; Tingey, D.G. Genesis of fibrous calcite and emerald by amagmatic processes in the southwestern Uinta Mountains, Utah. *Rocky Mt. Geol.* **2008**, *43*, 1–21. [[CrossRef](#)]
121. Tapponnier, P.; Mattauer, M.; Proust, F.; Cassaigneau, C. Mesozoic ophiolites, sutures, and large-scale tectonic movements in Afghanistan. *Earth Planet. Sci. Lett.* **1981**, *52*, 335–371. [[CrossRef](#)]
122. Sabot, B.; Cheilletz, A.; de Donato, P.; Banks, D.; Levresse, G.; Barrès, O. Afghan emeralds face Colombian cousins. *Chron. R. Min. BRGM* **2000**, *541*, 111–114.
123. Sabot, B.; Cheilletz, A.; de Donato, P.; Banks, D.; Levresse, G.; Barrès, O. The Panjsher-Afghanistan emerald deposit: New field and geochemical evidence for Colombian style mineralisation. In Proceedings of the European Union Geoscience XI, Strasbourg, France, 8–13 April 2001; Section OS 06. p. 548.
124. An, Y. The geological characteristics of the emerald deposit in Tashen Kuergan, Xinjiang. *Xinjiang Non-Ferrous Met.* **2009**, *29*, 9–10.
125. Wise, M.A. New finds in North Carolina. *ExtraLapis Engl.* **2002**, *2*, 64–65.
126. Speer, W.E. Hiddenite district, Alexander Co, North Carolina. In Fieldtrip Guidebook. In *Proceedings of the Southeastern Section 57th Annual Meeting*; Charlotte, NC, USA, 10–11 April 2008, The Geological Society of America: Boulder, CO, USA, 2008; 28p.
127. Wise, M.A.; Anderson, A.J. The emerald- and spodumene-bearing quartz veins of the Rist emerald mine, Hiddenite, North Carolina. *Can. Mineral.* **2006**, *44*, 1529–1541. [[CrossRef](#)]
128. Grundmann, G.; Morteani, G. “Smaragdminen der Cleopatra”: Zabara, Sikait und Umm Kabo in Ägypten. *Lapis* **1993**, *7–8*, 27–39.
129. Grundmann, G.; Morteani, G. Emerald formation during regional metamorphism: The Zabara, Sikeit and Umm Kabo deposits (Eastern Desert, Egypt). In *Geoscientific Research in Northeast Africa*; Schandemeier, T., Ed.; A.A. Balkema: Rotterdam, The Netherlands, 1993; pp. 495–498.
130. Grundmann, G.; Morteani, G. Multi-stage emerald formation during Pan-African regional metamorphism: The Zabara, Sikait, Umm Kabo deposits, South Eastern desert of Egypt. *J. Afr. Earth Sci.* **2008**, *50*, 168–187. [[CrossRef](#)]
131. Surour, A.A.; Takla, M.A.; Omar, S.A. EPR spectra and age determination of beryl from the Eastern Desert of Egypt. *Ann. Geol. Surv. Egypt* **2002**, *25*, 389–400.
132. Giuliani, G.; France-Lanord, C.; Coget, P.; Schwarz, D.; Cheilletz, A.; Branquet, Y.; Giard, D.; Pavel, A.; Martin-Izard, A.; Piat, D.H. Oxygen isotope systematics of emerald—Relevance for its origin and geological significance. *Miner. Deposita* **1998**, *33*, 513–519. [[CrossRef](#)]
133. Duarte, L.D.C.; Pulz, G.M.; D’el-Rey Silva, L.J.H.; Ronchi, L.H.; de Brun, T.M.M.; Juchem, P.L. Microtermometria das inclusões fluidas na esmeralda do distrito mineiro de Campos Verdes, Goiás. In *Caracterização e Modelamento de depósitos Minerais*; Ronchi, L.H., Althoff, F.J., Eds.; Eitoras Unisinos: São Leopoldo, RS, Brazil, 2003; pp. 267–292.
134. Olivera, J.A.P.; Ali, S.H. Gemstone mining as a development cluster: A study of Brazil’s emerald mines. *Resour. Policy* **2011**, *36*, 132–141. [[CrossRef](#)]
135. Salvi, S.; Giuliani, G.; Andrianjakavah, P.R.; Moine, B.; Beziat, D.; Fallick, A.E. Fluid inclusion and stable isotope constraints on the formation of the Ianapera emerald deposit, Southern Madagascar. *Can. Mineral.* **2017**, *55*, 619–650. [[CrossRef](#)]
136. de Wit, M.J.; Hart, R.A.; Hart, R.J. The Jamestown ophiolite complex, Barberton mountain belt: A section through 3.5 Ga oceanic crust. *J. Afr. Earth Sci.* **1987**, *6*, 681–730. [[CrossRef](#)]
137. Biondi, J.C.; Poidevin, J.L. Idade da mineralização e da sequência Santa Terezinha (Goiás, Brasil). In Proceedings of the Boletim de Resumos Espandidos XXXVIII Congresso Brasileiro de Geologia, Camboriú, Brasil, 23–28 October 1994; pp. 302–304.
138. Ribeiro-Althoff, A.M.; Cheilletz, A.; Giuliani, G.; Féraud, G.; Barbosa Camacho, G.; Zimmermann, J.L. Evidences of two periods (2 Ga and 650–500 Ma) of emerald formation in Brazil by K-Ar and <sup>40</sup>Ar/<sup>39</sup>Ar dating. *Int. Geol. Rev.* **1997**, *39*, 924–937. [[CrossRef](#)]
139. Calligaro, T.; Dran, J.-C.; Poirot, J.-P.; Querré, G.; Salomon, J.; Zwaan, J.C. PIXE/PIGE characterization of emeralds using an external micro-beam. *Nucl. Instrum. Meth. B* **2000**, *161–163*, 769–774. [[CrossRef](#)]

140. Höll, R.; Maucher, A.; Westenberger, H. Synsedimentary diagenetic ore fabrics in the strata- and time-bound scheelite deposits of Kleinarltal and Felbertal in the Eastern Alps. *Miner. Deposita* **1972**, *7*, 217–226. [[CrossRef](#)]
141. Raith, J.G.; Montanuiversität Leoben, Austria. Personal communication, 2010.
142. Kozlik, M.; Raith, J.G.; Gerdes, A. U-Pb, Lu-Hf and trace element characteristics of zircon from the Felbertal scheelite deposit (Austria): New constraints on timing and source of W mineralization. *Chem. Geol.* **2016**, *421*, 112–126. [[CrossRef](#)]
143. Maluski, H.; Matte, P. Ages of alpine tectonometamorphic events in the northwestern Himalaya (northern Pakistan) by  $^{39}\text{Ar}/^{40}\text{Ar}$  method. *Tectonophysics* **1984**, *3*, 1–18.
144. Grundmann, G.; Morteani, G. Alexandrite, emerald, sapphire, ruby and topaz in a biotite-phlogopite fels from the Poona, Cue district, Western Australia. *Austral. Gemmol.* **1998**, *20*, 159–167.
145. Vapnik, Y.; Moroz, I. Fluid inclusions in Panjshir emerald (Afghanistan). In Proceedings of the 16th European Current Research on Fluid Inclusions, Faculdade de Ciências do Porto, Porto, Portugal, 17–20 July 2001; Noronha, F., Doria, A., Guedes, A., Eds.; Memoria n° 7: New York, NY, USA; pp. 451–454.
146. Lapointe, M.; Anderson, A.J.; Wise, M. Fluid inclusion constraints on the formation of emerald-bearing quartz veins at the Rist tract, Heddenite, North Carolina. *Atl. Geol. Abstr.* **2004**, *4*, 146.
147. Diamond, L.W. Introduction to gas-bearing aqueous fluid inclusions. In *Fluid Inclusions: Analysis and Interpretation*; Samson, I., Anderson, A., Marshall, D., Eds.; Mineralogical Association of Canada: Quebec City, QC, Canada, 2003; Volume 32, pp. 101–158.
148. Bodnar, R.J. Introduction to aqueous-electrolyte fluid inclusions. In *Fluid Inclusions: Analysis and Interpretation*; Samson, I., Anderson, A., Marshall, D., Eds.; Mineralogical Association of Canada: Quebec City, QC, Canada, 2003; Volume 32, pp. 81–100.
149. Audétat, A.; Gunter, D.; Heinrich, C. Formation of a magmatic-hydrothermal ore deposit: Insights with LA-ICP-MS analysis of fluid inclusions. *Science* **2012**, *279*, 2091–2094.
150. Diamond, L.W.; Marshall, D.; Jackman, J.; Skippen, G.B. Elemental analysis of individual fluid inclusions in minerals by Secondary Ion Mass Spectrometry (SIMS): Application to cation ratios of fluid inclusions in an Archaean mesothermal gold-quartz vein. *Geochim. Cosmochim. Acta* **1990**, *54*, 545–552. [[CrossRef](#)]
151. Rosasco, G.; Roedder, E.; Simmons, J. Laser-excited Raman spectroscopy for non-destructive analysis of individual phases in fluid inclusions in minerals. *Science* **1975**, *190*, 557–560. [[CrossRef](#)]
152. Delhaye, M.; Dhamelincourt, P. Raman microprobe and microscope with Laser excitation. *J. Raman Spectrosc.* **1975**, *3*, 33–43. [[CrossRef](#)]
153. Dhamelincourt, P.; Schubnel, H. La microsonde moléculaire à laser et son application à la minéralogie et la gemmologie. *Rev. Gemmol. AFG* **1977**, *52*, 11–14.
154. Burruss, R.C. Raman spectroscopy of fluid inclusions. In *Fluid Inclusions: Analysis and Interpretation*; Samson, I., Anderson, A., Marshall, D., Eds.; Mineralogical Association of Canada: Quebec City, QC, Canada, 2003; Volume 32, pp. 279–290.
155. Burke, E.A.J. Raman microspectrometry of fluid inclusions. *Lithos* **2001**, *55*, 139–158. [[CrossRef](#)]
156. Taylor, R.; Fallick, A.; Breaks, F. Volatile evolution in Archean rare-element granitic pegmatites: Evidence from the hydrogen-isotopic composition of channel H<sub>2</sub>O in beryl. *Can. Mineral.* **1992**, *30*, 877–893.
157. Marshall, D.; Meisser, N.; Ellis, S.; Jones, P.; Bussy, F.; Mumenthaler, T. Formational conditions for the Binntal emerald occurrence, Valais, Switzerland: Fluid inclusion, chemical composition and stable isotope studies. *Can. Mineral.* **2017**, *55*, 725–741. [[CrossRef](#)]
158. Groat, L.A.; Giuliani, G.; Marshall, D.D.; Turner, D. Emerald deposits and occurrences: A review. *Ore Geol. Rev.* **2008**, *34*, 87–112. [[CrossRef](#)]
159. Sheppard, S.M.F. Characterization and isotopic variations in natural waters. In *Stable Isotopes in High Temperature Geological Processes*; Valley, J.W., Taylor, H.P., O’Neil, J.R., Eds.; Mineralogical Association of America: Chantilly, VA, USA, 1986; Volume 16, pp. 165–183.
160. Giuliani, G.; Dubessy, J.; Ohnenstetter, D.; Banks, D.; Branquet, Y.; Feneyrol, J.; Fallick, A.E.; Martelat, E. The role of evaporites in the formation of gems during metamorphism of carbonate platforms: A review. *Miner. Deposita* **2017**, *53*, 1–20. [[CrossRef](#)]
161. Yardley, B.W.D.; Bodnar, R.J. Fluids in the Continental Crust. *Geochem. Perspect.* **2014**, *3*, 1–127. [[CrossRef](#)]
162. Yardley, B.W.D.; Cleverley, J.S. *The Role of Metamorphic Fluids in the Formation of Ore Deposits*; Geological Society: London, UK, 2013; pp. 1–393.

163. Williams, A.E.; McKibben, M.A. A brine interface in the Salton Sea Geothermal System, California: Fluid geochemical and isotopic characteristics. *Geochim. Cosmochim. Acta* **1989**, *53*, 1905–1920. [[CrossRef](#)]
164. Bohlke, J.K.; Irwin, J.J. Laser microprobe analyses of Cl, Br, I, and K in fluid inclusions: Implications for sources of salinity in some ancient hydrothermal fluids. *Geochim. Cosmochim. Acta* **1992**, *56*, 203–225. [[CrossRef](#)]
165. Poujol, M.; Robb, L.J.; Respaut, J.P. Origin of gold and emerald mineralization in the Murchinson greenstone belt, Kaapval craton, South Africa. *Mineral. Mag.* **1998**, *62A*, 1206–1207. [[CrossRef](#)]
166. Beus, A.A. *Geochemistry of Beryllium and Genetic Types of Beryllium Deposits*; W.H. Freeman: San Francisco, CA, USA; London, UK, 1966; 401p.
167. Smirnov, V.L. Deposits of beryllium. In *Ore deposits of the U.S.S.R.*; Pitman Publications: London, UK, 1977; Volume 3, pp. 320–371.
168. Franz, G.; Gilg, H.A.; Grundmann, G.; Morteani, G. Metasomatism at a granitic pegmatite-dunite contact in Galicia: The Franqueira occurrence of chrysoberyl (alexandrite), emerald, and phenakite: Discussion. *Can. Mineral.* **1996**, *34*, 1329–1331.
169. Zwaan, J.C.; Touret, J. Emeralds in greenstone belts: The case of Sandawana, Zimbabwe. *Münchener Geologische Hefte* **2000**, *28*, 245–258.
170. Franz, G.; Morteani, G. Be-minerals: Synthesis, stability, and occurrence in metamorphic rocks. In *Beryllium: Mineralogy, Petrology, and Geochemistry*; Grew, E.S., Ed.; Mineralogical Society of America: Washington, DC, USA, 2002; Volume 50, pp. 551–589.
171. Martin-Izard, A.; Paniagua, A.; Moreiras, D. Metasomatism at a granitic pegmatite-dunite contact in Galicia: The Franqueira occurrence of chrysoberyl (alexandrite), emerald and phenakite. *Can. Mineral.* **1995**, *33*, 775–792.
172. Martin-Izard, A.; Paniagua, A.; Moreiras, D.; Acevedo, R.D.; Marcos-Pascual, C. Metasomatism at a granitic pegmatite-dunite contact in Galicia: The Franqueira occurrence of chrysoberyl (alexandrite), emerald, and phenakite: Reply. *Can. Mineral.* **1996**, *34*, 1332–1336.
173. Korzhinskii, D.S. *Theory of Metasomatic Zoning*; Clarendon Press: Oxford, UK, 1970.
174. Sahu, S.S.; Singh, S.; Staphy, J.S. Lithological and structural controls on the genesis of emerald occurrences and their exploration implications in and around Gubarabanda area, Singhbhum crustal province Eastern India. *J. Geol. Soc. India* **2018**, *92*, 291–297. [[CrossRef](#)]
175. Zwaan, J.C.; Kanis, J.; Petsch, J. Update on emeralds from the Sandawana mines, Zimbabwe. *Gems Gemol.* **1997**, *33*, 80–101. [[CrossRef](#)]
176. Holmes, A. The oldest dated minerals of the Rhodesian shield. *Nature* **1954**, *173*, 612–614. [[CrossRef](#)]
177. Christensen, J.N.; Selverstone, J.; Rosenfeld, J.L.; DePaolo, D.J. Correlation by Rb/Sr geochronology of garnet growth histories from different structural levels within the Tauern Window, Eastern Alps. *Contrib. Mineral. Petr.* **1994**, *118*, 1–12. [[CrossRef](#)]
178. Vance, D.; O’nyions, R.K. Isotopic chronometry of zone garnets growth kinetics and metamorphic histories. *Earth Planet. Sci. Lett.* **1990**, *114*, 113–129. [[CrossRef](#)]
179. Gilg, A.; Technische Universität München, Germany. Personal communication, 2009.
180. Lake, D.J. Are there Colombian-type emeralds in Canada’s Northern Cordillera? Insights from regional silt geochemistry, and the genesis of emerald at Lened, NWT. M.Sc. Thesis, University of British Columbia, Vancouver, BC, Canada, 2017.
181. Escobar, R. Geology and geochemical expression of the Gachalá emerald district, Colombia. *Geol. Soc. Am. Abstr. Program* **1978**, *10*, 397.
182. Beus, A.A. Sodium—A geochemical indicator of emerald mineralization in the Cordillera Oriental, Colombia. *J. Geochem. Explor.* **1979**, *11*, 195–208. [[CrossRef](#)]
183. Ringsrud, R. The Coscuez mine: A major source of Colombian emeralds. *Gems Gemol.* **1986**, *22*, 67–79. [[CrossRef](#)]
184. Cheilletz, A.; Giuliani, G. The genesis of Colombian emeralds: A restatement. *Miner. Deposita* **1996**, *31*, 359–364. [[CrossRef](#)]
185. Rohtert, W.R.; Independant geologist. Personal communication, 2017.
186. Gutiérrez, L.H.O. Evaluación magnetométrica, radiométrica y geoelectrica de depósitos esmeraldíferos. *Geofísica Colombiana* **2003**, *7*, 13–18.

187. Arif, M.; Henry, D.J.; Moon, C.J. Cr-bearing tourmaline associated with emerald deposits from Swat, NW Pakistan: Genesis and its exploration significance. *Am. Mineral.* **2010**, *95*, 799–809. [[CrossRef](#)]
188. Wise, M.A. Crystal Morphology of quartz, calcite, pyrite and rutile; Potential tool for emerald exploration in the Hiddenite area (North Carolina). *Geol. Soc. Am. Abstr. Programs* **2012**, *44*, 25.
189. Murphy, D.C.; Lipovsky, P.S.; Stuart, A.; Fonseca, A.; Piercey, S.J.; Groat, L. What about those emeralds, eh? Geological setting of emeralds at Regal Ridge (SE Yukon) provides clues to their origin and to other places to explore. *Geol. Assoc. Canada Mineral. Assoc. Canada Abstr. Program* **2002**, *28*, 154.
190. Lewis, L.L.; Hart, C.J.R.; Murphy, D.C. Roll out the beryl. In *Yukon Geoscience Forum*; Publications du Gouvernement du Canada: Yukon Territory, NT, Canada, 2003.



© 2019 by the authors. Licensee MDPI, Basel, Switzerland. This article is an open access article distributed under the terms and conditions of the Creative Commons Attribution (CC BY) license (<http://creativecommons.org/licenses/by/4.0/>).